Journal of Science & Technology

About the Journal

Pertanika is an international peer-reviewed journal devoted to the publication of original papers, and it serves as a forum for practical approaches to improving quality in issues pertaining to tropical agriculture and its related fields. *Pertanika* began publication in 1978 as the Journal of Tropical Agricultural Science. In 1992, a decision was made to streamline *Pertanika* into three journals to meet the need for specialised journals in areas of study aligned with the interdisciplinary strengths of the university. The revamped Journal of Science & Technology (JST) aims to develop as a pioneer journal focusing on research in science and engineering, and its related fields. Other *Pertanika* series include Journal of Tropical Agricultural Science (JTAS); and Journal of Social Sciences and Humanities (JSSH).

JST is published in **English** and it is open to authors around the world regardless of the nationality. It is currently published two times a year, i.e. in **January** and **July.**

Goal of *Pertanika*

Our goal is to bring the highest quality research to the widest possible audience.

Quality

We aim for excellence, sustained by a responsible and professional approach to journal publishing. Submissions are guaranteed to receive a decision within 12 weeks. The elapsed time from submission to publication for the articles averages 5-6 months.

Indexing of *Pertanika*

Pertanika is now over 30 years old; this accumulated knowledge has resulted in *Pertanika* journals being indexed in SCOPUS (Elsevier), EBSCO, AGRICOLA, and EconLit. etc. JST is indexed in EBSCO.

Future vision

We are continuously improving access to our journal archives, content, and research services. We have the drive to realise exciting new horizons that will benefit not only the academic community, but society itself.

We also have views on the future of our journals. The emergence of the online medium as the predominant vehicle for the 'consumption' and distribution of much academic research will be the ultimate instrument in the dissemination of research news to our scientists and readers.

Aims and scope

Pertanika Journal of Science and Technology aims to provide a forum for high quality research related to science and engineering research. Areas relevant to the scope of the journal include: *bioinformatics, bioscience, biotechnology and biomolecular sciences, chemistry, computer science, ecology, engineering, engineering design, environmental control and management, mathematics and statistics, medicine and health sciences, nanotechnology, physics, safety and emergency management,* and related fields of study.

Editorial Statement

Pertanika is the official journal of Universiti Putra Malaysia. The abbreviation for *Pertanika* Journal of Science & Technology is *Pertanika* J. Sci. Technol.

Pertanika Journal of

SCIENCE & TECHNOLOGY

Selected Articles from:
International Advanced Technology Congress (ATCi 2009)

VOL. 19 (S) OCT. 2011
(Special Issue)

Guest Editors:
Saied Pirasteh and Biswajeet Pradhan

A scientific journal published by Universiti Putra Malaysia Press

Editorial Board

2011-2013

Editorial Board

Pertanika Editorial Office

Office of the Deputy Vice Chancellor (R&I),
1st Floor, IDEA Tower II, UPM-MTDC Technology Centre
Universiti Putra Malaysia, 43400 Serdang, Selangor, Malaysia
Tel: +603 8947 1622, 8947 1620
E-mail: ndeeps@admin.upm.edu.my

Publisher

The UPM Press
Universiti Putra Malaysia
43400 UPM, Serdang, Selangor, Malaysia
Tel: +603 8946 8855, 8946 8854 • Fax: +603 8941 6172
penerbit@putra.upm.edu.my
URL: http://penerbit.upm.edu.my

Preface

The International Advanced Technology Congress (ATCi) was established in early 2000 to promote academic teaching and research on cutting-edge engineering and technologies at the international level. ATCi seeks to ensure that the views of the engineering teaching and research community are fully represented in the discussions that take place on future Malaysian research agendas and it also provides a permanent scientific forum where engineers and researchers can meet and exchange ideas and experiences at the Malaysian level.

The ATCi 2009 was organized between 3rd to 5th November 2009 at PWTC, Kuala Lumpur, Malaysia. The theme of this congress was "*Meeting Globalization Challenges Through Advanced Technology*" and is made up of five conferences as follows:

- Conference on Advanced Materials and Nanotechnology (CAMAN 2009)
- Conference on Alternative and Renewable Energy (CARE 2009)
- Conference on Intelligent Systems and Robotics (CISAR 2009)
- Conference on SMART Farming (SMARTFarming 2009)
- Conference on Spatial and Computational Engineering (SPACE 20009)

The SPACE 2009 call for full-papers of original and unpublished fundamental scientific research in all fields of geoinformation science, engineering and advanced technologies resulted in 44 submissions, of which 18 were accepted for publication in this volume (acceptance rate 45%). These figures indicate that having full-paper submissions leading to high-quality scientific edition is a promising model for future ATCi conferences.

The scientific papers published here, cover a number of basic topics within Geoinformation Science. The papers included in this edited volume span fundamental aspects of geoinformation processing, spatiotemporal modeling and various applications. We believe that the papers comprise innovative research and take Geoinformation Science one step further.

Organizing the programme of an International Conference and also editing a volume of scientific papers necessarily requires time and effort. We therefore would like to gratefully acknowledge the efforts of the authors and reviewers of this book, who in adhering to a strict timetables, helped to finalize this special issue. We thank the local organizing committee (University Putra Malaysia), Prof. Dr. Borhanuddin Mohd Ali (the Director of Institute of Advanced Technology), Prof. Dr. Azmi Zakaria for giving all kind of local support to make this special issue happen. We are also thankful to Dr. Nayan Kanwal, The Executive Editor of Pertanika journals for his kind cooperation to release this issue.

Saied Pirasteh
Biswajeet Pradhan
Universiti Putra Malaysia

Guest Editors
September 2011

Pertanika Journal of Science & Technology
Vol. 19 (S) Oct 2011

Contents

Pertanika Journal of Science & Technology
Vol. 19 (S) Oct 2011

Contents

ISSN: 0128-7680
Pertanika J. Sci. & Technol. **19 (S)**: 1 - 9 (2011)

Nonlinear Boolean Permutations

Abdurashid Mamadolimov[1*], Herman Isa[1], Miza Mumtaz Ahmad[2] and Moesfa Soeheila Mohamad[1]

[1]Information Security Cluster,
Malaysian Institute of Microelectronic Systems (MIMOS Bhd.),
Technology Park Malaysia, 57000 Kuala Lumpur, Malaysia
[2]School of Mathematical Sciences, Universiti Kebangsaan Malaysia,
43600 Bangi, Selangor, Malaysia
[*]E-mail: rashid.mdolimov@mimos.my

ABSTRACT

A Boolean permutation is called nonlinear if it has at least one nonlinear component function. All nonlinear Boolean permutations and their complements are called non-affine Boolean permutations. Any non-affine Boolean permutation is a potential candidate for bijective S-Box of block ciphers. In this paper, we find the number of n-variable non-affine Boolean permutations up to multiplicative n and show a simple method of construction of non-affine Boolean permutations. However, non-affinity property is not sufficient for S-Boxes. Nonlinearity is one of the basic properties of an S-Box. The nonlinearity of Boolean permutation is a distance between set of all non-constant linear combinations of component functions and set of all non-affine Boolean functions. The cryptographically strong S-Boxes have high nonlinearity. In this paper, we show a method of construction of 8-variable highly nonlinear Boolean permutations. Our construction is based on analytically design (8, 1), (8, 2), and (8, 3) highly nonlinear vectorial balanced functions and random permutation for other component functions.

Keywords: Boolean permutation, S-Box, block cipher, nonlinearity

INTRODUCTION

A Boolean function is a map from F_2^n to F_2 and a vectorial Boolean function is a map from F_2^n to F_2^m. Vectorial Boolean functions are usually called S-Boxes and are used as basic component of block ciphers. For example, the S-Boxes used in Data Encryption Standard (DES) have n=6 and m=4 and the S-Box used in the Advanced Encryption Standard (AES) has n=m=8. Large S-Boxes ($n \geq 8$, $m \geq 8$) are stronger than small one. Usually, $n \geq m$ and if n=m then vectorial Boolean function is called Boolean transformation. If Boolean transformation is bijective, then it is called Boolean permutation. In cryptology, Boolean permutations are called bijective S-Boxes. Each component function of Boolean permutation is a Boolean function. Boolean permutation is called linear (affine) if each component function is linear (affine). In bijective S-Boxes, non-affine Boolean permutations are used.

In this paper, we find bounds for the number of n-variable non-affine Boolean permutations. Lower and upper bounds differs by multiple of n. These bounds prove that the set of all affine Boolean permutations is a very small subset of all Boolean permutations. Therefore, non-affine Boolean permutations are not rare.

Received: 1 August 2010
Accepted: 22 June 2011
[*]Corresponding Author

The nonlinearity of Boolean permutation is the (Hamming) distance between the set of all non-constant linear combinations of component functions and the set of all non-affine Boolean functions. Non-affinity property alone is insufficient for S-Boxes. The linear cryptanalysis introduced by Matusi (1994), which is based on finding affine approximation to the action of cipher (Matusi, 1994). The linear attack on a function is successful if nonlinearity of a function is low. Highly nonlinear functions possess the best resistance to the linear attack. Therefore, nonlinearity is an essential property for Boolean permutations used as bijective S-Boxes.

Upper bounds of nonlinearity for different classes of functions exist (Maxwell, 2005; Budaghyan, 2005; Sulak, 2006). For *n*-variable Boolean permutations, when *n* is even, functions with nonlinearity $2^{n-1} - 2^{\frac{n}{2}}$ are known. It is conjectured that this value is the highest possible nonlinearity for the *n* even case. In this case each component function's highest nonlinearity is $2^{n-1} - 2^{\frac{n}{2}-1} - 2$.

The problem in constructing highly nonlinear bijective S-Boxes has been studied in (Cui and Cao, 2007; Jin *et al*., 2006; Sakalauskas and Luksys, 2007). Methods of construction could be separated into two groups: analytic and algorithmic. Almost all analytical methods of construction are based on finite field theory. Vectorial Boolean functions can be considered also as a map from finite field F_{2^n} to finite field F_{2^m}. The power map $x \to x^d$, where $x \in F_{2^n}$ has been systematically studied in (Budaghyan, 2005). A power map is a Boolean permutation if and only if gcd $(d, 2^n - 1) = 1$. Some highly nonlinear power permutations are known (Budaghyan, 2005). For example, the power permutation $x^{2^{n-2}} = \begin{cases} x-1, \text{ if } x \neq 0 \\ 0, \text{otherwise} \end{cases}$, where $x \in F_{2^n}$, which in fact is the inverse function, has the known highest nonlinearity when *n* is even. AES's S-Box is based on 8-variable inverse function. The second group of construction of highly nonlinear Boolean permutations is algorithmic (Watanabe *et al*., 2007; Clark *et al*., 2005; Fuller *et al*., 2005; Seberry *et al*., 1993). Usually, algorithmic method is done by increasing the nonlinearity in steps. As a rule, the cryptographic properties of such algorithmic S-Boxes are not optimal.

We suggest a construction of Boolean permutations by analytically designing (8, 1), (8, 2) and (8, 3) highly nonlinear vectorial balanced functions and randomly permuting other component functions.

PRELIMINARIES

Let F_2 be the finite field with two elements and let $(F_2^n, \oplus)$ be the vector space over F_2, where $\oplus$ is used to denote the addition operator over both F_2 and the vector space F_2^n (Pieprzyk, 1989; Nyberg, 1993;1994).

An *n*-variable Boolean function (filter) is a map

$$f = f(x_1, \ldots, x_n) : F_2^n \to F_2$$

The (Hamming) weight *wt(f)* of a Boolean function *f* on *n* variables is the weight of this string, that is, the size of the support $sp(f) = \{x \in F_2^n : f(x) = 1\}$ of the function. The function *f* is said to be balanced if $wt(f) = 2^{n-1}$. The (Hamming) distance between two Boolean functions *f* and *g* is $d(f,g) = |\{x : f(x) \neq g(x)\}|$. Clearly, the distance between Boolean functions *f* and *g* is equal to the weight of sum of these functions i.e., $d(f,g) = wt(f \oplus g)$.

If we denote by *B(n)* the set of all *n*-variable Boolean functions then we have $|B(n)| = 2^{2^n}$.

An (*n,m*) vectorial Boolean function (S-Box) is a map.

$F = F(x_1,\ldots,x_n) = (f_1(x_1,\ldots,x_n),\ldots,f_n(x_1,\ldots,x_n)) : \mathrm{F}_2^n \to \mathrm{F}_2^m$. Clearly, each component function $f_i, i = 1,\ldots,m$ is an n-variable Boolean function. An (n,n) vectorial Boolean function is called n-variable Boolean transformation.

An (n,m) vectorial Boolean function is called balanced if it takes every value of F_2^m the same number of times. If a Boolean transformation is balanced then it takes every value of F_2^n one time. A balanced n-variable Boolean transformation is called n-variable Boolean permutation. Clearly, n-variable Boolean permutation is bijective function from F_2^n into itself.

Let $F = F(x_1,\ldots,x_n) = (f_1(x_1,\ldots,x_n),\ldots,f_n(x_1,\ldots,x_n))$ be a Boolean transformation and let $c \cdot F = c_1 f_1 \oplus \ldots \oplus c_n f_n, c = (c_1,\ldots,c_n) \in F_2^n, c \neq 0$ be non-constant linear combination of component functions. A Boolean transformation is a Boolean permutation if and only if each non-constant linear combination of component functions is balanced.

If we denote the set of all (n,m) vectorial Boolean functions, n-variable Boolean transformations and n-variable Boolean permutations as *BF(n,m), BT(n)* and *BP(n)* respectively, then we have $|BF(n,m)| = 2^{m\cdot 2^n}$, $|BT(n)| = 2^{n\cdot 2^n}$ and $|BP(n)| = 2^n!$.

The unique representation of n-variable Boolean function f as a polynomial over F_2 in n variables of the form $f(x_1,\ldots,x_n) = \sum_{\alpha \in F_2^n} c(\alpha)(\prod_{i=1}^{n} x_i^{\alpha_i})$ is called the algebraic normal form (ANF) of f. The degree of the ANF of f is denoted by $d^\circ(f)$ and is called the algebraic degree of the function f.

An n-variable Boolean function is called linear (affine) if its ANF is $f(x_1,\ldots,x_n) = c_1x_1 \oplus \ldots \oplus c_nx_n$, $(f(x_1,\ldots,x_n) = c_0 \oplus c_1x_1 \oplus \ldots \oplus c_nx_n)$ where $c_i \in F_2, i = (0,)1,\ldots,n$. Clearly, Boolean function f is affine if $d^\circ(f) \leq 1$and f is linear if it is affine and $f(0)$=0.

An (n,m) vectorial Boolean function $F = (f_1,\ldots,f_m)$ is called linear (affine) if each component function $f_1,\ldots,f_m$ is linear (affine). In this paper we concentrate on non-affine Boolean permutations.

Let $\mathrm{A}(n)$ be the set of all n-variable affine Boolean functions. The nonlinearity N_f of an n-variable Boolean function f is defined as $N_f = \min_{g \in A(n)} d(f,g)$, i.e., the nonlinearity of function f is a distance between function f and the set $\mathrm{A}(n)$ of all n-variable affine Boolean functions. Clearly, $N_f = 0$ if and only if f is an affine function. It is known that for any n-variable Boolean function f, the nonlinearity N_f satisfies the following relation: $N_f \leq 2^{n-1} - 2^{n/2-1}$. Functions achieving the equality are called bent functions which exist when n is even. However, bent functions are not balanced. Let f be a balanced n-variable Boolean function ($n \geq 3$). Then the nonlinearity of function f is given by

$$N_f \begin{cases} 2^{n-1} - 2^{n/2-1} - 2, & n \text{ even} \\ \lfloor\lfloor 2^{n-1} - 2^{n/2-1} \rfloor\rfloor, & n \text{ odd}, \end{cases}$$

where $\lfloor\lfloor x \rfloor\rfloor$ denotes the largest even integer less than or equal to x.

We can compute nonlinearity N_f of 8-variable Boolean function f by following way:

$$N_f = \min_{(c_0,c_1,\ldots,c_8) \in F_2^9} wt(f \oplus c_0 \oplus c_1x_1 \oplus c_8x_8).$$

The nonlinearity N_F of an (n,m) vectorial Boolean function F is defined as $N_F = \min_{c \in F_2^m, c \neq 0} N_{c\cdot F}$ In the other words, the nonlinearity of function F is a distance between the set of all non-constant linear combinations of component functions of F and the set $\mathrm{A}(n)$ of all n-variable affine Boolean functions. This shows that $N_F = 0$ if F is affine. However, the condition $N_F = 0$ does not explain the affinity of F. It is known that for any (n,m) vectorial Boolean function F, the nonlinearity, N_F satisfies $N_f \leq 2^{n-1} - 2^{n/2-1}$. Functions achieving the equality are called perfectly nonlinear and

can exist only when n is even and $m \leq \frac{n}{2}$. If n is odd and n=m then we have $N_f \leq 2^{n-1} - 2^{\frac{n-1}{2}}$. Functions with nonlinearity $2^{n-1} - 2^{\frac{n}{2}}$ are known for even n and n=m, and it is conjectured that this value is the highest possible nonlinearity.

THE NUMBER OF NON-AFFINE BOOLEAN PERMUTATIONS

We denote the set of all non-affine n-variable Boolean permutations by *NABP(n)*. Note that $NABP(n) \subset BP(n) \subset BT(n)$.

Theorem. Let $\mu(n) = 2^n! - (2^{n-1}!)^2 \cdot (2^{n+1} - 2)$. Then the number of non-affine Boolean permutations satisfies

$$\mu(n) \leq \left| NABP(n) \right| \leq n \cdot \mu(n)$$

Proof: For proving the left side of inequality, it is enough to show that we can construct $\mu(n)$ different non-affine n-variable Boolean permutations. Clearly, an n-variable Boolean permutation is just permutation of F_2^n vectors. Our method of construction contains two steps:

i. Choose balanced non-affine n-variable Boolean function as first component function f_1 of Boolean permutation.

i. Choose two permutations of F_2^{n-1} vectors and set the permuted vectors as values of $(0, f_2, ..., f_n)$ and $(1, f_2, ..., f_n)$, respectively.

The resulting function $F = (f_1, f_2, ..., f_n)$ is a non-affine Boolean permutation.

Any non-constant affine function is balanced. Since, $\left| A(n) \right| = 2^{n+1}$ and the number of constant affine functions is 2, the number of balanced affine Boolean functions is $2^{n+1} - 2$ while the number of n-variable balanced Boolean functions is $\left(\frac{2^n}{2^{n-1}}\right)$. Therefore the number of balanced n-variable non-affine Boolean function is $\left(\frac{2^n}{2^{n-1}}\right) - (2^{n+1} - 2)$. The number of permutations in step ii) is $(2^{n-1}!)^2$. Thus, we have

$(2^{n-1}!)^2 \cdot \left(\left(\frac{2^n}{2^{n-1}}\right) - (2^{n+1} - 2)\right) = 2^n! - (2^{n-1}!)^2 \cdot (2^{n+1} - 2) = \mu(n)$ distinct non-affine Boolean permutations.

To prove the right side of inequality, we first construct $n \cdot \mu(n)$ non-affine Boolean permutations. Then we show that each non-affine Boolean permutation can be obtained by our construction. In the above construction if we take i-th component as balanced non-affine fixed function for each i=1,2,…,n then we have $n \cdot \mu(n)$ non-affine Boolean permutations. Let $F = (f_1, ..., f_n)$ be any non-affine Boolean permutation. Then F has at least one non-affine component function f_i. Clearly, the Boolean permutation $F = (f_1, ..., f_n)$ can be obtained by permuting the vectors of F_2^n such that in the obtained Boolean permutations i-th component function is same with f_i.

Table 1 showed us the number of functions of three classes for some small n.

TABLE 1
The number of functions of three classes

n	$\lvert BT(n)\rvert$	$\lvert BP(n)\rvert$	$\lvert NABP(n)\rvert$
1	4	2	0
2	256	24	0
3	16,777,216	40,320	$\geq$ 32,256
8	$\approx 10^{614}$	$\approx 10^{513}$	$\approx 10^{512}$

CONSTRUCTION HIGHLY NONLINEAR 8-VARIABLE BOOLEAN PERMUTATIONS

In the above construction we choose non-affine Boolean function as first component and after permuting of F_2^{n-1} vectors by first component we obtain non-affine Boolean permutation. If we choose a highly nonlinear Boolean function as the first component we can obtain highly nonlinear Boolean permutation.

We extend the construction to having highly nonlinear balanced (8, 2) and (8, 3) vectorial Boolean functions as first two and first three component functions of Boolean permutation, respectively.

Note that 8-variable highly nonlinear Boolean permutation is eight 8-variable Boolean functions $f_1(x_1,\ldots,x_8),\ldots,f_8(x_1,\ldots,x_8)$, where each non-constant linear combination of these functions is balanced and has high nonlinearity.

We note that the highest known nonlinearity for 8-variable Boolean permutations is 112, while each their component function's highest nonlinearity is 118.

The following construction is filled in.

A. Design of the First Component Function

We want to design highly nonlinear balanced Boolean function. We consider the function

$$g_1(x_1,\ldots,x_8) = x_1x_4 \oplus x_3x_6 \oplus x_2x_5 \oplus x_4x_5 \oplus x_7x_8 \oplus x_1x_2x_7 \oplus x_3x_4x_7 \oplus x_5x_6x_7$$

This function is bent and $N_{g_1} = wt(g_1) = 120$. The function

$$g_2(x_2,x_4,x_6,x_8) = x_4 \oplus x_8 \oplus x_2x_8 \oplus x_4x_6 \oplus x_2x_4x_6 \oplus x_2x_6x_8$$

is a balanced function and has highest nonlinearity ($N_{g_2} = 4$) in F_2^4. Let

$$f_1(x_1,\ldots,x_8) = \begin{cases} g_2(x_2,x_4,x_6,x_8), & \text{if } (x_1,x_3,x_5,x_7) \\ g_1(x_1,\ldots,x_8), & \text{otherwise} \end{cases}$$

Since $g_1(0,x_2,0,x_4,0,x_6,0,x_8) = 0$ for all $(x_2,x_4,x_6,x_8) \in F_2^4$, $wt(g_1)$=120 and g_2 is balanced then f_1 is a balanced function. We have $N_{f_1} = 116$. We use the function f_1 as first component function for Boolean permutation. Note that instead of g_2 we can use any balanced Boolean function in F_2^4 with nonlinearity 4. The total number of such functions is 10920.

B. Design of the First Two Component Functions

We want to design two functions, f_1 and f_2, where f_1, f_2 and $f_1 + f_2$ are balanced and have high nonlinearity.

We consider the following two functions:

$$f_1'(x_1,\ldots,x_8) = x_1x_2 \oplus x_1x_3 \oplus x_1x_4 \oplus x_1x_5 \oplus x_1x_7 \oplus x_2x_3 \oplus x_2x_4 \oplus x_2x_6 \oplus x_2x_8 \oplus x_3x_5 \oplus x_3x_7 \oplus x_3x_8 \oplus x_4x_6 \oplus x_4x_7 \oplus x_4x_8 \oplus x_5x_6 \oplus x_5x_6 \oplus x_5x_8 \oplus x_6x_7 \oplus x_6x_8 \oplus x_2x_3 \ldots x_8,$$

$$f_1'(x_1,\ldots,x_8) = x_1x_2 \oplus x_1x_4 \oplus x_1x_6 \oplus x_1x_8 \oplus x_2x_3 \oplus x_2x_5 \oplus x_2x_7 \oplus x_3x_4 \oplus x_3x_6 \oplus x_3x_7 \oplus x_4x_5 \oplus x_4x_6 \oplus x_5x_6 \oplus x_5x_7 \oplus x_5x_8 \oplus x_6x_8 \oplus x_7x_8 \oplus x_1x_3x_4 \ldots x_8$$

We have $wt(f_1') = 136$, $wt(f_2') = 118$, $wt(f_1' + f_2') = 122$ and $\min\{N_{f_1'}, N_{f_2'}, N_{f_1'+f_2'}\} = 118$. We change 8 values of function f_1': $f_1'(5)$, $f_1'(20)$, $f_1'(30)$, $f_1'(103)$, $f_1'(119)$, $f_1'(155)$, $f_1'(212)$, $f_1'(240)$ from 1 to 0. We also change 10 values of function f_2': $f_2'(30)$, $f_2'(32)$, $f_2'(38)$, $f_2'(78)$, $f_2'(103)$, $f_2'(119)$, $f_2'(140)$, $f_2'(167)$, $f_2'(212)$, $f_2'(240)$ from 0 to 1. Let obtained functions be f and f_2, respectively. Then we have $wt(f_1) = wt(f_2) = wt(f_3) = 128$ and $N_{f_1} = N_{f_2} = N_{f_1+f_2} = 112$.

C. *Design of the First Three Component Functions*

We want to design three f_1, f_2 and f_3 functions, where functions $f_1, f_2, f_3, f_1 + f_2, f_1 + f_3, f_2 + f_3$ and $f_1 + f_2 + f_3$ are balanced and have high nonlinearity.

Let f_1, f_2 be the functions from section B and f_3 be f_1 from section A. Then we have

$$wt(f_1) = wt(f_2) = wt(f_3') = wt(f_1 + f_2) = wt(f_1 + f_2 + f_3') = 128,$$
$$wt(f_1) + f(f_3') = 142, wt(f_2 + f_3') = 130 \text{ and}$$

$$N_{f_1} = N_{f_2} = N_{f_1+f_2} = 112, N_{f_3'} = 116, N_{f_1+f_3'} = 106, N_{f_1+f_2+f_3'} = 108.$$

We change (0 becomes 1, 1 becomes 0) 14 values of function f_3': $f_3'(11)$, $f_3'(12)$, $f_3'(87)$, $f_3'(88)$, $f_3'(90)$, $f_3'(91)$, $f_3'(106)$, $f_3'(107)$, $f_3'(114)$, $f_3'(115)$, $f_3'(158)$, $f_3'(159)$, $f_3'(185)$, $f_3'(186)$. Let the resulting function be f_3. Then we will have

$$wt(f_1) = wt(f_2) = wt(f_3) = wt(f_1 + f_2) = wt(f_1 + f_3) =$$
$$wt(f_2 + f_3) = wt(f_1 + f_2 + f_3) = 128 \text{ and}$$
$$N_{f_1} = N_{f_2} = N_{f_1+f_2} = 112, N_{f_3} = 108, N_{f_1+f_3} = 106, N_{f_1+f_3} = 104.$$

D. *Random Generation and Result of Experiment*

We have three types of constructions, A, B and C. In *Case A* two random permutations of F_2^7 vectors set as values of $(0, f_2, ..., f_8)$ and $(1, f_2, ..., f_8)$. The number of 8-variable Boolean permutations obtained in this way is $(128!)^2$. In *Case B* four random permutations of F_2^6 vectors set as values of $(0, 0, f_3, ..., f_8)$, $(0,1, f_3, ..., f_8)$, $(1,0, f_3, ..., f_8)$, $(1,1, f_3, ..., f_8)$. The number of 8-variable Boolean permutations obtained in this way is $(64!)^4$. While in *Case C* eight random permutations of F_2^5 vectors set as values of $(0,0,0, f_4, ..., f_8)$, $(0,0,1, f_4, ..., f_8)$, …, $(1,1,1, f_4, ..., f_8)$. The number of 8-variable Boolean permutations obtained in this way is $(32!)^8$.

The results of experiment with 100,000 generations for each of the three cases are showed in Table 2 and *Fig. 1*.

TABLE 2
Nonlinearity distribution

Nonlinearity	Frequency		
	Case A	Case B	Case C
0-74	0	0	0
76	1	0	0
78	6	0	1
80	9	1	20
82	67	15	69
84	291	66	274
86	1141	287	1117
88	4129	1350	3946
90	13029	5230	12880
92	31565	17103	30831
94	38420	38331	39062
96	11192	37617	11622
98	150	0	178
100-112	0	0	0
Total	100000	100000	100000

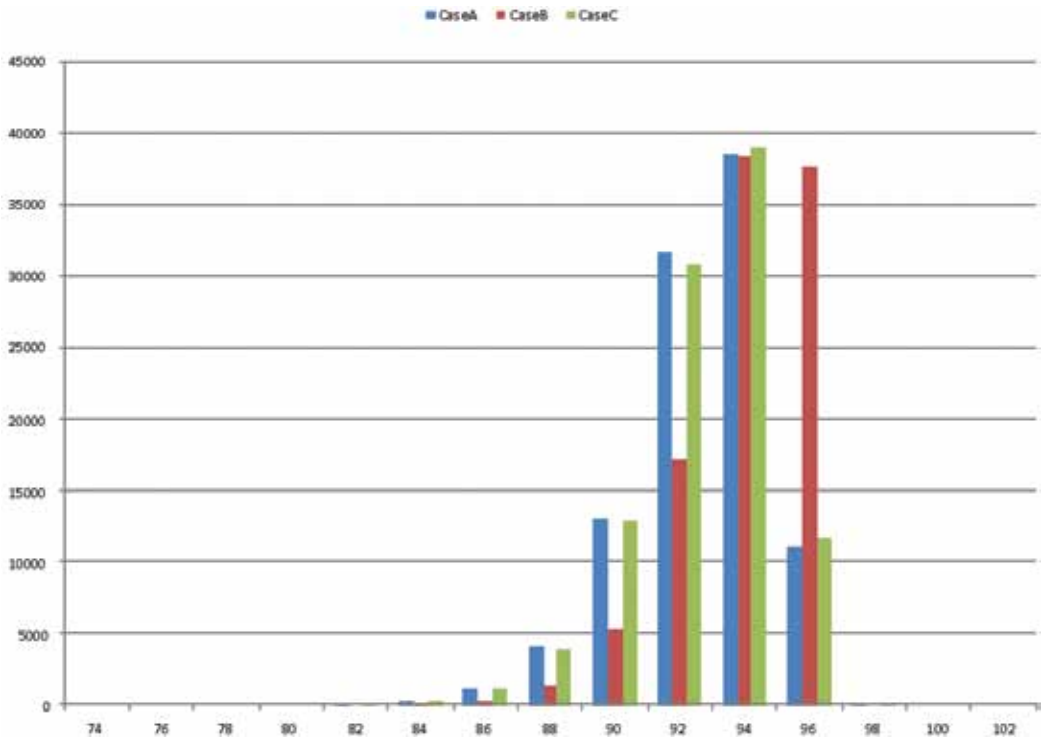

Fig. 1: Nonlinearity distribution

In Table 3, the comparison of our generated Boolean permutation and known 8-variable bijective S-Boxes is shown. Note that the first seven S-Boxes in this table are based on inverse function in F_{2^8} and they are linearly equivalent to each other.

TABLE 3
Comparison of 8 × 8 Bijective S-Boxes

No.	Cipher	Nonl.	Design techn.
1	AES	112	Finite field
2	Grand-Cru	112	Finite field
3	Mugi	112	Finite field
4	Q	112	Finite field
5	Scream	112	Finite field
6	Camellia	112	Finite field
7	Square	112	Finite field
8	Hierocrypt	106	Unknown
9	Skipjack	100	Unknown
10	Our	98	Anal.+ Ran.
11	Khazad	96	Random
12	Anubis	94	Random

CONCLUSIONS

Non-affine Boolean permutations are not rare. However, highly nonlinear ($\geq$ 98, in n=8 case) Boolean permutations are not many.

We suggest a new method of construction of highly nonlinear 8-variable Boolean permutations. Our construction technique combines both the analytical and random approach, by analytically design the first three component functions and randomly generate the remaining components.

From each 8-variable S-Box, approximately 10^{19} linearly equivalent S-Boxes can be obtained and all these S-Boxes have the same nonlinearity. It is not possible to consider S-Box as "new", if it is linearly equivalent to one of the known cipher's S-Box. However, the S-Box obtained from our construction S-Box with parameters in Table 3 is a new one.

The suggested construction can be generalized for any S-Box size.

REFERENCES

Budaghyan, L. (2005). The equivalence of Almost Bent and Almost Perfect nonlinear functions and their generalization. PhD Dissertation, Otto-von-Guericke-University, Magdeburg, Germany.

Clark, J., Jacob, J., & Stepney, S. (2005). The design of S-Boxes by simulated annealing. *New Generation Computing, 23*(3), September 2005, 219-231.

Cui, L., & Cao, Y. (2007). A new S-Box structure named affine-power-affine. *International Journal of Innovative Computing, Information and Control, 3*(3), 751-759.

Fuller, J., Millan, W., & Dawson, E. (2005). Multi-objective optimization of bijective S-Boxes. *New Generation Computing, 23*(3), September 2005, 201-218.

Jin, S-Y., Baek, J-M., & Song, H-Y. (2006). Improved Rijndael-like S-Box and its transform domain analysis. *Sequences and Their Applications – SETA 2006.* LNCS, *4086*, 153-167.

Matsui, M. (1994). Linear cryptanalysis method for DES cipher. In *Advances in Cryptology-EUROCRYPT'93, LNCS* (pp. 386-397). Springer-Verlag.

Maxwell, M. S. (2005). Almost perfect nonlinear functions and related combinatorial structures. PhD Dissertation, Iowa State University, Ames, Iowa.

Nyberg, K. (1993). On the construction of highly nonlinear permutations. In *Advances in Cryptology, EUROCRYPT'92, Springer Verlag, LNCS 658* (pp. 92-98).

Nyberg, K. (1994). Differential uniform mappings for cryptography. In *Advances in Cryptology, Proc. Eurocrypt'93, LNCS 765* (pp. 55-64).

Pieprzyk, J. (1989). Nonlinearity of exponent permutations. In *Advances in Cryptology, Proceedings of EuroCrypt'89, LNCS* (pp. 80-92). Berlin, Germany: Springer-Verlag,

Sakalauskas, E., & Luksys, K. (2007). Matrix power S-Box construction. Cryptology ePrint Archive: Report, no. 214. Retrieved from http://eprint.iacr.org/2007/214.

Seberry, J., Zhang, X-M., & Zheng, Y. (1993). Systematic generation of Cryptographically Robust S-Boxes. In *Proceedings of the First ACM Conference on Computer and Communications Security* (pp. 171-182). The Association for Computing Machinery, New York.

Sulak, F. (2006). Constructions of bent functions. M. Scien. Thesis, Middle East Technical University, Turkey.

Watanabe, A., Haruki, H., Sh. Shimotomai, Saito, T., Nagase, T., Yoshioka, Y., & Hasegawa, Y. (2007). A new mutable nonlinear transformation algorithm for S-Box. *AINA Workshops,* (1), 246-251.

ISSN: 0128-7680
Pertanika J. Sci. & Technol. **19 (S)**: 11 - 14 (2011)

On Nonspherical Partial Sums of Fourier Integrals of Continuous Functions from the Sobolev Spaces

Ravshan Ashurov
Institute of Advanced Technology (ITMA), Universiti Putra Malaysia,
43400 UPM, Serdang, Selangor, Malaysia
E-mail: ashurovr@yahoo.com

ABSTRACT

The partial integrals of the N-fold Fourier integrals connected with elliptic polynomials (not necessarily homogeneous; principal part of which has a strictly convex level surface) are considered. It is proved that if $a + s > (N - 1)/2$ and $ap = N$ then the Riesz means of the nonnegative order s of the N-fold Fourier integrals of continuous finite functions from the Sobolev spaces $W_p^a(R^N)$ converge uniformly on every compact set, and if $a + s > (N - 1)/2$ and $ap = N$, then for any $x_0 \in R^N$ there exists a continuous finite function from the Sobolev space such, that the corresponding Riesz means of the N-fold Fourier integrals diverge to infinity at x_0. AMS 2000 Mathematics Subject Classifications: Primary 42B08; Secondary 42C14.

Keywords: *N*-fold Fourier integrals, elliptic polynomials, continuous functions from the Sobolev spaces, uniformly convergence

INTRODUCTION

Let Ω be an arbitrary domain in R^N, $\Omega \subseteq R^N$. Consider an arbitrary non-negative elliptic differential operator $A(x,D)$ with smooth coefficients and the domain of definition $C_0^\infty(\Omega)$ (i.e. infinitely differentiable functions on Ω with a compact support). Let us denote by A an arbitrary non-negative self-adjoint extension in $L_2(\Omega)$ of the operator $A(x, D)$. According to the spectral theorem there exists a family of spectral projectors $\{E_\lambda\}$ such that for every $f \in L_2(\Omega)$ one has

$$Af(x) = \int_0^\infty \lambda \, dE_\lambda \, f(x),$$

where $E_\lambda f(x)$ is called the eigenfunction expansions of f. According to Gärding theorem, each projector E_λ is an integral operator with the kernel $\theta(x, y, \lambda)$, called the spectral function (Gärding, 1954).

The Riesz means of nonnegative order s of eigenfunction expansions $E_\lambda f(x)$ are defined as

$$E_\lambda^s f(x) = \int_0^\lambda \left(1 - \frac{t}{\lambda}\right)^s dE_t f(x) \tag{1}$$

In particular, if the operator $A(x, D)$ has constant coefficients and $\Omega = R^N$, then $E_\lambda f(x)$ coincides with the partial integrals of N-fold Fourier integrals of the function $f \in L_2(R^N)$.

In the present paper we study the uniform convergence of the spectral resolutions $E_\lambda^s f$ and their Riesz mean $E_\lambda^s f$ for functions belonging to the Sobolev space $W_p^a(\Omega)$ (for the definition and basic properties of the spaces $W_p^a(\Omega)$ see the monograph (Sobolev, 1963)).

Received: 1 August 2010
Accepted: 22 June 2011

Definitive sufficient conditions for the uniform convergence on any compact set $K \subset \Omega$ of $E_\lambda^s f$ to the finite function (i.e. with compact support) f belonging to $W_p^a(\Omega)$ (even to the broader Nikol'skii classes $H_p^a(\Omega)$ $H_p^a(\Omega)$) were established by Sh.A. Alimov (1967; 1978), and they are as follows:

$$a + s \geq \frac{N-1}{2}, ap > N \tag{2}$$

where $p \geq 1, s \geq 0, a > 0$.

These conditions ensure the uniform convergence of eigenfunction expansions of Schrödinger operator with singular potentials too (Sh.A. Alimov and Joó, 1983).

The relations (2) were first found for the Laplace operator in the work of Il'in [5] for $s = 0$. Moreover, Il'in proved (*see* [3]), that for uniform convergence the first condition here is best possible. Namely, if $a + s < (N-1)/2$ then there exists a finite function $f \in C^a(\Omega)$ for which the means $E_\lambda^s f$ are unbounded at some point.

As for the condition $ap > N$, it guarantees, according to imbedding theorems, the function in question to be continuous, and if the opposite inequality $ap \leq N$ is satisfied, then there exists an unbounded finite function $f \in W_p^a(\Omega)$ whose Riesz means clearly cannot converge to it uniformly. In this connection the following question arises: is the assertion on uniform convergence valid if in conditions (2) the inequality $ap > N$ is replaced by the equality $ap = N$ and it is additionally required that the function f be continuous in the domain Ω? In the paper [6] Sh.A. Alimov gave a complete answer to this question in case of the Laplace operator. Namely, he proved that in case $ap = N$ the sum $a + s$ is essential, i.e. if $a + s < (N-1)/2$ then we have the uniform convergence, and if $a + s < (N-1)/2$ then we do not.

To prove these theorems Sh.A. Alimov, distinguishing the leading term of the spectral expansion (Il'in, 1957), obtained an extremely convenient for studying representation of $E_\lambda^s f$ for the functions f from $W_2^a(\Omega)$ (*see* Lemma 4). The proof of this representation essentially based on the mean value formula for the eigenfunctions of the Laplace operator. Even in case of the Shrödinger operator, where we have the mean value formula but with the remainder term, this representation is not proved yet.

In this paper we investigate the same question for elliptic differential operators (not necessarily homogeneous) with constant coefficients and an arbitrary order, considering in R^N.

THE MAIN RESULTS

Let $A(D)$ be an arbitrary elliptic differential expression with constant coefficients and order m:

$$A(D) = \sum_{|\alpha| \leq m} a_\alpha D^\alpha$$

Note this operator is not necessarily homogeneous, i.e. the coefficients a_α with $|\alpha| < m$ is not necessarily zero.

If we consider $A(D)$ on $L_2(R^N)$ with the domain of definition $C_0^\infty(R^N)$, i.e. infinitely differentiable functions with a compact support, then we will have essentially self-adjoint operator (see, for example (Alimov *et al*., 1991; Sobolev, 1963). Let us denote a unique self-adjoint extension of this operator by A. As mentioned above an eigenfunction expansion in this case coincides with the Fourier expansion and has the following form:

$$E_\lambda f(x) = (2\pi)^{-N/2} \int_{A(\xi) < \lambda} \hat{f} e^{ix\xi} d\xi$$

where $\hat{f}(\xi)$ is the Fourier transform of $f(x)$ and $A(\xi)$ is the symbol of the expression $A(D)$, i.e.

$$A(\xi) = \sum_{|\alpha| \le m} a_\alpha \xi^\alpha.$$

The Riesz means of a nonnegative order s of $E_\lambda f$ are defined as in (1). Observe if $s = 0$ then

$$E_\lambda^0 f(x) = E_\lambda f(x).$$

If we define

$$\theta^s(x,\lambda) = (2\pi)^{-N} \int_{A(\xi)<\lambda} \left(1 - \frac{A(\xi)}{\lambda}\right)^s e^{ix\xi} d\xi \tag{3}$$

then by the definition of the Fourier transform one has

$$E_\lambda^s f(x) = \int_{R^N} f(y)\theta^s(x-y,\lambda)dy. \tag{4}$$

The function $\theta(x,\lambda) = \theta^0(x,\lambda)$ is called the spectral function of the operator A while $\theta^s(x,\lambda)$ is called the Riesz means of the spectral function.

The following homogeneous polynomial $A_0(\xi) = \sum_{|a|=m} a_\alpha \xi^\alpha$ is called a principal symbol of the elliptic polynomial $A(\xi)$. Obviously, the asymptotic behavior of the function $\theta^s(x,\lambda)$ essentially depends on the geometry of the set $C = \{\xi \in R^N : A_0(\xi) \le 1\}$. When the surface

$$\partial C = \{\xi \in R^N : A_0(\xi) = 1\} \tag{5}$$

is strictly convex, i.e. when the Gaussian curvature is positive at every point of this surface, then we have the best possible estimate for the Riesz means of the spectral function.

We denote by $W_{0,p}^a(R^N)$ the class of functions belonging to $W_p^a(R^N)$ and having compact support (i.e. finite functions).

The main results of the paper are the following theorems.

Theorem 1. *Let $A(\xi)$ be an arbitrary elliptic polynomial with strictly convex surface* (5). *Let $G \subset R^N$ and suppose that the numbers $s \ge 0$, $p \ge 1$ and the integer $a > 0$ are related by*

$$a + s > \frac{N-1}{2}, ap = N.$$

Then for any function $f \in W_{0,p}^a(R^N)$ continuous in the domain G the following equality holds uniformly on each compact set $K \subset G$:

$$\lim_{\lambda \to \infty} E_\lambda^s f(x) = f(x).$$

Theorem 2. *Let $A(\xi)$ be an arbitrary elliptic polynomial with a strictly convex surface* (5), *and let x_0 be an arbitrary point of R^N. Suppose that the numbers $s \ge 0$, $p \ge 1$, and the integer $a > 0$ are related by*

$$a + s = \frac{N-1}{2}, ap = N.$$

Then there exists a continuous function $f \in W_{0,p}^{a}(R^N)$ *such that*

$$\overline{\lim_{\lambda \to \infty}} E_{\lambda}^{s} f(x_0) = +\infty .$$

These theorems are true in fact for finite functions from the broader Nikol'skii classes $H_p^a(R^N)$ where the index $a > 0$ may assume any (not necessarily integer) values. But for these functions the proofs will be technically more complicated.

We also note, that these theorems were proved in case of homogeneous elliptic operators $A_0(D) = \sum_{|\alpha|\le m} a_\alpha D^\alpha$ (Alimov *et al*., 1991). In case of the operators $A_0(D)$ the sets $\{\xi \in R^N : A_0(\xi) \le \lambda\}$ form a family of enclosing sets, whereas the domains $\{\xi \in R^N : A(\xi) \le \lambda\}$ are in general not similar for different values of λ. Therefore, investigation of the Riesz means (4) for non-homogeneous elliptic operators more complicated.

CONCLUSION

Let $A(D)$ be a non-homogeneous elliptic operator with strictly convex surface (5). We investigated the corresponding Riesz means of the Fourier integrals (4). Consider the Sobolev class $W_p^a(R^N)$ and let $ap = N$. In this case functions from this class are not necessarily continuous. Therefore we cannot expect the uniform convergence of multiple Fourier integrals to these functions. Now let us consider only those functions of $W_p^a(R^N)$ which are continuous (i.e. consider a subspace). As it is shown in Theorems 1 and 2, for uniform convergence of the Riesz means (4) of order s for functions from this subspace the sum $a + s$ is essential. In other words, if this sum is greater than $(N - 1)/2$ then we have uniform convergence and otherwise we do not.

ACKNOWLEDGEMENTS

This paper has been supported by the Ministry of Higher Education of Malaysia under Research Grant (FRGS, Fasa 2/2009, Grant number 01-11-09-713FR/F1).

REFERENCES

Gärding, L. (1954). Eigenfunction expansions connected with elliptic differential operators. *Proc. 12 Congr. Scand. Math. Lund* (pp. 44-55).

Il'in, V. A. (1957). On the uniform convergence of expansions by eigenfunctions under summation in the order of increasing eigenvalues. *Dokl.Akad. Nauk SSSR*, *114*, 698-701

Sh. A. Alimov. (1976). *On spectral decompositions of functions in* H_p^a. *Mat. Sb., Nov. Ser., 101*(1), 3-21. English translation: Math. USSR, Sb. 30, 1-16, Zbl. 344.46069.

Sh. A. Alimov. (1978). Decomposability of continuous functions from the Sobolev classes with respect to eigenfunctions of the Laplacian, Sibirsk. *Mat. Zh*., *19*(4), 721-734.

Sh. A. Alimov Joó, I. (1983). On the eigenfunction expansions associated with the Schrodinger operator having spherically symmetrical potential. *Acta Sci. Math. (Szeged), 45*(1), 5-18.

Sh. A. Alimov, Ashurov, R. R., & Pulatov, A. K. (1991). Multiple Fourier series and Fourier integral. *Encyclopaedia of Mathematical Sciences*, *42*, 3-95.

Sobolev, S. L. (1963). *Applications of functional analysis in mathematical physics.* Leningrad: LGU (1950). English translation: Providence, Rhode Island. Am. Math. Soc. 1963 (239 pp.) Zbl. 123,90.

ISSN: 0128-7680
Pertanika J. Sci. & Technol. **19 (S)**: 15 - 22 (2011)

Quantum Markov Chains on a Caylay Tree

Farrukh Mukhamedov
Department of Computational & Theoretical Sciences,
Faculty of Science, International Islamic University Malaysia,
25200 Kuantan, Pahang, Malaysia
E-mail: farrukh_m@iiu.edu.my

ABSTRACT

In the present paper we provide a construction of Quantum Markov chain on a Cayley tree. Moreover, we give a concrete example of such chains, which is shift invariant and has the clustering property.

Keywords: Quantum Markov Chain, Cayey tree

INTRODUCTION

Markov fields play an important role in classical probability, in physics, in biological and neurological models and in an increasing number of technological problems such as image recognition. It is quite natural to forecast that the quantum analogue of these models will also play a relevant role. One of the basic open problems in quantum probability is the construction of a theory of quantum Markov fields, that is quantum Markov processes with a (possibly) multi-dimensional index set. In the papers (Accardi and Fidaleo, 2001;2003; Liebscher, 2001) a first attempts to construct a quantum analogue of classical Markov fields have been done. These papers extend to fields the notion of *quantum Markov state* introduced in Accardi and Frigerio (1983) as a sub–class of the *quantum Markov chains* introduced in Liebscher (2001). Note that in such papers quantum Markov fields were considered over multidimensional integer lattice Z^d. This lattice has so called amenability condition. Therefore, it is natural to investigate quantum Markov fields over non-amenable lattices. One of the simplest non-amenable lattice is a Cayley tree. First attempts to investigate Quantum Markov chains over such trees was done in Dobruschin (1968), such studies were related to investigate thermodynamic limit of valence-bond-solid models on a Cayley tree (Affleck *et al*., 1988). The mentioned considerations naturally suggest the study of the following problem: the extension to fields of the notion of generalized Markov chain.

The present paper is a first step towards the solution of such a problem. We define a notion of Quantum Markov chains over a Cayley tree. Note that in Accardi *et al*. (2007) a more general definition of such chains has been defined. An hierarchy property of the Cayley tree allows us to provide a construction of Quantum Markov chains over a such a tree.

The point is that, as we know from Dobrushin's seminal work (Dobruschin, 1968), the natural localization for fields on a discrete set L is given by the finite subsets of L and their complements. This localization, when restricted to the 1–dimensional case, does not lead to the usual probabilistic localization but, in a certain sense to its *dual* (or *time reversal*), corresponding to the conditioning of the past on the future rather than conversely. This leads to different structures of the Markov

Received: 1 August 2010
Accepted: 22 June 2011

chains in the two cases, a fact already noted in Accardi (1975) where these two types were called *Markov chains* and *inverse Markov chains* respectively.

PRELIMINARIES

In this section, we are going give a construction of Quantum Markov chains over a Cayley tree.

Recall that a Cayley tree Γ^k of order $k \geq 1$ is an infinite tree whose each vertices have exactly $k+1$ edges. If we cut away an edge $\{x, y\}$ of the tree Γ^k, then Γ^k splits into connected components, called semi-infinite trees with roots x and y, which will be denoted respectively by $\Gamma^k(x)$ and $\Gamma^k(y)$. If we cut away from Γ^k the origin O together with all $k+1$ nearest neighbor vertices, in the result we obtain $k+1$ semi-infinite $\Gamma^k(x)$ trees with $x \in S_0 = \{y \in \Gamma^k: d(O, y) = 1\}$.

Hence we have

$$\Gamma^k = \bigcup_{x \in S_0} \Gamma^k(x) \cup \{O\}.$$

Therefore, in the sequel we will consider semi-infinite Cayley tree $\Gamma^k_+ = (L, E)$ with the root x_0. Let us set

$$W_n = \{x \in L: d(x, x_0) = n\}, \Lambda_n = \bigcup_{k=0}^{n} W_k$$
$$E = \{\{x, y\} \in E: x, y \in \Lambda_n\}.$$

Denote

$$S(x) = \{y \in W_{n+1}: d(x, y) = 1\}, x \in W_n,$$

this set is called a set of *direct successors* of x.

From these one can see that

$$\Lambda_m = \Lambda_{m-2} \cup \Big(\bigcup_{x \in W_{m-1}} \{x \cup S(x)\} \Big) \tag{2.1}$$

$$E_m, \quad E_{m-1} = \bigcup_{x \in W_{m-1}} \bigcup_{y \in S(x)} \{\{x, y\}\} \tag{2.2}$$

To each $x \in L$ it is associated an Hilbert space H_x of dimension $d_H(x) \in N$. In the present paper we will assume that $d := d_H(x) = d_H < +\infty$, (independent of x).

Given $\Lambda \subseteq {}_{fin}L$ we define $H_\Lambda := \bigotimes_{x \in \Lambda} H_x$. We will use the notation $B_\Lambda := B(H_\Lambda)$ for each $\Lambda \subseteq {}_{fin}L$ and B_L is the inductive C^*-algebra, that is, $B_L := \varinjlim B_\Lambda$ for $\Lambda \uparrow L$. As a C^*-algebra B_L is isomorphic to the (unique) infinite C^*-tensor product $\otimes_{x \in L} B_x$. In what follows, by $S(B_\Lambda)$ we will denote the set of all states defined on the algebra B_Λ.

Now we are going to introduce a coordinate structure in Γ^k_+. Every vertex x (except for x^0) of Γ^k_+ has coordinates $(i_1,...,i_n)$, here $i_m \in \{1, \ldots, k\}$, $1 \leq m \leq n$ and for the vertex x^0 we put (0). Namely, the symbol (0) constitutes level 0 and the sites $(i_1,...,i_n)$ form level n of the lattice. In this notation for $x \in \Gamma^k_+$, $x = (i_1,...,i_n)$ we have

$$S(x) = \{(x, i): 1 \leq i \leq k\},$$

where (x, i) means that $(i_1,...,i_n,i)$. Then for $1 \le i \le k$, we define a shift γ_i by

$$\gamma_i(x) = (i,x) = (i,i_1,\dots i_n).$$

We can consider such a shift as a shift homomorphism on B_L.

Consider a triplet $C \subset B \subset A$ of unital C^*-algebras. Recall that a *quasi-conditional expectation* with respect to the given triplet is a completely positive identity preserving linear map $E : A \to B$ such that $E(ca) = cE(a)$, $a \in A$, $c \in C$. Notice that, as the quasi-conditional expectation E is a real map, one has $E(ac) = E(a)c$, $a \in A$, $c \in C$ as well.

Definition 2.1. A state ϕ on B_L is called a *Quamtum Markov chain associated* to $\{W_n\}$ if there exist a quasi-conditional expectation E_n with respect to the triple $B_{W_{n-1}} \subset B_{W_n} \subset B_{W_{n+1}}$ for each $n \in N$ and an initial state ρ on B_{W_1} such that

$$\phi = \lim_{n\to\infty} \rho o E_1 o E_2 o L o E_n$$

in the weak-* topology.

CONSTRUCTION OF QUANTUM MARKOV CHAINS

Let be given a positive operator $w_0 \in B_{(0),+}$ and two family of operators $\left\{K_{<x,y>} \in B_{\{x,y\}}\right\}_{\{x,y\}\in E}$, $\left\{h_x \in B_{x,+}\right\}_{x\in L}$ such that

$$\begin{gathered} \mathrm{Tr}(w_0 h_0) = 1 \\ \mathrm{Tr}\left(\prod_{i=1}^{k} K_{<x,(x,i)>} \prod_{i=1}^{k} h_{(x,i)} \prod_{i=1}^{k} K^*_{<x,(x,k+1-i)>}\right) = h_x \end{gathered} \tag{3.1}$$

for every $x \in L$, where $Tr_\Lambda : B_L \to B_\Lambda$ is a normalized partial trace for any $\Lambda \subseteq_{fin} L$ and $\mathrm{T_r}$ is a normalized trace on B_L.

Denote

$$K_n = w_0^{1/2} \prod_{\{x,y\}\in E_1} K_{<x,y>} \prod_{\{x,y\}\in E_2,E_1} K_{<x,y>} L \prod_{\{x,y\}\in E_n,E_{n-1}} K_{<x,y>} \prod_{x\in W_n} h_x^{1/2}, \tag{3.2}$$

where by definition we put

$$\prod_{\{x,y\}\in E_m,E_{m-1}} K_{<x,y>} := \prod_{x\in W_n} \prod_{i=1}^{k} K_{<x,(x,i)>} \tag{3.3}$$

Now define $W_{n]} = K_n K_n^*$. It is clear that $W_{n]}$ is positive. Recall that a sequence $\{W_{n]}\}$ is *projective* with respect to $\mathrm{Tr}_{n]} = \mathrm{Tr}_{\Lambda_n}$ if

$$\mathrm{Tr}_{n-1]}(W_{n]}) = W_{n-1]}$$

is valid for all $n \in N$.

Theorem 3.1 Let (3.1) be satisfied. Then $\{W_{n]}\}$ is a projective sequences of density operators.
Proof. From (3.2) one has

$$W_{n]} = w_0^{1/2} \prod_{m-1}^{n-1} \left(\prod_{\{x,y\} \in E_m, E_{m-1}} K_{<x,y>} \right) \prod_{\{x,y\} \in E_n, E_{n-1}} K_{<x,y>}$$
$$\prod_{x \in W_n} h_x \left(\prod_{\{x,y\} \in E_n, E_{n-1}} K_{<x,y>} \right)^* \prod_{m-1}^{n-1} \left(\prod_{\{x,y\} \in E_{n-m}, E_{n-m-1}} K_{<x,y>} \right)^* w_0^{1/2}.$$

We know that for different x and x' taken from W_{n-1} the algebras $B_{x \cup S(x)}$ and $B_{x' \cup S(x')}$ commute, therefore from (3.3) one finds

$$\prod_{\{x,y\} \in E_n, E_{n-1}} K_{<x,y>} \prod_{x \in W_n} h_x \left(\prod_{\{x,y\} \in E_n, E_{n-1}} K_{<x,y>} \right)^* = \prod_{x \in W_n} \prod_{i=1}^{k} K_{<x,(x,i)>} \prod_{i=1}^{k} h_{(x,i)} \prod_{i=1}^{k} K^*_{<x,(x,k+1-i)>^*}$$

Hence from the condition (3.1) we find

$$\begin{aligned} Tr_{n]}(W_{n]}) &= w_0^{1/2} \prod_{m-1}^{n-1} \left(\prod_{\{x,y\} \in E_m, E_{m-1}} K_{<x,y>} \right) \\ &\times \prod_{x \in W_{n-1}} Tr_x \left(\prod_{i=1}^{k} K_{<x,(x,i)>} \prod_{i=1}^{k} h_{(x,i)} \prod_{i=1}^{k} K^*_{<x,(x,k+1-i)>} \right) \\ &\times \prod_{m-1}^{n-1} \left(\prod_{\{x,y\} \in E_{n-m}, E_{n-m-1}} K_{<x,y>} \right)^* w_0^{1/2} \\ &= w_0^{1/2} \prod_{m-1}^{n-1} \left(\prod_{\{x,y\} \in E_m, E_{m-1}} K_{<x,y>} \right) \times \prod_{x \in W_{n-1}} h_x \left(\prod_{\{x,y\} \in E_{n-m}, E_{n-m-1}} K_{<x,y>} \right)^* w_0^{1/2} \\ &= W_{n-1]} \end{aligned}$$

Similarly, from (3.1), one can show that $W_{n]}$ is density operator, i.e. $\mathrm{Tr}(W_{n]}) = 1$.
Define a state on B_{Λ_n} by

$$\phi(x) = \mathrm{Tr}(W_{n+1]} x), x \in B_{\Lambda_n}$$

Assume that h_x is invertible for all $x \in L$ and define

$$E_n(a) = \mathrm{Tr}_{n]} \left(\prod_{x \in W_n} h_x^{-1/2} \prod_{\{x,y\} \in E_{n+1}, E_n} K_{<x,y>} \prod_{x \in W_{n+1}} h_x^{-1/2} a \times \prod_{x \in W_{n+1}} h_x^{-1/2} \left(\prod_{\{x,y\} \in E_{n+1}, E_n} K_{<x,y>} \right)^* \prod_{x \in W_n} h_x^{-1/2} \right)$$

for each $n \geq 0$ and $a \in B_{\Lambda_{n+1}}$. Similar to the above proof, we get that E_n is a quasi-conditional expectation with respect to the triple $B_{W_{n-1}} \subset B_{W_n} \subset B_{W_{n+1}}$. One can see that

$$\phi_n(a) = \mathrm{Tr}(h_0^{1/2} w_0 h_0^{1/2} E_0 \circ E_1 \circ L \circ E_{n-1} \circ E_n(a)).$$

Therefore, according to Theorem 3.1 we can define a Quantum Markov chain on B_L by $\phi = \lim \phi_n$ in the weak-* topology.

If $h_x = h$ and $K_{<x,y>} = K$, for all $x \in L$ and $\{x, y\} \in E$, and w_0 satisfies the initial condition

$$\mathrm{Tr}_{(i)} = \left(w_0 \prod_{j=i}^{k} K_{<0,j>} \prod_{j=i}^{k} h_j \left(\prod_{j=i}^{k} K_{<0,j>} \right)^* \right) = h_i^{1/2} w_0 h_i^{1/2},$$

ϕ is shift-invariant for γ_i. Indeed, from the last equality we have

$$\mathrm{Tr}\left(h_0^{1/2} w_0 h_0^{1/2} E_0(\,\cdot\,)\right) = \mathrm{Tr}\left(h_i^{1/2} w_i h_i^{1/2} \cdot\right)$$

on B_i, hence

$$\begin{aligned}\phi_n\left(\gamma^i(a)\right) = \mathrm{Tr}\big(&h_i^{1/2} w_i h_i^{1/2} E_1 \circ E_2 \circ L \circ E_{n-1} \circ E_n\left(\gamma^j(a)\right)\big)\\ &\mathrm{Tr}\left(h_0^{1/2} w_0 h_0^{1/2} E_0 \circ E_1 \circ L \circ E_{n-2} \circ E_{n-1}(a)\right)\\ &\phi(a)\end{aligned}$$

for all $a \in B_{\Lambda_{n-1}}$. In the third equation, we use $h_0 = h_1 = h$ and $K_{<x,y>} = K$. Furthermore, the γ_i invariant Quantum Markov chain ϕ satisfies clustering property for γ_i if

$$\lim_{n\to\infty} \phi\left(a\gamma_i^n(b)\right) = \phi(a)\phi(b).$$

AN EXAMPLE

In this section, we provide more concrete examples of Quantum Markov chains on a Cayley tree. For the sake of simplicity we consider a semi-infinite Cayley tree $\Gamma_+^2 = (L, E)$ of order 2. Our starting C^*-algebra is the same B_L but with $B_x = M_2(C)$ for $x \in L$. By $e_{ij}^{(x)}$ we denote the standard matrix units of $B_x = M_2(C)$.

For every edge $\{x, y\} \in E$ put

$$K_{<x,y>} = \exp\{\beta H_{<x,y>}\}, B \in R \tag{4.1}$$

where

$$H_{<x,y>} = e_{12}^{(x)} \otimes e_{21}^{(y)} + e_{21}^{(x)} \otimes e_{12}^{(y)}. \tag{4.2}$$

Now we are going to find a solution $\{h_x\}$ and w_0 of equations (3.1) for the defined $\{K_{<x,y>}\}$. Note that from (4.1),(4.2) for every $K_{<x,y>}$ one can see that

$$K_{<x,y>} = K_{<x,y>}^* \tag{4.3}$$

for all $\{x, y\} \in E$.

Assume that $h = \alpha I$ for every $x \in V$. Hence, thanks to (1.3), the equations (3.1) can be rewritten as follows

$$\begin{aligned}&\alpha \mathrm{Tr}_0(w_0) = 1\\ &\alpha^2 \mathrm{Tr}_x\left(K_{<x,(x,1)>} K_{<x,(x,2)>}^2 K_{<x,(x,1)>}\right) = \alpha I,\end{aligned}$$

for every $x \in L$.

One can see that

$$\begin{aligned}H_{<x,y>}^{2n} &= H_{<x,y>}^2 = e_{11}^{(x)} \otimes e_{22}^{(x)} + e_{22}^{(x)} \otimes e_{11}^{(x)}\\ H_{<x,y>}^{2n-1} &= H_{<x,y>}\end{aligned}$$

for every $n \in N$. Then we get

$$K^2_{<x,y>} = I + (\sinh 2\beta)H_{<x,y>} + (\cosh 2\beta - 1)H^2_{<x,y>}$$

$$\mathrm{Tr}_x(K^2_{<x,y>}) = \frac{\cosh 2\beta + 1}{2} I = \cosh^2 \beta I$$

for every $\{x, y\} \in E$. Hence, for $x \in L$ and $y, z \in S(x)$, one finds

$$\begin{aligned}\mathrm{Tr}_x(K_{<x,y>}, K^2_{<x,z>}, K_{<x,y>}) &= \mathrm{Tr}_x(K_{<x,y>}\mathrm{Tr}_{xy}(K^2_{<x,z>})K_{<x,y>}) \\ &= (\cosh^4 \beta) I.\end{aligned}$$

Therefore we obtain $\alpha = \cosh^{-4}\beta$ and $\mathrm{Tr}(w) = \cosh^4 \beta$. Next, consider the initial condition (3.1). Since

$$\mathrm{Tr}_1(w_0 K_{<0,1>}, K^2_{<0,2>}, K_{<0,1>}) = (\cosh^2 \beta)\mathrm{Tr}_1(w_0 K^2_{<0,1>}),$$

by putting $w_0 = \sum_{i,j=1,2} a_{ij} e^0_{ij}$, we have

$$\begin{aligned}&\mathrm{Tr}_1(w_0 K_{<0,1>}, K^2_{<0,2>}, K_{<0,1>}) = \frac{\cosh^2 \beta}{2} \\ &\times((a_{11} + a_{22})I + (\cosh 2\beta - 1)(a_{11}e_{22} + a_{22}e_{11}) + (\sin 2\beta)(a_{12}e_{12} + a_{21}e_{21}))\end{aligned}$$

Therefore we have the solution $w_0 = I$. Therefore, ϕ generated by the above notations is γ_1-invariant d-Markov chain. Similary, it is easily seen that ϕ is also γ_2-invariant. Finally we show the clustering property.

Theorem 4.1. A state ϕ generated by the above notations satisfies clustering property w.r.t. γ_1.

Proof. To show the clustering property, it is enough to prove for any $a \in B_0 = M_2(C)$

$$\lim_{n\to\infty} E_0 \circ E_1 \circ L \circ E_{n-1} \circ E_n(\gamma_1^{n+1}(a)) = \phi(a) I.$$

Indeed, for $a, b \in B_0$, we have

$$\begin{aligned}\lim_{n\to\infty} \phi(\gamma_1^n(a)b) &= \lim_{n\to\infty} \mathrm{Tr}(h_0^{1/2} w_0 h_0^{1/2} E_0(E_1 \circ L \circ E_{n-1} \circ E_n(\gamma_1^{n+1}(a))b)) \\ &= \phi(a)\mathrm{Tr}(h_0^{1/2} w_0 h_0^{1/2} E_0(b)) \\ &= \phi(a)\phi(b).\end{aligned}$$

Assume $\gamma_1^{n+1}(a) \in B_y$ and $y, z \in S(x)$, then essentialy, we can restrict E_n to $E_n \mid B_{x,y,z}$. From a simple calculation, we have

$$\begin{aligned}\mathrm{Tr}_x(K_{<x,y>}K_{<x,z>}e^{(y)}_{11}K_{<x,z>}K_{<x,y>}) &= (\cosh^2 \beta) \times \mathrm{Tr}_x(K_{<x,y>}e^{(y)}_{11}K_{<x,y>}) \\ &= \frac{\cosh^4 \beta}{2} I.\end{aligned}$$

Similary, we get

$$\mathrm{Tr}_x\left(K_{<x,y>}K_{<x,z>}e_{22}^{(y)}K_{<x,z>}K_{<x,y>}\right) = \frac{\cosh^4\beta}{2}I,$$
$$\mathrm{Tr}_x\left(K_{<x,y>}K_{<x,z>}e_{12}^{(y)}K_{<x,z>}K_{<x,y>}\right) = \cosh^2\beta\sinh 2\beta e_{12}^{(x)},$$
$$\mathrm{Tr}_x\left(K_{<x,y>}K_{<x,z>}e_{21}^{(y)}K_{<x,z>}K_{<x,y>}\right) = \cosh^2\beta\sinh 2\beta e_{21}^{(x)}.$$

Therefore, we obtain that

$$\lim_{n\to\infty} E_0 \circ E_1 \circ L \circ E_{n-1} \circ E_n\left(\gamma_1^{n+1}(a)\right) = \mathrm{Tr}(a) = \phi(a)I$$

which implies the assertion. Similarly, one can prove that ϕ satisfies clustering property w.r.t. γ_2.

CONCLUSIONS

Let us note that a first attempt of consideration of quantum Markov fields began in Accardi and Fidaleo (2001; 2003) for the regular lattices (namely for Z^d). But there, concrete examples of such fields were not given. In the present paper we have defined a notion of Quantum Markov chain to fields, i.e. to Cayley trees. Note that such a tree is the simplest hierarchical lattice with *non-amenable* graph structure. This means that the ratio of the number of boundary sites to the number of interior sites of the tree tends to a nonzero constant in the thermodynamic limit of a large system, i.e. the ratio W_n/V_n tends to $(k-1)/(k+1)$ as $n \to \infty$, where k is the order of the tree. Here quantum Markov chains have been considered on discrete infinite tensor products of C^*–algebras over trees. A tree structure allowed us to give a construction of quantum Markov chains. We provided a concrete example of such chains, which are shift invariant and have the clustering property. Note that Quantum Markov chains describe ground states of quantum systems over trees. Certain particular examples of such systems were considered in (Affleck *et al*., 1988; Fannes *et al*., 1992).

ACKNOWLEDGEMENTS

The author thanks the MOHE grant FRGS0308-91.

REFERENCES

Accardi, L. (1975). On the noncommutative Markov property. *Func. Anal. Appl.*, *9*, 1-8.

Accardi, L., & Fidaleo, F. (2001). On the structure of quantum Markov fields. In W. Freudenberg (Ed.), *World Scientific, QP–PQ Series 2003*, *15*, 1-20. *Proceedings Burg Conference,* 15-20 March 2001.

Accardi, L., & Fidaleo, F. (2003). Quantum Markov fields, Inf. Dim. Analysis, Quantum Probab. *Related Topics*, *6*, 123-138.

Accardi L., Fidaleo F., & Mukhamedov, F. (2007). Markov states and chains on the CAR algebra, Inf. Dim. Analysis, Quantum Probab. *Related Topics*, *10*, 165-183.

Accardi, L., & Frigerio, A. (1983). Markovian cocycles. *Proc. Royal Irish Acad., 83A*, 251-263.

Affleck, L., Kennedy, E., Lieb, E. H., & Tasaki, H. (1988). Valence bond ground states in isortopic quantum antiferromagnets. *Commun. Math. Phys.*, *115*, 477-528.

Dobrushin, R. L. (1968). Description of Gibbsian random fields by means of conditional probabilities. *Probability Theory and Applications*, *13*, 201-229.

Fannes, M., Nachtergaele, B., & Werner, R. F. (1992). Ground states of VBS models on Cayley trees. *J. Stat. Phys*., *66*, 939-973.

Liebscher, V. (2003). Markovianity of quantum random fields. In W. Freudenberg (Ed.), *World Scientific*, *QP–PQ Series, 15*, 151-159. *Proceedings Burg Conference,* 15-20 March 2001.

ISSN: 0128-7680
Pertanika J. Sci. & Technol. **19 (S)**: 23 - 30 (2011)

A Review of Property Mass Valuation Models

Ebrahim Jahanshiri*, Taher Buyong and Abdul Rashid Mohd. Shariff
Spatial and Numerical Modeling Laboratory,
Institute of Advanced Technology, Universiti Putra Malaysia,
43400 UPM, Serdang, Selangor, Malaysia
**E-mail: e.jahanshiri@gmail.com*

ABSTRACT

Mass valuation of properties is important for purposes like property tax, price indices construction, and understanding market dynamics. There are several ways that the mass valuation can be carried out. This paper reviews the conventional MRA and several other advanced methods such as SAR, Kriging, GWR, and MWR. SAR and Kriging are good for modeling spatial dependence while GWR and MWR are good for modeling spatial heterogeneity. The difference between SAR and Kriging is the calculation of weights. Kriging weights are based on the spatial dependence or so called the semi-variogram analysis of the price data whereas the weights in SAR are based on the spatial contiguity between the sample data. MWR and GWR are special types of regression where study region is subdivided into local sections to increase the accuracy of prediction through neutralizing the heterogeneity of autocorrelations. MWR assigns equal weights for observations within a window while GWR uses distance decay functions. The merits and drawbacks of each method are discussed.

Keywords: Spatial prediction, property price indices, spatial econometrics

INTRODUCTION

For long, it has been a problem to assess property values accurately. Assessors and appraisers are known to be able to estimate values of properties through their accumulated knowledge. However, the challenges are (i) the accuracy and consistency of these valuations that refers to the weights that appraiser gives to specify the quality of the appraised value, and (ii) the speed of which the appraising process can take place. Correct and up-to-date assessment of property values is not only important to owners of the properties and real estate agencies but also to the local governments whom must define the taxes to be imposed on the properties based on their values. It is also a requirement that property values must be regularly updated in order for the taxes to be accurate and fair.

Over the past decades, property valuation has evolved from simple empirical judgments to automated valuation models and their applications have extended from single property to mass valuation (Clapp, 2003). Manual methods of expert valuation although effective, are subjective, inconsistent, and prone to errors (Adair and McGreal, 1988; Benjamin *et al*., 2004). For large jurisdictions that encompass thousands or millions of properties, manual valuation if possible, is time consuming. Therefore, automated valuation models are invented to solve for these types of problems. Automated valuation models consist of a database of property values and their characteristics and, current transactions of the properties, in a region of interest. The second major part of automated valuation models is the statistical method that is used to estimate property prices. The third part is the output and graphical user interface to do the communication and visualization of the output

Received: 1 August 2010
Accepted: 22 June 2011
*Corresponding Author

of the models. The methods of mass property valuation for so long have been confined to sales comparison method and Multiple Regression Analysis (MRA). However, apparent deficiencies of these methods have been the motivation for the usage of body of methods that are invented and borrowed from other disciplines to increase the accuracy of valuation. Improved accuracy of the new methods is possible by explaining parts of error of regression through consideration of the spatial autocorrelation and spatial heterogeneity. These effects are materialized when there is influence in terms of human communication and market demands on the property prices. Currently, these new methods are divided into two main sections that either deal with spatial autocorrelation or spatial heterogeneity. Both of these streams have their own sound theoretical basis although they may need to be merged to be more effective. A few methods like moving window kriging tries to deal with both of these effects. This paper aims to provide a review on methods of mass valuation and their improvements in the spatial domain that have been made in recent years. The composition of the paper is as follows: Section two provides the taxonomy of property mass valuation methods. Section three presents MRA, the de facto standard of mass appraisal model. Section four discusses models for spatial regression and prediction which includes spatial autoregressive models, geostatistical models, and local models. Section five provides future research directions and Section six concludes the paper by highlighting the important points.

TAXONOMY OF MASS VALUATION METHODS

MRA model is the de facto standard for mass valuation of properties. The model originated from non spatial discipline did not address peculiarities of spatial data like property data. Several other models emerge that largely aim to modify the MRA model to take care of spatial effects. The spatial econometrics research contributed the global Spatial AutoRegressive (SAR) models. These models are known as the Spatial Lag Model (SLM). Spatial Error Model (SEM), General Spatial Model, and Spatial Durbin Model (SDM). The geographic research contributed local models of Geographically Weighted Regression (GWR) and Moving Window Regression (MWR). The geostatistics research contributed the various kriging models including Regression Kriging (RK) and Moving Window Kriging (MWK). *Fig. 1* shows the taxonomy of mass valuation models.

MULTIPLE REGRESSION ANALYSIS (MRA)

MRA is a statistical methodology that utilizes the relationship between two or more independent variables (characteristics of properties like size of living area, number of bedrooms, number of bathroom, and so on) and a dependent variable (price of properties). The dependent and independent variables are regressed using properties of known prices to determine the established relationships (coefficients) between the two types of variables (Adair and McGreal, 1988). The determined coefficients are then used for the prediction of prices of unsold properties in the same stock. MRA determines the coefficients with the least possible error (Benjamin *et al*., 2004) using the Ordinary Least Squares (OLS), maximum likelihood (ML), or Weighted Least Squares (WLS) estimation techniques with OLS being the most popular (Ambrose, 1990; Beach and MacKinnon, 1978). The OLS method minimizes the sum of square of residuals or errors. The regression coefficients that are derived based on OLS shall be best linear unbiased estimator (BLUE).

However, there are some drawbacks on the use of MRA in property valuation relating to spatial autocorrelation and heteroscedasticity, the two spatial effects inherent in property data (Mark and Goldberg, 1988; Fletcher *et al*., 2000). Spatial autocorrelation means that the residuals are spatially correlated; off diagonal elements of the variance-covariance matrix of the estimated residuals deviate from zero indicating that the two observations that define the elements are spatially correlated.

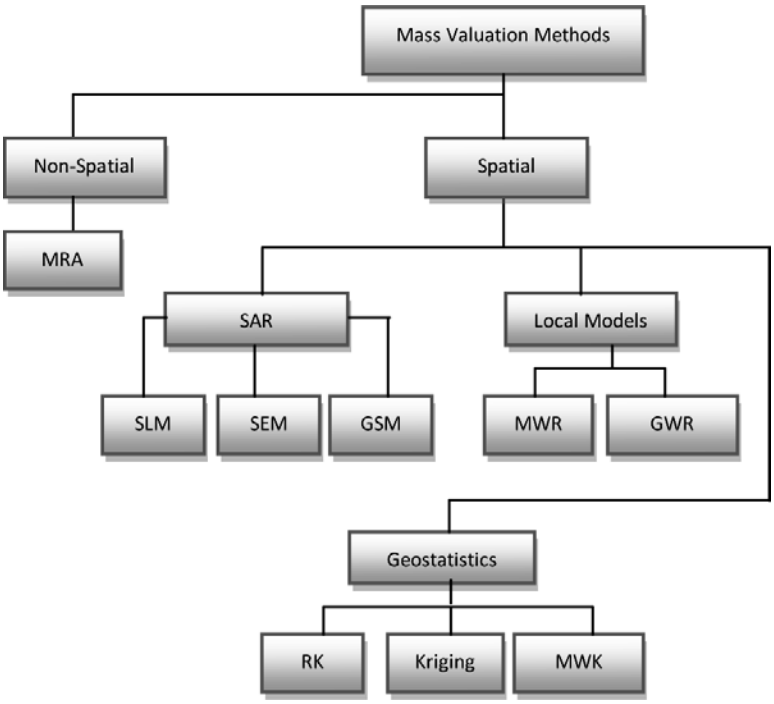

Fig. 1: Mass valuation models

Spatial autocorrelation is the result poor of specification of the regression model which may be due to incomplete or missing spatial variables that accounted spatial dependence and spatial heterogeneity in property data. The inclusion of spatial variables makes the models more complete from the point of view of regressing spatial phenomena. Unaccounted spatial dependence and spatial heterogeneity also makes the residuals deviate from normal distribution. Heteroscedasticity is partly due to spatial dependence and heterogeneity, and partly due to non-spatial reasons. It is difficult to separate the effects but accounting for spatial dependence and heterogeneity may reduce heteroscedasticity.

Varieties of ways are available for assessing the presence of spatially correlated residuals and heteroscedasticity (Belsley *et al*., 2004). Spatially autocorrelated residuals and heteroscedasticity violate the presumption of OLS that the residuals must be uncorrelated and normally distributed with zero mean and constant variance, i.e., $e \sim N(0, \sigma^2 I)$. This makes the OLS estimated coefficients biased and unsuitable for inference. The ending effect is that the predicted property prices are unreliable.

Appraisal communities in the developed and developing countries have realized the power of computerized mass appraisal and statistical methodology. MRA technique, given its medium accuracy, flexibility, and ease of use is the preferred method that is embedded into the valuation systems especially for tax purposes (Tretton, 2007).

SPATIAL REGRESSION AND PREDICTION

The major reason for the low predictive capability of the MRA is ignoring spatial dependence and spatial heterogeneity. Spatial dependence can be seen when we consider that not only the price of a property is influenced by the prices of the surrounding properties but the characteristics of a property

are also influenced by the characteristics of surrounding properties. Spatial heterogeneity can be seen when unit price of land varies from urban to suburban, to rural areas, across a region of interest. Regression methods have advance to incorporate spatial effects. It was shown that regression errors can be reduced and consequently increasing its predictive capability by adding independent variables describing the spatial characteristics of the properties like in spatial autoregressive models or devising a regression procedure to capture spatial heterogeneity like in local models (Paez *et al*., 2008; Buyong and Valivalo, 2010; Fotheringham *et al*., 2002). On the other hand, spatial dependence in property prices is exploited in the prediction of the prices in the method of geostatistical kriging (Gallimore *et al*., 1996; Bonrassa *et al*., 2003; McCluskey and Borst, 2007). We will discuss these advances in the following subsections.

Spatial Autoregressive Models

Spatial AutoRegressive (SAR) models, also called spatial models is a group of models that improves the accuracy of property price prediction of the MRA model by incorporating spatial dependence of properties in the functional model. The spatial dependence parameters are estimated along with the regression coefficients. First is the Spatial Lag Model (SLM) that models the dependency of property prices; the price of a property is dependent on the prices of its neighboring properties. Second is the Spatial Error Model (SEM) that models the spatial dependence of the error terms; an error induced by a property is dependent on the error of nearby properties. Third is the General Spatial Model (GSM) that model both the dependence of prices and errors of neighboring properties; it combines the SLM and SEM into one model. Last is the Spatial Durbin Model (SDM) that models the dependency neighboring property characteristics (Militino *et al*., 2004; Anselin, 1988; Anselin and Bera, 1998; Anselin and Lozano-Gracia, 2009). When spatial dependence are explicitly modeled, the model specifications are more complete and thus, are able to produce more accurate prediction (Ismail *et al*., 2008; Cohen and Coughlin, 2008).

SAR models incorporate spatial weight matrices that are based on the concept of spatial neighbors. Two most commonly used strategies to define spatial neighbors are Delaunay triangulation and *k* nearest neighbors when properties are represented by their centroids. Properties that are spatial neighbors to a subject property receive the value of one while those that are not spatial neighbors receive zero values. It is normal to try various values of *k* until satisfactory results are obtained when the *k* nearest neighbors strategy is used. When the rows and columns of the weight matrix arranged such that the subject property is at the main diagonal, the weight matrices are usually sparse and banded. Literature regarding the application of these models in the property price valuation shows improvement in the property price prediction.

Geostatistical Kriging

Geostatistical kriging is another technique to deal with the spatial autocorrelation. This technique does not fall into the category of regression models since it primarily deals with the property prices and tries to predict the price of unsold properties using the spatial relationship between the prices of sold properties. The spatial autocorrelation first needs to be rectified through a process called variography and then the information that is derived from the variography of the price data will be used to form simultaneous equations or kriging system to determine the price of unsold properties. Variography starts with calculating the differences or semi-variances between all pairs of data that are a specific distance apart. By plotting the semi-variances against different distances and modeling these relationships, we can estimate the degree of relationship (or differences to be more exact) in entire region and therefore we can use this information to predict the price of any unsold property (Chica-Olmo, 2007).

The method of geostatistical kriging has some drawbacks. First, although it gives more weight to the surrounding points, it is a global method, that is, like the MRA, it uses the entire dataset to predict the price of unsold properties while as we have mentioned in Section I, the nature and degree of spatial dependence is different in different parts of the region. To tackle this problem, the method of moving window kriging is used so that for any unsold property, we will use the spatial dependence information only in that specific window rather than the global information. Beside prices, there is other property characteristic information available. The method of co-kriging uses other important highly correlated property characteristics in the neighboring properties to predict the price of the unsold property. This method is theoretically sound since the price of a property is not only influenced by the prices of its neighboring properties but also by the characteristics of the neighboring properties. This method adds more difficulty in computational aspects because the spatial dependence information now comes from more than one variable across the region. Co-kriging, however, ignores the characteristics of the unsold property that its price is going to be predicted which can be seen as a drawback of the method. Normally, cokriging is used in the situations where the secondary variables (property characteristics) are observed less sparsely than the primary variables (property prices) which seldom happen in property data.

To deal with this problem, another method called regression kriging (RK) is used that is based on the simple MRA model but with added spatial dependence information. Regression kriging that is usually used in the literature (Dubin, 1999; 2003; Anselin *et al*., 2004) takes the residuals of simple MRA method and performs a kriging on them so that for each unsold property there will be a predicted error. This error will then be added back to the MRA analysis and then price will be calculated for that specific property using its own property characteristics (independent variables). Variations of this method could be invented using the spatial lag or spatial Durbin models.

Local Models

Spatial heterogeneity plays a major role in modeling spatial phenomena because spatial heterogeneity might be more important than the spatial dependence especially in modeling property prices. Local models have been developed to capture spatial heterogeneity; the MRA model is repeatedly regressed in several smaller areas until the region of interest is covered. If the nature of the spatial relationships is different at different places in a study region, we can estimate the coefficients and then do the prediction locally such that the determined relationships are confined in the well defined neighborhoods, called windows.

The windows of local models can be of various forms, shapes, and sizes. The most convenient for property price modeling, however, is windows of irregular-shaped boundaries with varying sizes depending on the distribution of neighboring properties to be included in the windows.

Regression windows may be centered at data points (sold houses) or non-data points (unsold houses). If data points are a lot less, as usually happen in property price modeling, it might be better to center regression windows at data points because of less total computer regression time; If regression windows are centered at non-data points, the advantage occurs during prediction; the center of regression windows, being non-data points, can be predicted directly using the determined coefficients. It is not possible to do this if regressions are centered at data points. Extra work is required to determine in which regression window a predicted point lies and use coefficients of that window in the prediction. A weighted mean is required if the predicted point falls in more than one regression window. In property price modeling, we are convinced that centering regression windows at data points is a better deal.

Window regressions necessitate the use of a subset of data points for each window where these points are the closest to the center of regressions. The issue is how many data points to be considered. If spatial heterogeneity exists in a strict sense in a region of interest, each observation

should have a different value of coefficients and a global MRA model produces biased estimated coefficient. Local models reduce this biasness and require the coefficients to be the same for all observations in each window; coefficient values between local areas may vary. This can be achieved by considering observations very close to the regression points. This option, even though produces estimated coefficients with small bias, reduces the effective sample size producing coefficients with large variances and thus unreliable. Considering observations far from regression points may produce estimated coefficients with small variances and increasing reliability but with increasing bias. In line with the bias-variance trade-off is the issue of prediction accuracy. Too few observations produce prediction of lower accuracy but too many observations do not necessarily increase the accuracy of prediction significantly. The bias-variance trade-off in estimation and accuracy in prediction in local models must be effectively handled. We would like to use the optimum number of data points for each window to solve these issues. For the moment, the criterion is the accuracy of prediction and the most widely used strategy is the cross validation; it determines the optimum number of neighboring data points to be included in a regression.

Local models produced *k* sets of coefficients where *k* is the number of regression windows. As a result, local models make local statistics such as local R^2, local Moran, etc. to be available naturally. The *k* sets of coefficients also allow continuous map of coefficients to be made so that the dynamics of regression coefficients can be seen. Local models are mostly appraised in the literature for their ability to prove the non-stationarity of property prices because the different relationships in different parts of a region can be proved through mapping of regression coefficients in the region.

Geographically Weighted Regression

Geographically Weighted Regression (GWR) is the most popular local models. At each regression window, only a subset of observations nearest to the regression point enters the regression and these observations are weighted according to some distance decay functions. Observations near the regression point receive higher weight while observations further from regression point receive lower weight. Due to unequal weighting of observations, the WLS estimation is used instead of the OLS.

Moving Window Regression

Moving Window Regression (MWR) is another version of local models. The only difference between GWR and MWR is in the way weights are assigned to observations that are included in regression windows. Unlike in GWR, all observations that are included in regression windows are weighted equally in MWR. This is to say that observations will influence the subject property by the same amount no matter how far they are from the subject property. This weighting strategy makes MWR loses out to GWR because it contradicts to the theory of spatial dependence and thus make MWR less popular compared to GWR. On the other hand, MWR is simpler to implement because it uses OLS estimation due to equal weighting of observations.

FUTURE DIRECTIONS

Past research segregated spatial dependence and spatial heterogeneity in the effort to produce more accurate prediction. Since spatial effects in inherent in property data comprise both spatial dependence and heterogeneity, future research should focus on the combination of both effects on increasing the capacity of the error reduction in regression analyses.

The focus of spatial autoregressive, local and geostatistical models is primarily on the spatial domain. We know very well that property data have both the spatial dimension and time dimension. The interaction of the time and space on property data cannot be underestimated. Such effects

which are called spatiotemporal effects are now being investigated and their feasibility in property price modeling are considered by the researchers. Another trend of research is on the usage of the time based geostatistics or soft geostatistics and model based geostatistics that uses the Bayesian approaches for the increase of prediction accuracy. The Bayesian approaches in the regression analysis are also being used more frequently in the literature.

Another major research area is on the software development for the ease of conduct of the appraisal using thousands of transaction data that are now being increasingly accessible to valuation professionals. Software platforms like R system and Geoda framework have readymade sections for the development of the spatial weight matrices that could used by the other proprietary and non proprietary software (Anselin *et al*., 2004).

CONCLUSIONS

Speed, consistency, and accuracy of mass valuation are now a demand that appraisal communities are challenged with. Using the traditional method of MRA will result in high margin of error and therefore for most cases is unreliable. MRA however provides a benchmark on top of which other methods are built and tested. Most common problems associated with simple MRA are ignorance of spatial effects in the model. Spatial dependence which is the influence of near properties on each other is important and should be somehow considered in MRA. The nature of these effects is not the same everywhere however and this difference will create spatial variability, spatial heterogeneity, or market segmentation. The gust of all of the spatial models is to increase the influence of nearest neighbors or prevention of farthest neighbors to influence the prediction for unsold property. Spatial models aim to improve MRA by adding spatial dependence components to the formula using the connectivity weights either in the response variable (SLM) or error terms of regression (SEM). Geostatistical kriging aims to introduce a new type of prediction using the information inherent to the geographical distribution of price or its relation to the property characteristics of nearest neighbors. Local models try to segmentize the region based on specific windows and predicting for the unsold property based on those windows. The method of MWR gives equal weight to the neighbors influencing a subject property in the windows while GWR imposes spatially varying weights that more closely resembles the data generating process. GWR is useful for ascertaining the degree of spatial heterogeneity in the area.

REFERENCES

Adair, A., & McGreal, S. (1988). The application of multiple regression analysis in property valuation. *Journal of Property Valuation and Investment*, *6*, 57-67.

Ambrose, B. (1990). An analysis of the factors affecting light industrial property valuation. *Journal of Real Estate Research*, *5*, 355-70.

Anselin, L. (1988). *Spatial econometrics: Methods and models*. Springer.

Anselin, L., & Bera, A. (1998). Spatial dependence in linear regression models with an introduction to spatial econometrics. *Handbook of Applied Economic Statistics*, *155*, 1998.

Anselin, L., Ibnu, S., & Kho, Y. (2004). GeoDa: An introduction to spatial data analysis. *Geographical Analysis*, *38*, 5-22.

Anselin, L., & Lozano-Gracia, N. (2009). Spatial Hedonic Models *K. Patterson*, 2009.

Beach, C. M., & MacKinnon, J. G. (1978). A maximum likelihood procedure for regression with autocorrelated errors. *Econometrica*, *46*(Jan. 1978), 51-58.

Belsley, D. A., Kuh, E., & Welsch, R. E. (2004). *Regression diagnostics: Identifying influential data and sources of collinearity*. Wiley-IEEE.

Benjamin, J. D., Guttery, R. S., & Sirmans, C. F. (2004). Mass appraisal: An introduction to multiple regression analysis for real estate valuation. *Journal of Real Estate Practice and Education*, *7*, 65-77.

Brasington, D. M., & Hite, D. (2005). Demand for environmental quality: A spatial hedonic analysis. *Regional Science and Urban Economics*, *35*, 57-82.

Bourassa, S .C., Hoesli, M., & Peng, V. S. (2003). Do housing submarkets really matter? *Journal of Housing Economics*, *12*, 12-28.

Buyong, T., & Valivalo, S. (2010). Modeling residential property prices using geographically weighted regression. *Pacific Rim Property Research Journal, 2010.*

Chica-Olmo, J. (2007). Prediction of housing location price by a multivariate spatial method: Cokriging. *Journal of Real Estate Research*, *29*, 92.

Clapp, J. M. (2003). A semiparametric method for valuing residential locations: Application to automated valuation. *The Journal of Real Estate Finance and Economics*, *27*(Nov. 2003), 303-320.

Cohen, J. P., & Coughlin, C. C. (2008). Spatial hedonic models of airport noise, proximity, and housing prices. *Journal of Regional Science*, *48*, 859-878.

Dubin, R. (1988). Spatial autocorrelation. *Review of Economics and Statistics*, *70*.

Dubin, R. (2003). Robustness of spatial autocorrelation specifications: Some Monte Carlo evidence. *Journal of Regional Science*, *43*, 221-248.

Dubin, R., Pace, R. K., & Thibodeau, T. G. (1999). Spatial autoregression techniques for real estate data. *Journal of Real Estate Literature*, *7*, 79-96.

Fletcher, M., Gallimore, P., & Mangan, J. (2000). Heteroscedasticity in hedonic house price models. *Journal of Property Research*, *17*, 93-108.

Fotheringham, A. S., & Brunsdon, C., & Charlton, M. (2002). *Geographically weighted regression: The analysis of spatially varying relationships*. Wiley.

Gallimore, P., Fletcher, M., & Carter, M. (1996). Modelling the influence of location on value. *Journal of Property Valuation and Investment*, *14*, 6-19.

Ismail, S., Buyong, T., Sipan, I., Hashim, M. G., & Navaneethan, R. (2008). Spatial Hedonic Modelling (SHM) for mass valuation. *International Real Estate Research Symposium (IRERS)*. Kuala Lumpur, Malaysia.

Mark, J., & Goldberg, M. (1988). Multiple regression analysis and mass assessment: A review of the issues. *Appraisal Journal*, *56*, 89-109.

McCluskey, W. J., & Borst, R. A. (2007). Specifying the effect of location in multivariate valuation models for residential properties. *Property Management*, *25*, 312–343.

Militino, A., Ugarte, M., & García-Reinaldos, L. (2004). Alternative models for describing spatial dependence among dwelling selling prices. *Journal of Real Estate Finance and Economics*, *29*, 193-209.

Paez, A., Long, F., & Farber, S. (2008). Moving window approaches for hedonic price estimation: An empirical comparison of modelling techniques. *Urban Studies*, *45*, 1565.

Tretton, D. (2007). Where is the world of property valuation for taxation purposes going? *Journal of Property Investment and Finance*, *25*, 482-514.

ISSN: 0128-7680
Pertanika J. Sci. & Technol. **19 (S)**: 31 - 39 (2011)

Online 3D Terrain Visualization of GIS Data: A Comparison between Three Different Web Servers

Ruzinoor Che Mat*, Abdul Rashid Mohd. Shariff, Biswajeet Pradhan and Ahmad Rodzi Mahmud
Department of Biological and Agricultural Engineering,
Universiti Putra Malaysia, 43400 UPM, Serdang, Selangor, Malaysia
**E-mail: ruzinoor@rediffmail.com*

ABSTRACT

Geographical Information Systems (GIS) and three dimensional (3D) World Wide Web (WWW) applications usage are on the rise. The demand for online 3D terrain visualization for GIS data has increased. Current users demand for more complex data which have higher accuracy and realism. This is aided by the emergence of geo-browsers in the market which provide free service and also cater for the commercialized market. Other new technology driving the market is the use of software such as CityGML, Virtual Reality Markup Language (VRML)/ Entensive 3D (X3D), geoVRML, and Keyhole Markup Language (KML). These technologies also play an important role for this new era of online 3D terrain visualization. The aim of this paper is to implement the online 3D terrain visualization for GIS data by using VRML technology and launching the system into three different web servers. The data used for this system are contour data and high resolution satellite image (QUICKBIRD) for Universiti Putra Malaysia (UPM) area. Testing was done only for satellite image overlaid to 3D terrain data. The web servers used in this experiment were the Spatial Research Group Server in UPM, Universiti Utara Malaysia (UUM) web server, and ruzinoor.my web server. The comparison was based on the performance of web servers in terms of accessibility, uploading time, CPU usage, frame rate per second (fps), and number of users. The results from this experiment will be of help and guidance to the developers in finding the right web servers for the best performance on implementing online 3D terrain visualization for GIS data.

Keywords: Web map server, 3D terrain visualization, satellite image, web server, GIS

INTRODUCTION

In this new era of modern technology, the demand for accessing information is increasing tremendously due to the availability of Internet technology. The backbone of Internet technology involved different kinds of technology such as networking (LAN, MAN, WAN), World Wide Web (WWW), and Groupware. The WWW latest version is Web 3.0. Due to this, the WWW is now in the era of 3 dimensions (3D). Geo-browser such Google Earth, NASA World Win, and Virtual Earth emerged from this new era. The important part in all of these browsers is the 3D terrain data. That is why the demand for online 3D terrain visualization has increased and is a popular area of study. The success of these browsers is based on the web servers behind it. For example Google Earth and NASA World Win have their own powerful web servers. Most of the modern web servers have to process million of client requests on a daily basis. That is why it should be equipped with the capability to process multiple request concurrently (Praphamontripong *et al*., 2006). The aim of this study is to experiment the implementation of online 3D terrain visualization by using locally

Received: 1 August 2010
Accepted: 22 June 2011
*Corresponding Author

available web servers and test their performance. The Virtual Reality Markup Language (VRML) was used as backbone for developing online 3D terrain online draped with high resolution satellite imageries. The three web servers chosen for this experiment were Spatial Research Group (SRG) web server in UPM, Universiti Utara Malaysia (UUM) web server and ruzinoor.my web server. The criteria used to compare these three web servers were accessibility, loading time during office hours and out of office hours, CPU usage, frame rate per second (fps), and number of users at one time.

RELATED WORK

Research in 3D terrain visualization has emerged more than 10 years ago. Many researchers have shown an interest in this area. Praphamontripong *et al*. (2006) examined the performance analysis of asynchronous web server by using Proactor pattern. There presented the model based approach for the design time performance analysis of a web server which implement by using concurrent processing. Otherwise, Lu & Gokhale (2006) use a M/G/m queuing model to model the performance of web server which consider the response time of a client request. Furthermore, Mohd Syazwan & Nor Farzana (2008) have done the study on finding the factors that influencing the use of webcube web server from groupware and also acceptance issues from the users. They found that the lacks of webcube users in Universiti Utara Malaysia (UUM) were due to the service provided by the system which is not suitable to the users. In terms of 3D terrain visualization, Zhu *et al*. (2003) have proposed the hybrid 2D-3D interface for solving the problem of low bandwidth for implementing 3D terrain visualization. They also introducing tile based selective visualization for improving this system to increase the performance. Other than that, Ruzinoor *et al*. (2008) introduced the method of developing 3D web based terrain visualized by combining several software such as R2V, Arc View, Auto CAD, VRML, Chisel, and Dream weaver. This development has been successfully launched into the web server (Ruzinoor *et al*., 2009).

METHODOLOGY

The method used in this study consists of three steps which were data preparation, implementation, and testing. The detailed discussion on this matter will be explained in the following three sections.

Data Preparation

The data used in this study involved contour and high resolution satellite image data of UPM area. The contour data was provided by Department of Survey and Mapping Malaysia and satellite data by Taman Pertanian Universiti UPM. Both data need to be of the same exrent in order make the overlaying of image over the terrain data successful. AutoCAD and R2V software were used for editing the contour data and this was then exported into SHP files for the next process. PCI Geomatica software was used for cropping the satellite image to be the same extent as contour data. The file was saved in TIFF format. The last process is draping the satellite image over the 3D terrain data. These overlaying method is based on Ruzinoor [6] which used Arc GIS 9.2 software. This software was found to be the best on performing this task compared to other GIS software. The end product of this process is the VRML file of 3D terrain draped with satellite imageries which can be used online. For the purpose of testing the performance of online 3D terrain visualization of GIS data in three different web servers, only one file was used.

Implementation

Three web servers were chosen in this study; the Spatial Research Group web server in UPM, ruzinoor.my web server in Petaling Jaya and UUM Webcube web server. As mentioned by Praphamontripong *et al*. (2006) each modern web server employs the request/reply paradigm by using the HTTP protocol to communicate between itself and the clients. Normally web server provides only two types of request which is read request and write request. When both of requests were performed successfully the operation will be run in the client computer. But this is depends on the queuing process whether it is faster or slower. The location of Spatial Research Group Web Server was in the testing environment. The second web server ruzinoor.my was located 20 km from the location of testing and then the third web servers UUM webcube web server located 496 km from the testing location. The specifications and locations of these three servers are shown Table 1 – Table 3.

TABLE 1
Specifications of spatial research group web server

Spatial Research Group web server	
Domain	http://spatial.upm.edu.my
Location	Spatial Lab UPM
Provider	UPM
Type	Windows Server (XAMP)

TABLE 2
Specifications of ruzinoor.my web server

Ruzinoor.my web server	
Domain	http://www.ruzinoor.my
Location	Bandar Sunway, Petaling Jaya
Provider	Backbone Technologies (M) Sdn. Bhd.
Type	MYNIC Web Server

TABLE 3
Specifications of UUM web server

UUM web server	
Domain	http://staf.uum.edu.my
Location	Universiti Utara Malaysia Sintok
Provider	Universiti Utara Malaysia
Type	Webcube Groupweb

Data for the first web server was launched into address “http://spatial.upm.edu.my/ruzin- oor/-webupm/arcgis3d.wrl”. The data for the second web server was launched into address http://www.ruzinoor.my/webupm/arcgis3d.wrl, and data for the third web server into address “http://staf.uum.edu.my/ruzinoor/webupm/arcgis3d.wrl”. *Fig. 1* shows the online data for Spatial Research Group web server.

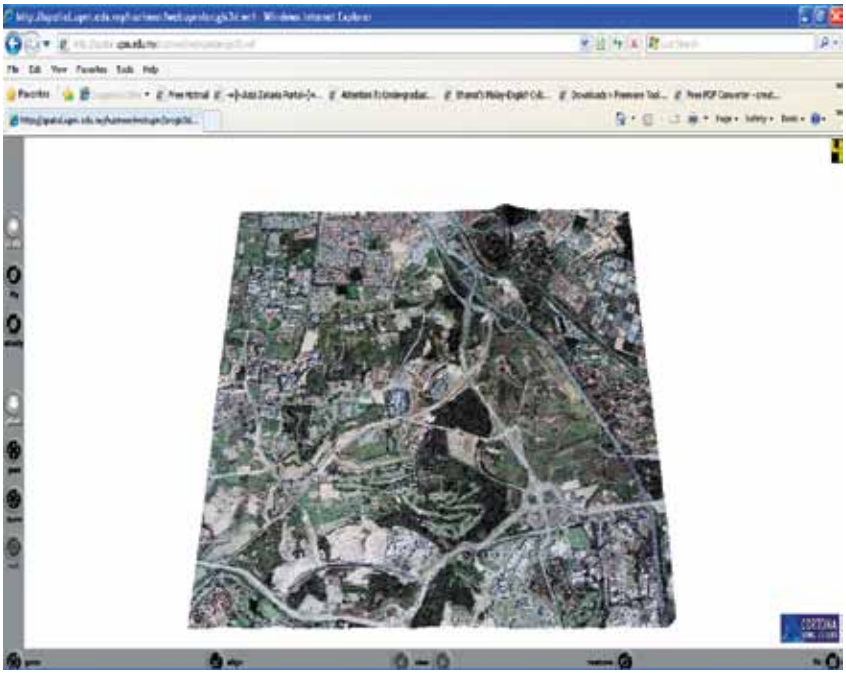

Fig. 1: Image of online data for Spatial Research Group web server

Testing

In order to test the three different web servers, the following criteria were used: accessibility, loading time, CPU usage, frame rate per second (fps), and number of users. The accessibility was tested based on how easy the web servers could be accessed in a certain time during the experiment. This is not the major criteria of testing because this test result could be determined based on other criteria. The major criteria tested were the loading time during office hours and out of office hours. This test was performed on a laptop with specifications as shown on Table 4.

TABLE 4
Specifications of laptop used for testing

	Laptop
Processor	Intel Core Duo Processor
Speed	1.66GHz, 667MHz FSB, 2MB L2 cache
Memory	2Gb DDR2
HDD	60Gb
Graphics	Intel Graphics Media Accelerator 950

The loading time was also tested with a different number of users accessing each web server at one time. The other two criteria tested were frame per second and the CPU usage. All of these tests were performed in one type of desktop computer with one type of actions which is walkthrough. The specifications for all of these computers were similar. Table 5 shows the specifications of this computer.

TABLE 5
Specifications of desktop computer used for testing

	Desktop computer
Processor	Intel Core 2 Duo Processor
Speed	2.40GHz, 800MHz FSB, 2MB L2 cache
Memory	2Gb DDR2 SDRAM
HDD	150Gb
Graphics	Onboard Graphic Cards

Based on the observations during the testing, different actions shown to have different value of frame per second and CPU usage. That is why the last criteria were tested based on different actions perform in one desktop computer (same specification as Table 4). The actions consist of four different types of interactions with online 3D terrain visualization which was fly, walk, rotate and pan. All of these tests were performed on three web servers.

RESULTS AND DISCUSSION

The first experiment measured the loading time in three different web servers running on one desktop computer. The measurement was performed by using stop watch and the result is produced in two decimal points. The result of this experiment is shown in Table 6. The graph for this result is shown in *Fig. 2*.

TABLE 6
Loading time during office hours and out of office hours

Criteria	SRG web server	Ruzinoor.my web server	UUM web server
Load time (office hours)	4.42 sec	7.96 sec	4.84 sec
Load time (Out of office hours)	1.25 sec	7.95 sec	1.69 sec

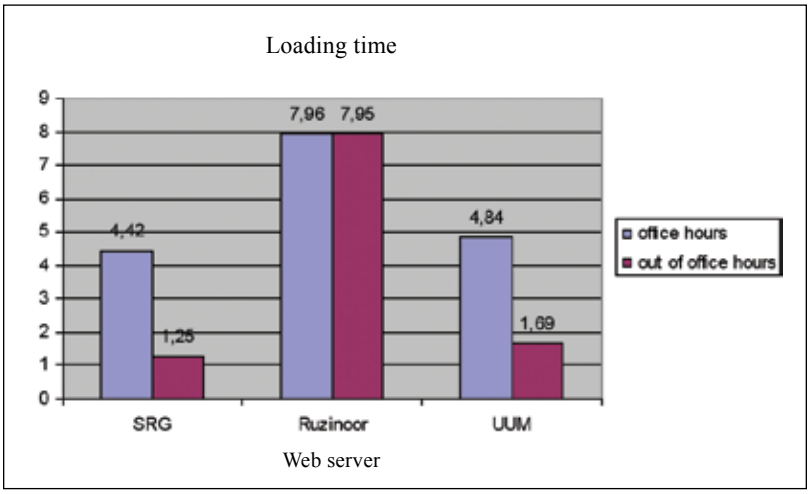

Fig. 2: Loading time in different web servers

The result shows that the best web server was Spatial Research Group Web Server which has the fastest loading time during office hours (4.42 sec) and out of office hours (1.25 sec). The worst web servers was ruzinoor.my which took more than 7 sec to load the file during office hours and also out of office hours. But overall the three web servers had taken less than 8 sec for loading the file which is not bad for accessing the system.

The second experiment was testing the loading time, frame per second (fps), and CPU usage by different number of users. All the users accessed the online system at the same time. The number of users started with 2 users, then, increased to 4, 6, and 8 users respectively. The result of this experiment is shown in *Fig. 3 – Fig 5*.

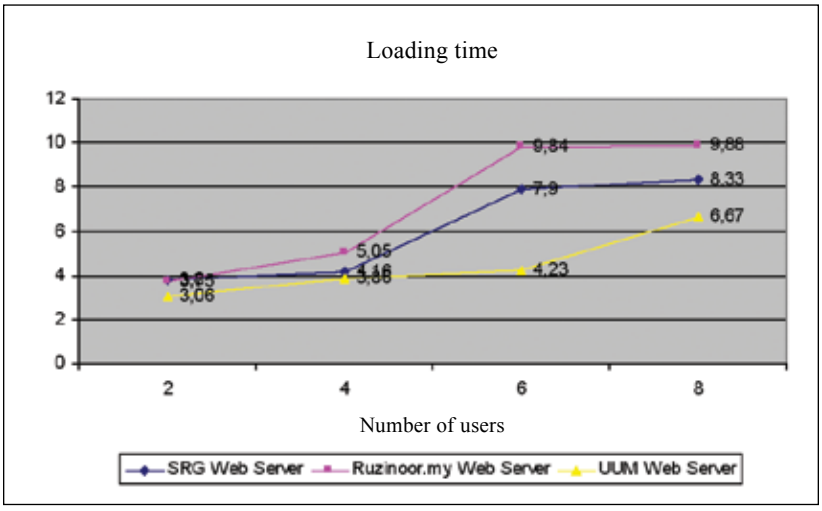

Fig. 3: Loading time in for different number of users

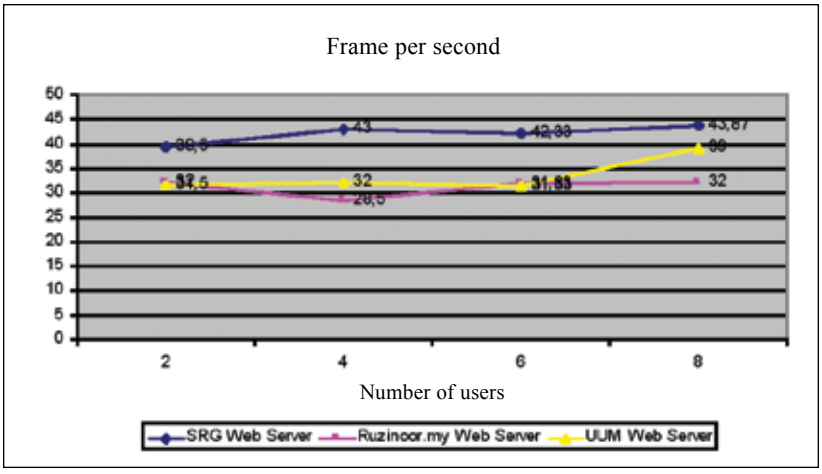

Fig. 4: Frame per second in for different number of users

The result for loading time in *Fig. 3* shows that when the number of users increased, the loading time becomes much slower. This may due to the time for loading the same file by many users at the same time slows the file accessibility from the same web server. Overall the UUM web server had the best loading time for the whole number of users compared to other web servers. This should not have occurred if we compare based on the location of the web server. The closer the web server is to the users, the faster should be the file loading time, and the further the distance, the slower time for loading. On average, the UUM web server had the fastest loading time for accessing the file online for the whole number of users. This may due to the network bandwidth and queuing process (read and write) for this web server at the best situation during the time was tested. That is why this web server stated the fastest loading time compared to others.

The results for frame per second in *Fig. 4* shows inconsistency of fps for three different web servers. In normal situations, when the number of users increased, the fps value should be lower but the results produced the opposite value of fps where when the number of users becoming eight, the fps value was the highest in most web servers. This may due to the network bandwidth and queuing process (read and write) for all web servers during the time of testing eight users is in the best situation which allowing the fps value to be the highest. As an average, the Spatial Research Group web server showed the lowest frame per second for accessing the file online for the whole number of users.

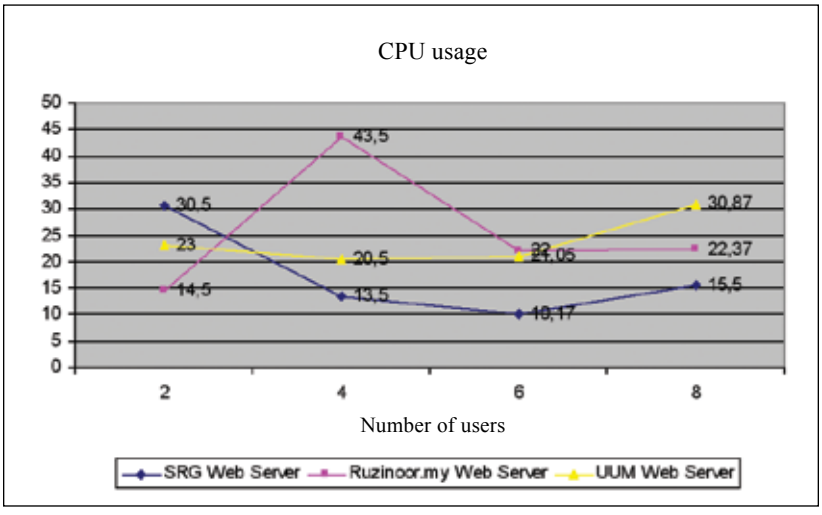

Fig. 5: CPU usage in for different number of users

The results for CPU usage in *Fig. 5* produced inconsistent values for the three web servers. In normal situations, when the number of users increases, the CPU usage should increase. However, in this situation most of the web servers produced the opposite results. The most inconsistent value for CPU usage was ruzinoor.my web server whereas the two users illustrated the highest value. As an average, the Spatial Research Group web server demonstrated the lowest CPU usage for accessing the file online for the whole number of users. This may due to the value of network bandwidth and queuing process (read and write) during the time for accessing the file was also inconsistent which sometime is lowest and sometime is highest. That is why most of the web servers giving the inconsistent value for the CPU usage.

The third experiment was testing the frame per second (fps) and CPU usage for different type of actions (refer *Fig. 6* and *Fig. 7*). This proved that different actions performed will produce different value of fps and CPU usage. In term of fps the pan actions produced the highest fps in all three web servers except for actions in Spatial Research Group web server which has a little bit fastest than pan actions. The actions which have the slowest value were rotate. This is may be due to the fact that actions involved much more movement of the object in online environment.

The second part was testing the CPU usage for different types of actions. The walk actions produced the best value which has the lowest CPU usage value for all of the actions tested. The rotate action was the weakest whereas CPU usage showed the highest value compared to the other actions. This is true where this action was the lowest in term of fps. These actions need more space for the actions which consume more CPU usage. Overall the best web server for performing different actions in term of fps was UUM web server and in term of CPU usage was ruzinoor.my.

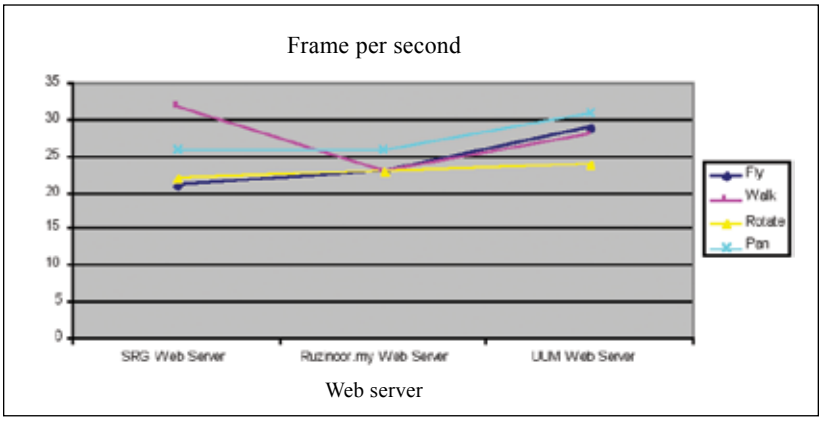

Fig. 6: Frame per second in for different actions

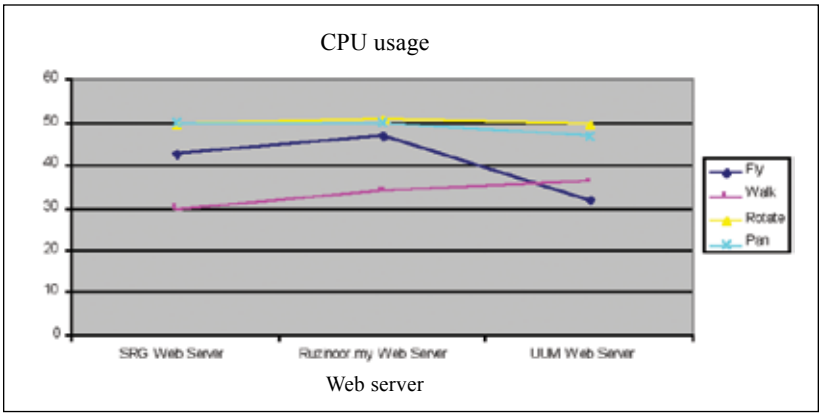

Fig. 7: CPU usage in for different actions

CONCLUSION

In conclusion, the best web servers to be used for implementation of online 3D terrain visualization was the Spatial Research Group Server. This is because it has the best value and is fastest for most of the test performed except for loading time involving different number of users and performance on different actions. In term of loading time in the second experiment, the location of the web server did not affect the file loading time. But in term of network bandwidth and queuing process (read and write) most of the web servers have inconsistent value where sometime is slower and sometime is faster. That is why in certain operation such as CPU usage the inconsistent value for web server is stated. The last experiment of this study produced opposite results where the Spatial Research Group Web server should be the best in term of fps and CPU usage because its location is the closest compared to other web server. But the Spatial Research Group web server stated the worst value on fps and CPU usage. It means that each web server has it own advantages in certain situation.

ACKNOWLEDGEMENTS

The authors would like to express their sincere appreciation to Taman Pertanian Univerisiti UPM for providing us the satellite image of UPM area. The most sincere thanks to Department of Survey and Mapping Malaysia (JUPEM) for providing us the latest contour data for UPM area. Without their help this study could not be finished.

REFERENCES

Lu, J., & Gokhale, S.S. (2006). Web server performance analysis. In *International Conference on Web Engineering*. Palo Alto, California, USA.

Nor Farzana, A. G., & Mohd Syazwan, A. (2008). Groupware technology acceptence as a knowledge sharing tool: A case study in UUM. In *Knowledge Management International Conference (KMICE 2008)* (pp. 381-385). Langkawi, Malaysia.

Praphamontripong, U., Gokhale, S., Gokhale, A., & Gray, J. (2006). Performance analysis of an asynchronous web server. In *Computer Software and Applications Conference 2006 (COMPSAC'06)* (pp. 22-28).

Ruzinoor, C. M., Abdul Rashid, M. S., Ahmad Rodzi, M., & Pradhan, B. (2008). Development of 3D web based terrain visualizer. In *International Symposium and Exhibition on Geoinformation 2008 (ISG 2008)*. Kuala Lumpur Malaysia.

Ruzinoor, C. W., Abdul Rashid, M. S., & Ahmad Rodzi Mahmud, M. (2009). Online 3D terrain visualization: A comparison of three different GIS software. In *International Conference on Information Management and Engineering*. Kuala Lumpur, Malaysia.

Zhu, C., Tan, E. C., & Chan, K. Y. (2003). 3D terrain visualization for web GIS. In *Map Asia 2003*. Kuala Lumpur Malaysia.

ISSN: 0128-7680
Pertanika J. Sci. & Technol. **19 (S)**: 41 - 49 (2011)

Integrated Partial Match Query in Geographic Information Retrieval

Rosilawati Zainol[1*], Zainab Abu Bakar[2] and Sayed Jamaludin Sayed Ali[3]
[1]Urban Studies & Planning Programme, Faculty of Arts & Social Sciences,
University of Malaya, 50603 Kuala Lumpur, Malaysia
[2]Department of Computer Science, Faculty of Computer and Mathematical Sciences,
[3]Department of Surveying Science and Geomatic,
Faculty of Architecture, Planning and Surveying,
Universiti Teknologi MARA, 40450 Shah Alam, Selangor, Malaysia
[*]E-mail: rosilawatizai@um.edu.my

ABSTRACT

This paper presents the evaluation of integrated partial match query in Geographic Information Retrieval (GIR). To facilitate the evaluation, Kuala Lumpur tourist related data is used as test collection and is stored in SuperWeb, a map server. Then the map server is customized to enhance its query capability to recognize word in partial or case sensitive between layers of spatial data. Query keyword is tested using the system and results are evaluated using experiments on sample data. Findings show that integrated partial match query provides more flexibility to tourist in determining search results.

Keywords: Partial match query, geographic information retrieval (GIR), integrated layers

INTRODUCTION

Tourists often feel frustrated when conducting online search for information on destinations they plan to visit (Pan and Fesenmaier, 2006; Radosevich, 1997; Stoltz, 1999). This is due to the abundant results they received when search is conducted (Pan and Fesenmaier, 2000; 2006). According to [8], tourists use different words to describe similar concept. Therefore it is difficult to design a specific query to search for specific results. Query becomes more complex when it involves geographic data. According to Clough *et al*. (2006), geographic information retrieval or better known as GIR involves the retrieval of documents based on both thematic and geographic content. Jones and Purves (2008) argued that GIR is an extension of Information Retrieval (IR) (Baeza-Yates and Ribeiro-Neto, 1999). GIR differs from GIS which stands for Geographic Information System in its structures, application, search engine, and relational database. GIR is more concerned on retrieving geospatial information and its relevancy. On the other hand, GIS emphasis more on exact spatial representatives and complex analysis at individual spatial object (Martins, 2008).

As a spatial component to classic IR, GIR concerns with the retrieval of spatial information (Geoffrey, 2006; Kunz, 2009). Even though some studies have shown that keyword search produces unsatisfactory results (Dridi, 2008), this study intends to show that partial keyword search with integrated capabilities and results summary is able to produce more flexible results as compared to the previous methods. Users have more choices and control to choose. This will enable them decide which results returned they prefer to view.

Received: 1 August 2010
Accepted: 22 June 2011
[*]Corresponding Author

CHALLENGES IN GEOGRAPHIC INFORMATION RETRIEVAL

Geographic Information Retrieval or GIR is a component of Information Retrieval (IR) that deals with geographic references. Thus its evaluation method is similar to methods in classic IR. Relevancy has become one of the important issues in GIR. Thus, the key challenge is to retrieve geographical information correctly and efficiently (Martins *et al*., 2005). Its main goal is to define index structures and techniques to efficiently store and retrieve documents using both the text and the geographic references contained within the text. Due to this aim, relevance has become one of the important issues and a challenge in GIR.

In meeting this challenge, scholars have come out with many models and techniques in handling GIR. Among the models include GeoCLEF, SPIRIT, Alexandria Digital Library project (Hill and Zheng, 1999), GREASE and Geographic co-occurrence (Overall and Rüger, 2007).

GeoCLEF for example, is a cross-language geographic retrieval track. Runs as part of Cross Language Evaluation Forum (CLEF), it provides the necessary framework to evaluate search tasks which involves spatial and multilingual aspects in GIR systems. On the other hand, SPIRIT which stands for Spatially-Aware Search Engine, uses geo-ontology and query expansion technique in search engine (Jones *et al*., 2003).

Many techniques in retrieving spatial information were also designed in GIR to produce efficient and relevant results. Among them include gazetteers, query expansion, geo-ontologies, and common sense geographic knowledge base (CSGKB). Gazetteers or place name resources are used to avoid vague terminology. In Alexandria Digital Library project, digitally georeferenced gazetteer is used to merge place names and geographic footprints (Doerr and Papagelis, 2007). A gazetteer has many roles. *Fig. 1* shows the major roles of a gazetteer.

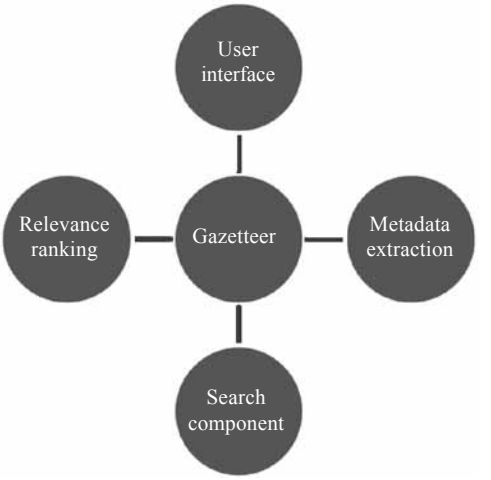

Fig. 1: Roles of a gazetteer [1]

Query expansion is another technique in GIR. It is used to expand query using words or phrases that have similar meaning in order to reduce query mismatch (Aly, 2008).

Geo-ontology, an approach used in SPIRIT, has four main areas of application: user's interpretation, system query formulation, metadata extraction and relevance ranking [26]. It is an enhancement technique of gazetteers. Furthermore in SPIRIT, it models both vocabulary and the spatial structure of places in information retrieval.

Common sense geographic knowledge base (CSGKB) can be viewed as the direct model of geographic world. It consists of geographic features and relationships which is based on qualitative spatio-temporal reasoning. Its structures composed of knowledge base, inference engine, geographic ontology and learner.

The task producing efficient and relevant documents in GIR is always evolving. Jones and Purves (2008) argued that the existing techniques in GIR have many shortcomings and needs to be improved further (Jones *et al*., 2003; Lin and Ban, 2008). *Fig. 2* shows the aspects to be improved outlined by Jones and Purves (2008) in order to produce a more efficient approach to GIR.

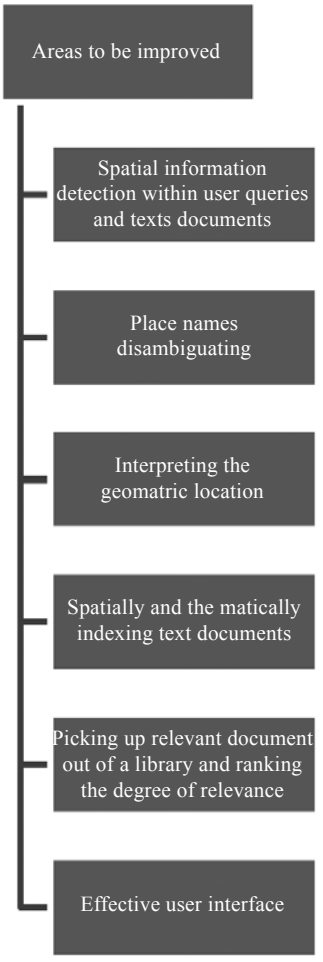

Fig. 2: Areas to be improved in GIR [2]

Since GIR is an evolving area of study, it will constantly be improved by scholars through various approaches. This study attempts to improve spatial information detection within user queries and to produce an efficient method in retrieving spatial information using integrated partial match query method.

TEST COLLECTIONS AND METHOD

Test collections in this study only cover the features related to tourism information in Kuala Lumpur. Query list of 92 keywords, on the other hand is gathered from 31 Bachelor Degree of Urban Studies & Planning Programme students in the University of Malaya. Finally, relevant judgment is obtained from five experts who have known Kuala Lumpur for more than 10 years.

Kuala Lumpur is the capital city of Malaysia. Being the most populated city in Malaysia, Kuala Lumpur has attracted more than 60 million domestic and foreign tourists in 2008 (Tourism Malaysia, 2009). Besides housing several governmental departments, Kuala Lumpur is a city that has many attractions which encompasses various categories such as shopping, semi nature, architecture, heritage and theme park. Thus test collections of Kuala Lumpur are divided into several layers. Each layer has attributes related to it. The detail of the layers and their attributes are shown in Table 1.

TABLE 1
Layers and their attributes with total number of documents

Category	Attributes	No. of documents
Accommodation	ID, Shape, Name, Category, Ranking, Year built, Tel. No., Fax No., Address, Email, Website, Longitude and Latitude, Brief	138
Attraction	ID, Shape, Name, Category, Year built, Tel. No., Address, Website, Longitude and Latitude, Brief	324
Eateries	ID, Shape, Name, Category, Tel. No., Address, Website, Longitude and Latitude, Brief	241
Auto teller machine	ID, Shape, Name, Location, Longitude and Latitude	244
Petrol station	ID, Shape, Name, Location, Longitude and Latitude	92
Landmark	ID, Shape, Name, Category, Longitude and Latitude, Brief	337

Query list which was obtained from the students can be divided according to several categories. The total numbers of keywords gathered are 92. However, only ten single keyword and abbreviations are used in this experiment. The detail of the query list is shown in Table 2.

TABLE 2
Query list

Category	Keyword
Attraction	Attraction, att, shopping, shop
Food	Food
Accommodation	Hotel
Recreation	Park, recreation
Heritage	Heritage
Facilities	Bank

Relevant judgment is obtained by interviewing five experts who live in Kuala Lumpur for more than ten years and are currently dealing with tourism sector. These experts include academicians and travel agents.

Methods used in this evaluation include recall and precision. Since GIR is a part of IR, evaluation technique focuses on the main criterion of relevance (Martins *et al*., 2005). Two most popular measures are precision and recall. For relevant item, recall,

$$r = \frac{cd}{n} \tag{1}$$

where r is recall, cd is the correct documents and n is the total number of documents and precision,

$$r = \frac{cd}{rd} \tag{2}$$

where p is precision, cd is the correct documents for relevant documents and rd is the total number of relevant documents. In addition the f measure combines recall with precision and is commonly used in problems when the negative results outnumber the positive ones (Martins *et al*., 2005). Thus, fl – measure equally weighs precision and recall and is given by

$$fl(p,r) = \frac{2pr}{p+r}. \tag{3}$$

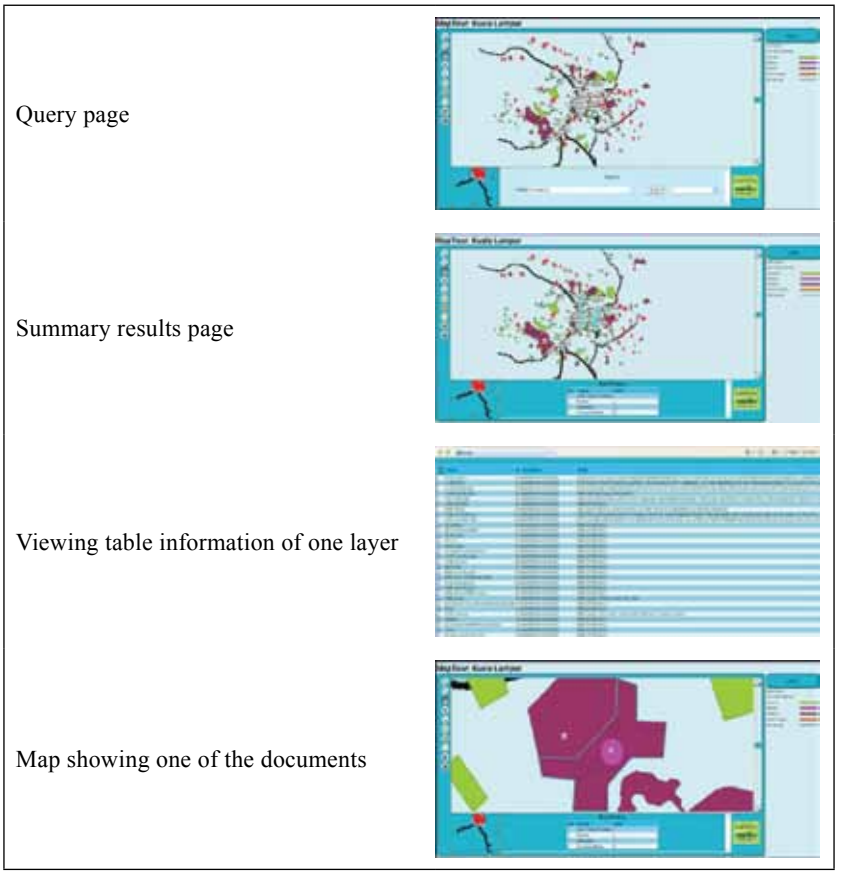

Fig. 3: Images of viewing results of a query

In addition, MapTour: Kuala Lumpur powered by SuperWeb, a map server application, is the product developed to examine the test collection. Some html and java scripts documents are customized to produce results of the experiments. Customization of these files has changed 80% the original SuperWeb search function. The new query function gives more flexibility to users in choosing the results that they looked for from a summary of results displayed. Furthermore, by clicking on the document of each layer from the summary will display the map of the desired location. *Fig. 3* shows the steps in viewing query function and results of "shopping".

RESULTS

Results collected from the experiment can be divided into two parts. One is the results appeared when keyword is typed in and the other is when viewing each layer from the previous results. The former shows results according to the layers in which the keyword appeared in any field in the

TABLE 3
Summary results of each keyword query

Keyword	Layer displayed	No of documents
Shopping	Auto teller machine	7
	Eateries	1
	Attraction	71
	Accommodation	95
Shop	Auto teller machine	9
	Eateries	3
	Attraction	72
	Accommodation	96
Food	Eateries	205
	Attraction	58
	Accommodation	1
Hotel	Eateries	25
	Attraction	2
	Accommodation	132
Attraction	Attraction	154
	Accommodation	5
Att	Attraction	161
	Landmark	10
Park	Attraction	8
	Landmark	7
	Eateries	2
	Accommodation	3
Recreation	Attraction	32
Heritage	Eateries	1
	Attraction	26
	Accommodation	2
Bank	Auto teller machine	172
	Landmark	5
	Attraction	1
	Accommodation	2

document. This technique is used to enhance query capabilities in looking at similar keyword that are related to any layers. However the results displayed are not ranked according the highest number of documents but rather provides opportunity to the user to make decision.

Instead of using query expansion Fu *et al*. (2005) integrated partial match query will display results summary at the first level of a query. This provides options for users to choose and accommodate similar name that has more than one meaning. For example, Masjid can represent a place where Muslims pray, or Jalan Masjid, since it is able to detect keyword "Masjid", which represents a street call Masjid. Thus this method will reduce the confusion. Table 3 shows the summary results of each keyword and abbreviation query.

Partial match query has better chance of retrieving more documents as compared to exact match query. However not all of the documents retrieved are relevant. Therefore, documents retrieved in Table 3 are evaluated based on the recall, precision and *f* value of each query in Table 2 using formula, recall $r = \frac{cd}{n}$, precision $p = \frac{cd}{rd}$ and $fl(p,r) = \frac{2pr}{p+r}$. Results of selected keywords and abbreviations are shown in Table 4.

TABLE 4
Results of recall and precision of the ten keywords

Keyword	N	Recall (%)	Precision (%)	*f* value (%)
Shopping	174	100	100	100
Shop	180	100	100	100
Food	264	100	100	100
Hotel	159	100	100	100
Attraction	324	49	0.6	1.19
Att	324	50	0.3	5.96
Park	32	100	59	74.21
Recreation	32	100	100	100
Heritage	28	100	97	98.48
Bank	244	73	99	84.03

Findings show that not all partial and exact match returns 100% recall and precision. For example, the keyword "shop" which is a part of the word shopping can yield 100% recall and precision. However, the abbreviation "att" which is a part of the word attraction does not produce desired results. Furthermore, this abbreviation picks up "Kampung Attap" as one of the results return when a query is conducted even though the results are not relevant.

Similarly with the word "park" which returns document that is not relevant such as Ampang Park, a shopping complex in Kuala Lumpur.

However, the advantage of this technique is that it is able to show the relationship between layers that are related. For example a tourist who is coming to Kuala Lumpur would like to obtain information on which hotel has shopping facilities nearby. They can just type in the word "hotel", the system will return with three related layers and one of them is attraction which is able to show shopping centers. They can also search the opposite way and view more related results. Thus they, the user are able to obtain two meaningful returns.

Besides this advantage, this technique has one shortcoming in which it is not able to track keyword if the word is labeled as the name of a layer. For example, "attraction" is one of the keyword chosen for testing. When a query is carried out, results return only 159 documents when the actual

total number of documents is 324. However, the abbreviation "att" returns more documents since it is able to track any partial word either with *att or att*.

Further revision to this technique is still being carried out. This technique only concentrates on a single keyword search. Thus, the next step in this study is to evaluate on query of more than one word. Words like "value for money", "popular attractions", "delicious food" and "budget hotel" are some of the words that will be evaluated in the second phase of this study.

CONCLUSION

Integrated partial match query technique with results summary capabilities can still be enhanced to provide a more precise and relevant information. Combined with semantic query capabilities this technique will be able to yield more relevant and precise document (Abdelmoty *et al*., 2007). Partial match query of multiple words with single meaning can be developed using semantic query capabilities.

ACKNOWLEDGEMENTS

The authors wish to thank Universiti Malaya for providing the funding to collect textual and spatial data of Kuala Lumpur.

REFERENCES

Abdelmoty, A. I., Smart, P., & Jones, C. B. (2007). Building place ontologies for the semantic web: Issues and approaches. In *Proceedings of the 4th ACM Workshop on Geographical Information Retrieval*. ACM: Lisbon, Portugal.

Aly, A. A. (2008). Using a query expansion technique to improve document retrieval. *International Journal Information Technologies and Knowledge*, *2*, 343-348.

Baeza-Yates, R., & Ribeiro-Neto, B. (1999). *Modern information retrieval*. Boston, MA: Addison Wesley.

Clough, P. D., Joho, H., & Purves, R. (2006). *Judging the spatial relevance of documents for GIR*.

Doerr, M., & Papagelis, M. (2007). A method for estimating the precision of placename matching. In *IEEE Transactions on Knowledge and Data Engineering*, *19*, 1089-1101.

Dridi, O. (2008). Ontology-based information retrieval: Overview and new proposition. In *Research Challenges in Information Science (RCIS 2008).*

Fu, C., Jones, B., & Abdelmoty, A. I. (2005). Ontology-based spatial query expansion in information retrieval. In *On the Move to Meaningful Internet Systems* 2005a. ODBASE 2005.

Furnas, G., *et al.* (1987). The vocabulary problem in human-system communication. *Communications of the ACM*, *30*, 964-971.

Geoffrey, A. (2006). GIR experimentation. In C. Peters, *et al*. (Eds.), *CLEF 2006* (pp. 881-888). Springer: Alicante, Spain.

Hill, L., & Zheng, Q. (1999). Indirect geospatial referencing through place names in the digital library: Alexandria Digital Library experience with developing and implementing gazetteers. In *1999 Annual Meeting of the American Society for Information Science.*

Jones, C., Abdelmoty, A., & Fu, G. (2003). Maintaining ontologies for geographical information retrieval on the web. In *On The Move to Meaningful Internet Systems 2003: CoopIS, DOA, and ODBASE*. Springer Berlin / Heidelberg.

Jones, C. B., & Purves, R. S. (2008). Geographical information retrieval. *Int. J. Geogr. Inf. Sci.*, *22*(3), 219-228.

Kunz, R. (2009). *Evaluation of spatial relevance in geographic information retrieval*. Department of Geography, University of Zurich: Zurich, Switzerland.

Lin, X., & Ban, Y. (2008). On the framework and key technologies of modern GIR systems. In *The International Archives of the Photogrammetry, Remote Sensing and Spatial Information Sciences* (pp. 269-276). Beijing.

Martins, B. (2008). *Geographic information retrieval*. Seminário Língua Natural 2008/2009.

Martins, B., Silva, M. J., & Chaves, M. S. (2005). Challenges and resources for evaluating geographical ir. In *ACM Workshop on Geographic Information Retrieval*. Bremen, Germany: ACM Press.

Overell, S. E., & Rüger, S. (2007). Geographic co-occurrence as a tool for GIR. In *Proceedings of the 4th ACM Workshop on Geographical Information Retrieval*. ACM: Lisbon, Portugal.

Pan, B., & Fesenmaier, D. R. (2000). A typology of tourism related web sites: Its theoretical foundation and implications. *Information Technology and Tourism*, *3*(3/4), 155-176.

Pan, B., & Fesenmaier, D. R. (2006a). Online information search: Vacation planning process. *Annals of Tourism Research*, *33*(3), 809-832.

Pan, B., & Fesenmaier, D. R. (2006b). Travel information search on the Internet and the implications for designing travel recommendation systems. In H.W.K.W.W.E. D.R. Fesenmaier (Eds.), *Travel destination recommendation systems: Behavioral foundations and applications*. CABI publishing: Oxfordshire.

Radosevich, L. (1997). Fixing web-site usability. *InfoWorld*, *19*, 81-82.

Stoltz, C. (1999). Each year, a bit less. In *Washington Post*.

Tourism Malaysia. (2009). Malaysia hotel guests by state. Retrieved on June 15, 2009 from http://www.tourism.gov.my/tourismmalaysia_corpx/rpt4_hotelguest.cfm?rpt=4.2009.

Zhang, Y., *et al*. (2008). A common sense geographic knowledge base for {GIR}. Science in China Series E: *Technological Sciences*, *51*(0), 26-37.

ISSN: 0128-7680
Pertanika J. Sci. & Technol. **19 (S)**: 51 - 58 (2011)

Digital Mapping Using Low Altitude UAV

Anuar Ahmad
Department of Geoinformatics,
Faculty of Geoinformation Science & Engineering,
Universiti Teknologi Malaysia,
81310 UTM Skudai, Johor, Malaysia
E-mail: anuarahmad@utm.my

ABSTRACT

Normally, topographic map is produced using aerial photogrammetry. The recent development in aerial photogrammetry is the use of large format digital aerial camera for producing topographic map, however, the cost of the camera is too expensive and many mapping organization around the world could not afford to purchase it. In certain application, there is a need to map small area with limited budget. This issue has been solved by using small format camera (i.e. conventional or digital) to produce digital map. This study concentrates on the use of unmanned aerial vehicle (UAV) for producing digital map. UAV has been widely used in military for reconnaissance, planning, combat, and etc. Today, UAV can be used by civilian for reconnaissance, monitoring, mapping, and others. The objectives of this study are to investigate the capability of UAV in producing digital map and assess the accuracy of mapping using UAV. In this study, a light weight fixed wing UAV was used as a platform and a high resolution digital camera was used to acquire aerial digital images of the study area. The aerial digital images were acquired at low altitude. After capturing the aerial digital images, ground control points and check points were established using GPS. Then the aerial digital images were processed using photogrammetric software. The output of the study is a digital map and digital orthophoto. For accuracy assessment, the root mean square error (RMSE) is used. Based on the assessment, the results showed that accuracy of sub-meter can be obtained using the procedure and method used in the study. In conclusion, this study shows that UAV can be used for producing digital map at sub-meter accuracy and it can also be used for diversified applications.

Keywords: Unmanned aerial vehicle, aerial photogrammetry, digital camera

INTRODUCTION

In aerial photogrammetry, normally the topographic map, orthophoto and other photogrammetric products are produced from the aerial photograph acquired using the large format aerial camera or commonly known as metric camera. The cost of acquiring the aerial photograph is very costly and need to be planned properly. Ideally, large format aerial camera is useful for mapping large area. This type of camera is not suitable and economical to be used for mapping small area. To overcome this problem, small format digital camera can be used to acquire aerial photograph. The small format digital camera has been widely used by many researches around the world for mapping purposes (Mills and Newton, 1996a, b; Ahmad, 2009). The aerial photograph acquired using small format digital camera is used not only for topographic mapping (Ahmad, 2006) but it could also be used for various applications such as for land slide (Ahmad *et al*., 2008), map revision in GIS, research

Received: 1 August 2010
Accepted: 22 June 2011

work, and any application which does not require high accuracy. The digital camera offers several advantages compared to large format metric camera. Some of the advantages include ease of use, handy, cheap, the images are in digital form which is ready to be used and does not need special aircraft. The digital camera can be placed in a balloon, light aircraft such as the microlight, and other platform (i.e based on their application). The use of digital camera also has been reported by several researchers for different applications.

In this study, a small airplane in the form of a glider or known as unmanned aerial vehicle (UAV) equipped with a small format digital camera, Global Positioning System (GPS) and Inertial Navigation System (INS) which form data acquisition system is used to acquire aerial photograph of the study area. The objectives of the study are to investigate the suitability of the data acquisition system in acquiring the aerial photograph for mapping purposes and to produce digital map and digital orthophoto from the aerial photograph.

UNMANNED AERIAL VEHICLE

Unmanned Aerial Vechicle (UAV) was developed by the United State (US) military for surveillance and reconnaissance purposes back in World War 1 and World War 2 as a prototype form. UAV is widely used in early 20th century between the year 1960s to 1980s. The number of research on UAV done by US and other countries around the world is increasing. UAV is also known as drones, remotely piloted vehicle (RPV), remotely piloted aircraft (RPA), and remotely operated aircraft (ROA). Today, UAV is available in various shape, size, weight, and applications. UAV is a light aircraft that fly without pilot and uses aerodynamic power to fly, able to fly on its own based on pre-programmed flight plans or a complex dynamic automation system (UAV Forum, 2008). There are also operating UAV for remote sensing application such as photogrammetric task in recording archeology site (Eisenbeiss, 2004); precision agriculture (Herwitz *et al*., 2002); GPS remote sensing measurement (Gent *et al*., 2005), thermal and hyperspectral sensing, search and rescue, industrial and chemical plant inspection, emergency operation and production of 3D vector map (Haarbrink and Koers, 2008). Table 1 shows the category of UAV defined by Unmanned Vehicle Systems-International (UVS).

TABLE 1
Category of UAV [7]

Category name	Mass (kg)	Range (km)	Flying altitude (m)	Endurance (h)
Micro	<5	<10	250	1
Mini	<250/30/150	<10	150/250/300	<2
Close range	25-150	10-30	3000	2-4
Medium range	50-250	30-70	3000	3-6
High alt. long endurance	>250	>70	>3000	>6

In this study, the CropCam UAV deployed is a Canadian product that has weight of 2.7 kg (*Fig. 1*). Table 2 shows the specification of the CropCam UAV. The CropCam UAV together with Pentax Optio A40 digital camera is used to acquire aerial photographs. This CropCam UAV is launched manually and landed on the same spot where it was launched. *Fig. 2* shows the CropCam UAV component and ground control station.

Fig. 1: CropCam UAV

TABLE 2
Specification of Cropcam UAV

Lenght	1.22 m
Wing span	2.44 m
Mass	2.72 kg
Engine	2.46 cc / 0.15 cu in
Oil tank	6 oz
Altitude	Up to 2200 feet in Canada
Flight endurance / 160 acre	20 minute
Camera	Pentax Optio A40
Average speed	60 kmj^{-1}
Minimum temperature	–10°C

Fig. 2: CropCam UAV and ground station

RESEARCH METHODOLOGY

Acquisition of Aerial Photograph Using UAV

The photographs of Universiti Teknologi Malaysia (UTM) main campus were acquired using both the large format metric camera and small format digital camera Pentax Optio A40. For the large format metric camera, the Wild RC30 metric camera with wide angle lens was used to acquire the aerial photographs of UTM by Department of Surveying and Mapping Malaysia (DSMM). The photographs were acquired in 2005 with the scale of 1:10 000. After the photography, the colour film was developed and scanned at 1000dpi using the photogrammetric scanner in DSMM. In this study, the large format aerial photograph acquired using the Wild RC30 camera was used as reference image.

For the Pentax Optio A40 digital camera, the aerial photographs (in digital form) were acquired by placing the digital camera underneath the CropCam UAV's wing. The photographic session is carried out by a company and a series of digital images were acquired. The digital images were acquired at an approximate 60% overlapped and 30% sidelapped. Since the format of the digital camera is small, the ground coverage is small too. Many small format aerial photographs were acquired using several flight lines. After each flight session, the digital images were downloaded into the notebook at the ground control station. *Fig. 3* shows an example of the aerial photograph acquired using the small format digital camera.

Fig. 3: An example of aerial photograph of partial area of UTM campus acquired using the digital camera

Establishment of Ground Control Point

In photogrammetry, it is a common practice that the ground control points (GCPs) are established after the aerial photography session. There are several methods that can be used to establish the GCP such as traversing and Global Positioning System (GPS). For the large format photograph several GCPs were selected which enclosed the overlapped area. For the digital images, many GCPs are required. For the establishment of GCPs, rapid static method was used for both the large format and small format aerial photographs.

Calibration of Digital Camera

In this study, a test field was built at Faculty of Geoinformation Science and Engineering, UTM. This test field is a 3D test field which comprise of 36 targets that are fixed with retro-reflective target. The test field was used to calibrate the digital camera. For the purpose of calibration, 10 photographs of the test field were acquired from five (5) camera locations (*Fig. 4*). The focus of the digital camera was set at infinity focus and the automatic function was disabled. At each camera location, two photographs were acquired where one is in landscape position and the other one is rotated 90 degree from its' original position i.e portrait position. During photography the camera flash is switched on and a piece of tissue paper was used to block the flash light so that not much light will be transmitted. If the flash is not covered then 'over saturated' will occur which might cause deterioration of the calibration results. Also during photography, convergent photographs were employed where the optical axis of the digital camera always pointing towards the centre of the test field and the dimension of the test field should occupy the entire format of the digital camera. Convergent configuration was employed since it will strengthen the geometry and with the purpose to recover focal length successfully as recommended (Foyer, 1996). Photography was done within short period of time. The photographs of the test field were acquired after the acquisition of aerial photographs.

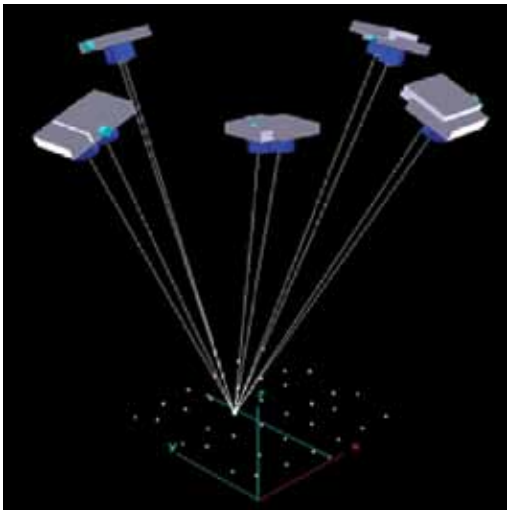

Fig. 4: Test field and location of digital camera

Processing Aerial Photograph

In this study, a digital photogrammetric software was used to process the digital images of the large format metric camera and the small format digital camera. The digital photogrammetric software was used to produce digital orthophoto and to produce digital map. For the large format aerial photograph, only a pair was used to generate the 3D stereoscopic model. In digital photogrammetric software, the 3D stereoscopic model was setup within short period. Then on screen digitizing is carried out to digitize some features (vectorization) in the stereoscopic model. The next step is to create DTM and subsequently create digital orthophoto. The vector and the orthophoto could be exported to other format such as CAD and GIS formats. The same procedure was repeated to process the aerial photograph from the small format digital camera.

Calibration of Digital Camera

After all the photographs from the digital cameras have been downloaded into the computer, image measurement is carried out. All the photographs of the test field were measured semi-automatically using close range photogrammetric software. This software can be used to determine the 3D coordinates of the points on the object (i.e retro-reflective targets) and the camera calibration parameters. The coordinates for the centre of the retro-reflective targets of the test field were determined using 'weighted mean' technique. The results of the camera calibration are tabulated in the following section.

RESULTS

From this study, two sets of results were produced. The first results comprised of camera calibration parameters obtained from calibrating the digital camera and the second results comprise of digital orthophoto obtained from the digital photogrammetric software.

Camera Calibration Parameters

Table 3 shows the estimated parameters together with their standard deviation. The camera calibration parameters consist of the focal length (c), principal point offset (x_p, y_p), radial (k^1, k^2, k^3) and tangential (p^1, p^2, p^3) lens distortion, "affinity"(b^1) and different in scale factor (b^1). All these parameters were then entered into the digital photogrammetric software for processing the aerial photograph except for affinity and scale factor parameters.

TABLE 3
Digital camera calibration parameters

Canon digital camera		
Parameter		Std. deviation
c (mm)	7.4753	4.511e-003
x_P (mm)	-0.0930	2.670e-003
y_P (mm)	0.1264	2.700e-003
k_1	4.17626e-003	1.004e-004
k_2	-9.22072e-005	2.088e-005
k_3	2.63634e-006	1.411e-006
p_1	2.05459e-004	1.802e-005
p_2	-6.14004e-004	1.841e-005
b_1	1.94918e-004	3.866e-005
b_2	7.89334e-005	4.294e-005 5

Digital Orthophoto

Before the production of the orthophoto, aerial triangulation is performed for the small format aerial photographs and followed by production of DTM. After the process of aerial triangulation, the 3D stereoscopic model is set up. From the 3D stereoscopic model, digitizing is carried out and check points were also digitized for the purpose of accuracy assessment. In this study, sub-meter accuracy of ±0.623m was achieved from the assessment. Table 4 shows the result of accuracy assessment.

Fig. 5 shows the mosaic of digital orthophoto produced from the digital photogrammetric software of the small format digital camera.

TABLE 4
Accuracy assessment

Pt ID	GPS (meter)			ERDAS imagine (meter)			Differences (meter)		
	X	Y	Z	X	Y	Z	ΔX	ΔY	ΔZ
1015	627391.613	171955.444	12.413	627391.651	171955.655	13.674	0.039	0.211	1.261
1016	627357.901	171945.050	11.724	627357.408	171944.646	12.185	0.493	0.403	0.461
1019	627420.304	171992.045	13.661	627420.573	171991.997	12.133	0.269	0.048	1.528
1020	627432.739	171995.588	13.805	627432.197	171995.647	12.890	0.542	0.060	0.915
1011	627313.775	172008.495	11.977	627313.570	172008.413	10.382	0.206	0.082	1.595
1012	627329.563	172008.759	12.015	627328.164	172009.035	10.589	1.399	0.277	1.426
						RMSE		**±0.623**	

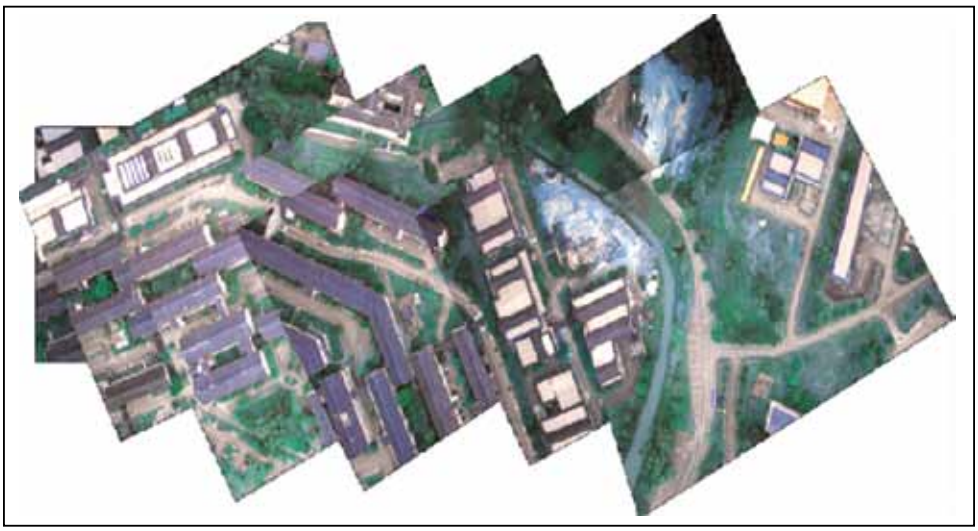

Fig. 5: Partial mosaic of UTM campus for the small format aerial photograph

CONCLUSION

From this study, it was found that the digital photogrammetric software is capable of producing digital orthophoto and digital map for both the large format metric camera and small format digital camera. However, the area covered by the digital camera is very small compared to the area covered by the large format metric camera. In this study, the digital orthophoto produced from the digital camera covers only a small area compared to the digital orthophoto produced from large format metric camera. For accuracy assessment, it cannot be denied that the accuracy for large format metric camera is superior. In another previous study, it was proved that high accuracy could be achieved by the large format metric camera compared to the accuracy achieved by the small format digital camera (Ahmad and Adnan, 2008). In this study, the accuracy achieved by the small format digital camera is at sub-meter level.

ACKNOWLEDGEMENT

The author wishes to thank the Ministry of Science, Technology and Innovation (MOSTI) in providing the E-Science grant for funding the research.

REFERENCES

Ahmad, A. (2006). Digital photogrammetry: An experience of processing aerial photograph of UTM acquired using digital camera. *Asia GIS Conference.* UTM Skudai, Malaysia. 4-6 March 2006.

Ahmad, A. (2009). Mapping using small format digital imagery and unmanned aerial vehicle platform. *10th South East Asia Survey Congress 2009 (SEASC 2009)*. Bali, Indonesia, 4-7 August 2009.

Ahmad, B., Ahmad, A., & Yahya, M. A. (2008). Landslide mapping and volume analysis using photogrammetric technique and potential use of unmanned aerial vehicle. *International Conference on Slope Malaysia*. Hotel Istana, Kuala Lumpur, Malaysia, 4-5 November 2008.

Ahmad, A., & Adnan, N. A. (2008). Digital photogrammetry: Comparison of digital orthophoto based on different dataset of diital images of aerial photograph. *7th International Symposium & Exhibition on Geoinformation*. PWTC, Kuala Lumpur, 13-15 October 2008.

Eisenbeiss, H. (2004). A mini unmanned aerial vehicle (UAV): System overview and image aquisition. *International Workshop on Processing and Visualization Using High-Resolution Imagery*. Pitsanulok, Thailand, 18-20 November 2004.

Fryer, J. G. (1996). Camera calibration. In K. B. Atkinson (Ed.), *Close range photogrammetry and machine vision* (pp. 156-179). Whittles Publishing, Caithness, Scotland, U.K.

Grant, M. S., Katzberg, S. J., & Lawrence, R. W. (2005). GPS Remote Sensing Measurements Using Aerosonde UAV. *AIAA 2005-7005*, Arlington, VA.

Haarbrink, R. B., & Koers, E. (2006). Helicopter UAV for photogrammetry and rapid response. Retrieved on January 9, 2008 from http://www.pegasus4europe.com/pegasus/workshop/documents/contributions/Haarbrink_UAV_full.pdf.

Herwitz, S. R., Johnson, L. F., Higgins, R. G., Leung, J. G., & Dunagan, S. E. (2002). Precision agriculture as a commercial application for solar-powered unmanned aerial vehicles. *AIAA 2002-3404*. Portsmouth,VA. Retrieved on January 14, 2008 from http://www.uavforum.com/library/librarian.htm.

Mills, J. P., & Newton, I. (1996a). A new approach to the verification and revision of large scale mapping. *ISPRS Journal of Photogrammetry & Remote Sensing*, *51*, 17-27.

Mills, J. P., & Newton, I. (1996b). Aerial photography for survey purposes with a high resolution, small format, digital camera. *Photogrammetric Record*, *15*(88), 575-587.

ISSN: 0128-7680
Pertanika J. Sci. & Technol. **19 (S)**: 59 - 67 (2011)

Groundwater Quality Mapping of an Alluvial Aquifer, Eshtehard, Iran

Leila Khodapanah* **and Wan Nor Azmin Sulaiman**
Department of Environmental Science, Faculty of Environmental Studies,
Universiti Putra Malaysia, 43400 UPM,
Serdang, Selangor, Malaysia
**E-mail: leyla.khodapanahy@gmail.com*

ABSTRACT

Eshtehard aquifer located in southwest of Tehran province, Iran, provides a large amount of water requirement for inhabitants of Eshtehard district. Monitoring and analyzing of groundwater quality are important for protecting groundwater as sustainable water resource. One of the most advanced techniques for groundwater quality interpolation and mapping is geostatistics methods. The purposes of this study are (1) to investigate major ions concentration and their relative abundance to provide an overview of present groundwater chemistry and (2) to map the groundwater quality in the study area using geostatistics techniques. In this investigation, ArcGIS 9.2 was used for predicting spatial distribution of some groundwater characteristics such as: Chloride, Sulfate, pH, and Conductivity. These methods are applied for data from 44 wells within the study area. The final maps show that the south parts of the Eshtehard aquifer have suitable groundwater quality for human consumption and in general, the groundwater quality degrades south to north and west to east of the Eshtehard plain along the groundwater flow path.

Keywords: Groundwater quality, GIS, geostatistics, Eshtehard, Iran

INTRODUCTION

Groundwater is the only reliable source for increasing water demand in arid and semi-arid regions around the world. Many regions in Iran are characterized by semi-arid climate. Eshtehard plain, located in west of Tehran, falls in a semi-arid type of climate. This aquifer provided the increasing water demand for irrigation, domestic, and industrial uses over the past century. The quality of water is as important as its quantity in any water supply planning especially for drinking purposes. The chemical, physical and bacterial characteristics of ground water determine its usefulness for municipal, commercial, industrial, agricultural, and domestic water supplies. Therefore, monitoring the quality of water is important because clean water is necessary for human health and the integrity of aquatic ecosystems (Babiker *et al*., 2007). However, due to cost and practicality, it is not feasible to establish monitoring stations in every location of study area to measure the pollutant concentration. Therefore, prediction of values at other locations based upon selectively measured values could be one of the alternatives. There are two main groupings of interpolation techniques: deterministic and geostatistical. Deterministic interpolation techniques create surfaces from measured points, based on either the extent of similarity (e.g. Inverse Distance Weighted) or the degree of smoothing (e.g. radial basis functions). Geostatistical interpolation techniques (e.g. kriging) utilize the statistical properties of the measured points. Using measured sample points from a study area, geostatistics can create prediction for other unmeasured locations within the same area The geostatistical techniques

Received: 1 August 2010
Accepted: 22 June 2011
*Corresponding Author

quantify the spatial autocorrelation among measured points and account for the spatial configuration of the sample points around the prediction location (ESRI, 2003). The accuracy of interpolation methods for spatially predicting soil and water properties has been analyzed in several studies (Nas and Berktay, 2006; LaMotte and Greene, 2007; Barca and Passarella, 2008). Thus this research has been done to investigate the spatial correlation of groundwater quality data set in Eshtehard aquifer and mapping groundwater quality in this area by using GIS and geostatistics techniques.

STUDY AREA

The study area is in Tehran province, about 100 km southwest of Tehran. This area lies between the longitudes of 48˚16' to 48˚50' and latitudes 35˚34' to 35˚47' (*Fig. 1*). It is surrounded by the Halghehdar Mountains to the north, Karaj plain to the east, Kordha and Ghezelban Mountains to the south and Hajiarab basin to the west. The area is characterized by a warm and dry climate in summer and cold and dry in winter, in way of modified Domartan method with an average annual temperature of 14.7˚C and a rainfall of 227 mm. The Eshtehard groundwater basin consists of the moderately permeable gravel formation and the overlying coarse sediments. The aquifer forms an east–west elongated topography deepening westward. The aquifer thickness ranges from 30 m in the east to more than 130 m in the west. Due to the lack of confining clay layers, the aquifer is considered typically unconfined. The groundwater flow is from west to east.

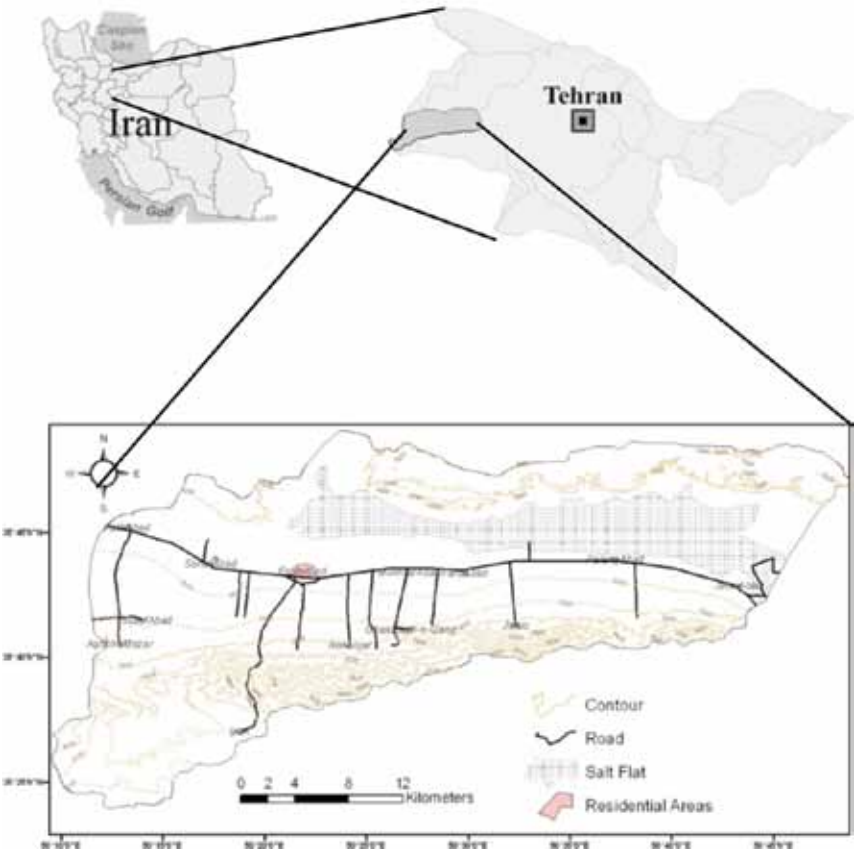

Fig. 1: Location of the study area

MATERIALS AND METHOD

Groundwater samples were taken directly from 44 sample points in May and October 2007. Water quality parameters (chloride, sulfate) were then analyzed in the laboratory of Tehran Regional Water Authority according to the methods given in the 19th edition of the Standard Methods of APHA (Fetouani *et al*., 2008). Sample pH was measured using a glass electrode pH meter. Electrical conductivity was measured using a platinum electrode conductivity meter. The analytical precision for the measured major ions was within ±5%. Summary statistics of the chemical data are listed in Table 1.

TABLE 1
Chemical compositions of groundwater samples

Parameter	Minimum	Maximum	Mean	WHO, 2004
SO4	23.54	1526	420.45	250
Cl	10.64	7332	1089.69	250
pH	7.11	8.54	8/00	6.5-9.2
EC	350	23600	4425.79	1500

In this study geostatistical interpolation techniques were used to obtain the spatial distribution of groundwater quality parameters over the area. As their name implies, geostatistical techniques create surfaces incorporating the statistical properties of the measured data. Many methods are associated with geostatistics, but they are all in the kriging family. Among the various forms of kriging, ordinary kriging has been used widely as a reliable estimation method (Yamamoto, 2003; Fetouani *et al*., 2008). Kriging is divided into two distinct tasks: quantifying the spatial structure of the data and producing a prediction. Quantifying the structure, known as variography, is where a spatial-dependence model is fitted to data set. To make a prediction for an unknown value for a specific location, kriging will use the fitted model from variography, the spatial data configuration, and the values of the measured sample points around the prediction location. According to the theory of regionalized variable, the value of a random variable Z at a point x is given as by Buyong (2007):

$$Z(x) = m(x) + \varepsilon'(x) + \varepsilon'' \tag{1}$$

where $m(x)$ is the deterministic function describing the structural component of Z at point x, $\varepsilon'(x)$ is the term denoting the stochastic, locally varying but spatially dependent residual from $m(x)$ called the regionalized variable, and ε'' is the residual having zero mean. If there is no trend in a region, $m(x)$ equals the mean value in the region. Therefore, the expected difference between any two points x and $x + h$ separated by a distance vector h will be zero. That is:

$$E[Z(x) - Z(x+h)] = 0 \tag{2}$$

where $Z(x)$ and $Z(x+h)$ are the values of the random variable Z at point x and $x + h$. It also assumed that the variance of differences depends only on the distance h between points, so that:

$$\begin{aligned} E\left[\{z(x) - z(x+h)\}^2\right] &= E\left[\{\varepsilon'(x) - \varepsilon'(x+h)\}^2\right] \\ &= 2\gamma(h) \end{aligned} \tag{3}$$

The term $\gamma(h)$ is called semivariance. We can write equation (1) as:

$$Z(x) = m(x) + \gamma(h) + \varepsilon'' \tag{4}$$

to show the equivalence between $\varepsilon'(x)$ and $\gamma(h)$. Thus, the semivariogram may be mathematically described as the mean square variability between two neighboring points of distance *h* as shown in Eq. 5 [9, 10]:

$$\gamma(h) = \frac{1}{2N(h)}\sum_{i=1}^{N(h)}[z(x_i + h) - z(x_i)]^2 \tag{5}$$

Where $\gamma(h)$ is the semivariogram expressed as a function of the magnitude of the lag distance or separation vector h between two pints, $N(h)$ is the number of observation pairs separated by distance *h* and $z(x_i)$ is the random variable at location x_i.

The experimental semivariogram, $\gamma(h)$ is fitted to a theoretical model such as Spherical, Exponential, Linear, or Gaussian to determine three parameters, such as the nugget (C_0), the sill (C) and the range (A_0). These models are defined as follow (Adhikary *et al*., 2009; Isaaks and Srivastava, 1989),

Spherical model:

$$\gamma(h) = C_0 + \left[1.5\left(\frac{h}{A_0}\right) - 0.5\left(\frac{h}{A_0}\right)^2\right] \qquad h \le A_0$$

$$\gamma(h) = C_0 + C \qquad h > A_0 \tag{6}$$

Exponential model:

$$\gamma(h) = C_0 + C\left[1 - \exp\left(-3\frac{h}{A_0}\right)\right] \tag{7}$$

Gaussian model:

$$\gamma(h) = C_0 + C\left[1 - \exp\left[-\left(\frac{3h}{A_0}\right)^2\right]\right] \tag{8}$$

In this study, a geostatistical software package, called ArcGIS Geostatistical Analyst Extension was used for the ordinary kriging estimations. The groundwater quality data has been checked by a histogram tool and normal QQ Plots to see if it shows a normal distribution pattern. For the data which are not normally distributed (SO_4^{2-} and Cl^-), the ArcGIS Geostatistical Analyst provides log transformations for converting skewed distributions into normal distributions.

For each water quality parameter, an analysis trend was made. The trend analysis tool from the ArcGIS Geostatistical Analyst provides a three-dimensional perspective of the groundwater quality data directional trends. This analysis demonstrates that the chloride and electrical conductivity data seem to exhibit a strong trend in the NE-SW direction. Three different semivariogram models (Spherical, Gaussian and Exponential) were fitted on computed experimental semivariograms.

Prediction performances were assessed by cross- validation (*Fig. 2*).

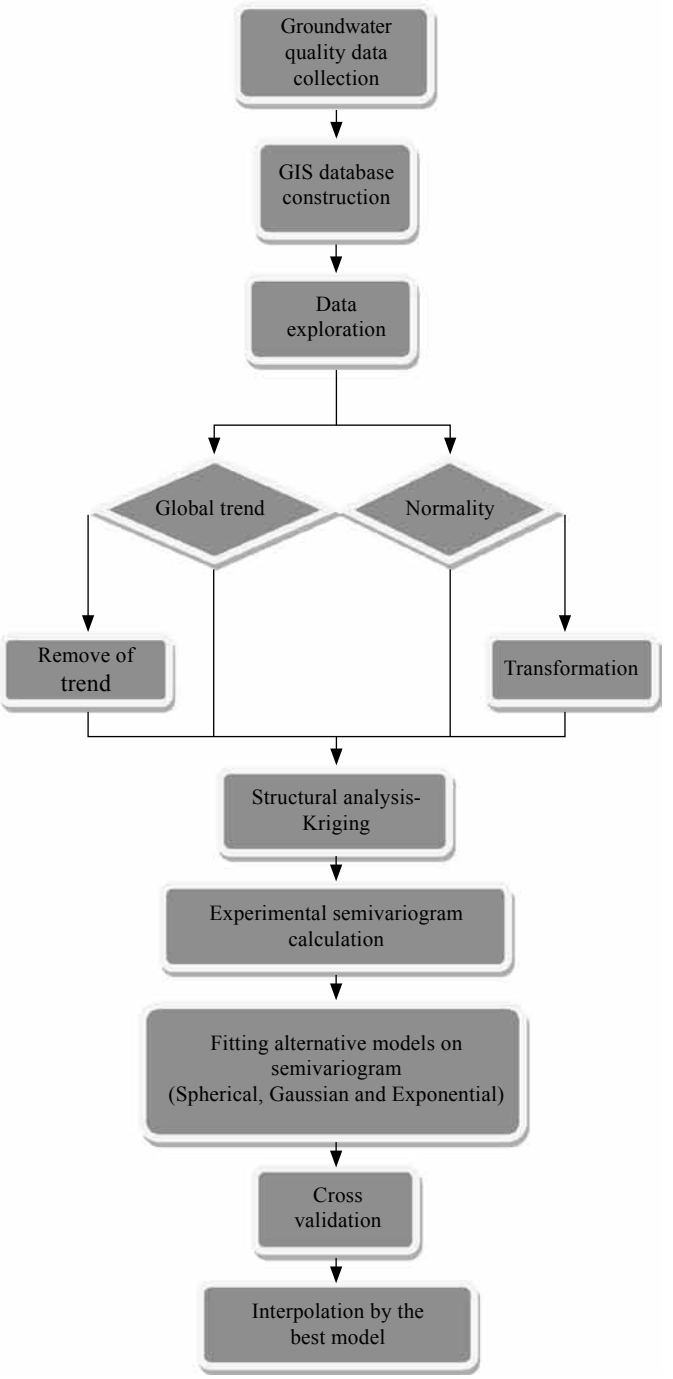

Fig. 2: Methodology flowchart

RESULTS AND DISCUSSION

The water quality evaluation in the area of study is carried out to determine their suitability for different purposes. The permissible limits for presence of different ions in groundwater have been defined by the World Health Organization as the standard quality for drinking water (WHO, 2008).

A statistical summary of the groundwater quality properties is presented in Table 1. In this study, the semivariogram models (Spherical, Exponential, and Gaussian) were tested for each parameter data set. Prediction performances were assessed by cross-validation. The objective of cross validation is to make an informed decision about which model provides the most accurate prediction.

For a model that provides accurate predictions, the mean error should be close to 0, the root-mean-square error and average standard error should be as small as possible (this is useful when comparing models), and the root-mean square standardized error should be close to 1 (ESRI, 2003).

After determination of the most suitable models by comparing the prediction errors, the spatial distribution of different groundwater quality elements were analyzed using Arc GIS. Subsequently, thematic maps for groundwater quality parameters were generated using ordinary kriging. Table 2 shows the best fitted models and their prediction errors using cross validation.

TABLE 2
Summary of best fitted models for different groundwater quality parameters

Parameters	Models	Prediction errors			
		Mean	Root-mean square	Average standard error	Root-mean-square standardized
SO_4	Spherical	-0.391	5.126	6.656	0.778
Cl	Guassian	-5.923	147.3	169.1	0.876
EC	Spherical	-2.007	42.72	47.79	0.935
pH	Spherical	-0.002	0.254	0.261	0.959

Groundwater quality maps resulting from kriging interpolation has been illustrated in *Fig. 3*. This figure shows the spatial distribution of pH, conductivity, sulfate, and chloride concentrations in study area, respectively.

pH

It was observed from the pH value that water samples were varying from 7.1 to 8.5 and these values are within the limits prescribed by WHO (Table 1). There are no water samples with pH values outside of the desirable ranges.

Electrical Conductivity (EC)

EC of the groundwater is varying from the conductivity values ranged from 350 to 23600 μmhos cm-1 at 25°C. The maximum limit of EC in drinking water is prescribed as 1500 μmhos cm-1 (Fetouani *et al*., 2008). In 55% of water samples the conductivity exceeds the permissible limit. As shown in *Fig. 3b*, the EC value increases from south to northwest and northeast along the groundwater flow path with the upper ranges being greater than 5,000 μmhos cm^{-1}.

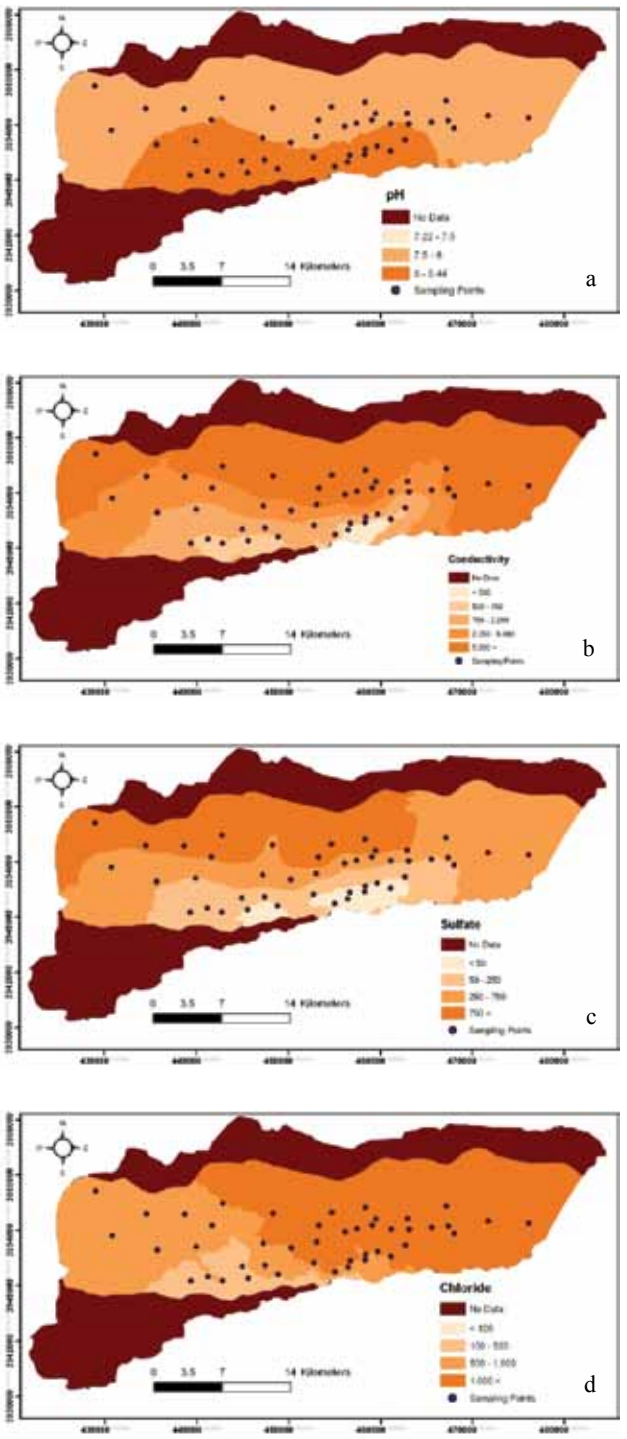

Fig. 3: Spatial distribution of a) pH, b) conductivity, c) sulfate and d) chloride

Chloride (Cl^-)

Chloride concentration is varying from 10.64 to 7332 mg l^{-1}. The large variation in Cl is mainly attributed to lithologic composition and anthropogenic activities prevailing in this region. Chloride concentration is very high in west and northwest of the study area which may indicate influence of geological formation and high rate of evaporation.

Chloride salts in excess of 100 mg l^{-1} give salty taste to water. When combined with calcium and magnesium, may increase the corrosive activity of water.

Sulfate ($SO4^{2-}$)

Sulfate concentration is varying from 23.54 to 1526 mg l^{-1} which exceeded the permissible limits in 50% of water samples. The groundwater samples with high concentration of sulfate are dominantly distributed in north and northeast of the area. It falls in an area of intensive land use (around the Eshtehrad city and cultivation area), that confirms an origin from the waste water discharge and agricultural fertilizers.

CONCLUSION

The groundwater samples have been evaluated for their chemical composition and suitability in Eshtehard aquifer. Spatial distribution map of groundwater quality parameters were generated through GIS and geostatistical techniques (ordinary kriging).

Because geostatistics is based on statistics can give an indication of how good the predictions are. The spatial variability maps showed that southern part of the study area has optimum groundwater quality and in general, the groundwater quality decreases south to north of the region. However chloride concentration in the groundwater was found to be increased from south and southwest to west and northwest.

Recommendations regarding improved cultural practices including the conjunctive use with good quality water, fertilizer and water management, and installation of subsurface drainage system should be taken up as effective practices to prevent soil salinization and provide sustainable water supply.

REFERENCES

Adhikary, P. P., Chandrasekharan, H., Chakraborty, D., & Kamble, K. (2009). Assessment of groundwater pollution in West Delhi, India using geostatistical approach. *Environ Monit Assess*. DOI 10.1007/s10661-009-1076-5.

APHA. (1995). *Standard methods for the examination of water and wastewater* (19th ed.). Washington, DC: American Public Health Association,

Babiker, I. S., Mohamed, M. A. A., & Hiyama, T. (2007). Assessing groundwater quality using GIS. *Water Resour Manage*, *21*, 699-715. DOI:10.1007/s11269-006-9059-6.

Barca, E., & Passarella, G. (2008). Spatial evaluation of the risk of groundwater quality degradation. A comparison between disjunctive kriging and geostatistical simulation. *Environ Monit Assess*, *137*, 261-273. DOI 10.1007/s10661-007-9758-3.

ESRI (Environmental System Research Institute). (2003). Using ArcGIS geostatistical analyst USA.

Fetouani, S., Sbaa, M., Vanclooster, M., & Bendra, B. (2008). Assessing ground water quality in the irrigated plain of Triffa (north-east Morocco). *Agricultural Water Management*, *95*(2), 133-142. DOI:10.1016/j.agwat.2007.09.009.

Isaaks, E. H., & Srivastava, R. M. (1989). *An introduction to applied geostatistics*. Oxford University, New York.

LaMotte, A. E., & Greene, E. A. (2007). Spatial analysis of land use and shallow groundwater vulnerability in the watershed adjacent to Assateague Island National Seashore, Maryland and Virginia, USA. *Environ Geol*, *52*, 1413-1421. DOI 10.1007/s00254-006-0583-8.

Nas, B., & Berktay, A. (2006). Groundwater contamination by nitrates in the City of Konya, (Turkey): A GIS perspective. *Journal of Environmental Management*, *79*, 30-37. DOI: 10.1016/j.jenvman.2005.05.010.

Taher Buyong. (2007). *Spatial data analysis for geographic information science*. Johor: Penerbit Universiti Teknologi Malaysia.

World Health Organization (WHO). (2008). *Guidelines for drinking water quality*. *Vol. 1 Recommendations* (3rd ed.). WHO, Geneva.

Yamamoto, J. K. (2003). An alternative measure of the reliability of ordinary kriging estimates. *Mathematical Geology*, *32*(4), 489-509. DOI:10.1023/A:1007577916868.

ISSN: 0128-7680
Pertanika J. Sci. & Technol. **19 (S)**: 69 - 76 (2011)

CropCam UAV for Land Use/Land Cover Mapping over Penang Island, Malaysia

Faez M. Hassan*, H. S. Lim and M. Z. Mat Jafri
School of Physics, Universiti Sains Malaysia,
Minden 11800 Penang, Malaysia
**E-mail: faiz_mm2000@yahoo.com*

ABSTRACT

The problem of difficulty in obtaining cloud-free scene at the equatorial region from satellite platforms can be overcome by using airborne imagery as an attempt for introducing an economical method of remote sensing data; which only requires a digital camera to provide near time data. Forty three digital images were captured using a high resolution digital camera model pentax optio A40 (12 megapixels)at a selected location in the same day in Penang Island from a low-altitude flying autopilot aircraft (CropCam) to generate land use/land cover (LULC) map of the test area. The CropCam was flown at an average altitude of 320 meters over the ground while capturing images which were taken during two flying missions for the duration of approximately 15 and 20 minutes respectively. The CropCam was equipped with a digital camera as a sensor to capture the GPS points based digital images according to the present time to ensure the mosaic of the digital images. Forty one images were used in providing a mosaic image of a bigger coverage of area (full panorama). Training samples were collected simultaneously when the CropCam captured the images by using hand held GPS. Supervised classification techniques, such as the maximum likelihood, minimum-to-distance, and parallelepiped were applied to the panoramic image to generate LULC map for the study area. It was found that the maximum likelihood classifier produce superior results and achieved a high degree of accuracy. The results indicated that the CropCam equipped with a high resolution digital camera can be useful and suitable tool for the tropical region, and this technique could reduce the cost and time of acquiring images for LULC mapping.

Keywords: CropCam, LULC, supervise classification, digital camera

INTRODUCTION

The increasing availability of remote sensing images, acquired periodically by satellite or airborne sensors on the same geographical area, makes it extremely interesting to devolve the monitoring systems which is capable of automatically producing and regularly updating land use/land cover (LULC) maps of the consider site (Bruzzone *et al*., 2002). Remote sensing technique has the ability to represent LULC categories by means of classification process. With the availability of multispectral remotely sensed data in digital form and the development in digital processing, remote sensing supplies a new prospective for LULC analysis (Weng, 2001). Remote sensing applications for agriculture and forestry often require images with a high temporal resolution (Grenzdoreff and Zuer, 2007); this is difficult and /or costly obtain, either by satellite imagery or conventional airborne data. Therefore, unmanned UAV equipped with GPS and digital camera, so called CropCam, has become the focus of our research as a development technique to collecting the data. Most researchers have examined the use of conventional aircrafts or satellite system to collect such imagery (Lim *et al*., 2009; Saleh, 2009). Unfortunately, both have limited ability to provide accurate and

Received: 1 August 2010
Accepted: 22 June 2011
*Corresponding Author

concurrent imagery in LULC mapping. Thus, alternative methods of acquiring imagery need to be evaluated. Our objective is to evaluate high resolution imagery using a variety of applications involving LULC mapping. The sensor used in this study was a 12.0 megapixel digital camera model Pentax optio A40 that enables the CropCam to acquire colour imagery with a 9.0 cm spatial resolution from the height of 320 meters above the ground. Supervised classification of remote sensing images had been widely used as a powerful means to extract various kinds of information concerning earth environment. The ability to acquire imagery at relatively low altitude (e.g. 200-640 m above the ground), afford UAVs the ability to acquire imagery below the majority of atmospheric conditions, such as cloud cover, that often plague other remote sensing systems. Atmospheric conditions such fog and haze can have an effect on UAV based systems, but to a lesser degree than other platforms that may have acquisitions heights of 10 to 100's of kilometers above the earth's surface (Tan *et al*., 2009). Another great advantage of a UAV based aerial imagery system is the ability to be quickly deployed and have imagery available almost concurrent. A part of this, the fact that some UAVs can hand lunched and skid landed in relatively small locations; eliminate the need for takeoff and landing strips, which may be at a significant distance from the emergency site. The main purpose of this study are to do LULC mapping using CropCam unmanned Aerial Vehicle (UAV) and digital camera to make a quick decision about the specific area can be made after processing the data.

STUDY AREA AND DATA ACQUISITIONS

The flying field site over Penang Island, Malaysia was chosen as the study area. The study area is balik pulua located between altitude 5° 39' N to 5° 41' N and longitude 100° 20' E to 100° 24' E (*Fig. 1*).

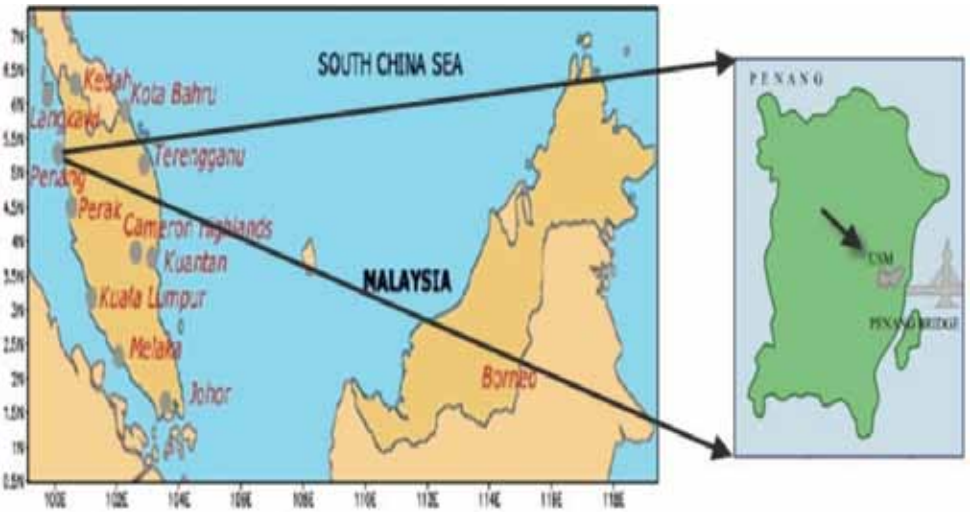

Fig. 1: The geographical features of the study area

A digital camera (*Fig. 2*) was used to capture RGB digital images from CropCam UAV (*Fig. 3*) at an altitude of 320 meters above the ground. The images were captured between 4 p.m. and 6 p.m. on the 9th January 2009. The images were acquired at approximately 60% overlapped and 30% sidelapped and covering around 900 meters square of the ground while flying over our area which had been chosen due to the fact that it is an open area without any near obstacle that can hinder safe

CropCam takeoff and landing. The images were taken under a suitable condition which was during a sunny day with a normal wind speed at approximately 5 knot/hour to ensure the flight stability and the camera's capability to capture accurate images; all images were taken also during two flight missions in one day for duration 15 and 20 minute respectively and with average CropCam speed at 60 m/sec during flying.

Fig. 2: Digital Camera- Pentax optio A40 (Pentax optio, 2009)

Fig. 3: CropCam Unmanned Aerial Vehicle (UAV)

REMOTE PLATFORM AND SENSOR

In this study, the CropCam was flown above the study area at an average of altitude of 320 meters during image acquisitions. The technical specifications for the CropCam platform are shown in Table 1.

The CropCam is a revolutionary mini agriculture plane that could change the way to manage the crops, fields, or any part of the agriculture operation by providing high resolution GPS based digital images for precision agriculture. CropCam is a radio controlled model glider which can be easily assembled and hand lunched, it can be fitted with a miniature autopilot, digital camera, Trimble GPS, and software that can provide images on demand. The CropCam was able to fly automatically from the moment it takes off and lands. It also provides high resolution GPS based images on demand.

TABLE 1
The technical specifications for the CropCam [8]

length	4 feet
Wing pan	8 feet
Weight	6 pounds
Engine	0.15 cu in/Axi Brushless
Fuel tank	6 oz/lithium polymer batteries
Altitude	(400-2200) feet in Canada (can be adjusted to meet our application)
Flight duration	20 minutes
Camera	Pentax digital optio A40

CropCam can be lunched using hands from a corner of the field and the powerful miniature autopilot and GPS did the navigate in a pattern over the field. Both the CropCam and the digital camera perform automatically to take GPS based digital imageries, each individual image is GPS based with latitude, longitude, and latitude (Pentax optio, 2009).

METHODOLOGY

Forty four digital imageries of the flying site were selected for LULC classification, sample of the images were shown in (*Fig. 4*). The images were acquired in three visible bands (red, green, and blue). The size of each raw high spatial resolution image was 4000 pixels by 3000 lines. Forty one images were mosaiced together to produce a bigger coverage area (*Fig. 5*). The mosaic image was separated in to three bands (RGB) for multispecialty analysis using PTGui Pro8.1.3 software. The PTGui is panoramic stitching software originally developed as a graphical user interface for

Fig. 4: Sample of raw images used in this study

panorama tools. PTGui currently a full featured photo stitching application (CropCam, 2008). A total of 20 training samples were collected simultaneously when the CropCam was capturing the images using hand held GPS and were used to register the mosaic image into an established geographic coordinate system UTM (*Fig. 6*).

Fig. 5: The mosaic image used for land cover/land use

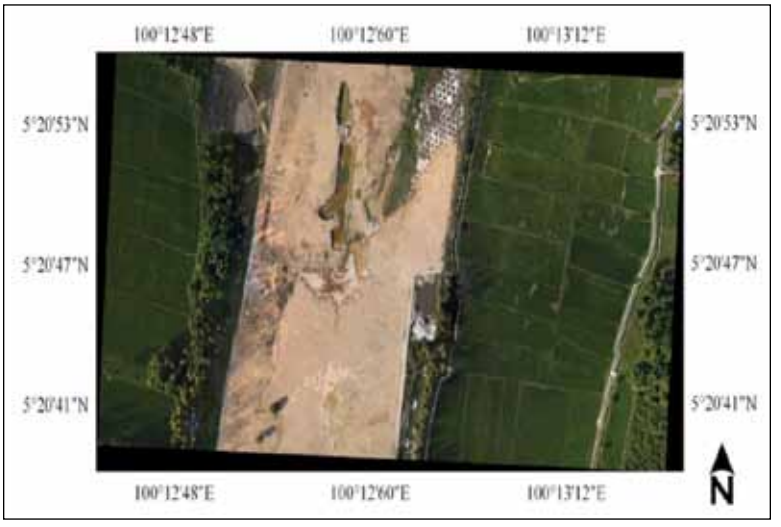

Fig.6: The geocoded mosaic image used for land cover/land use classification

All the images were taken in absolutely clear sky on the 9th January 2009.All image-processing tasks were carried out using PCI Geomatica version 10.3 digital image processing software.

Supervised classifications were operated in three basic steps: training, classification and accuracy assessment. The aim of the classification is to categorize all of pixels in the digital image into LULC classes in the ground. Training samples are needed for supervised classification; selection

of training areas in this study was based on the colour image. The areas were established using polygons. There are delineated by spectrally homogeneous sub area, which have, given class name. Many researches choose the maximum likelihood classifier in their studies (PTGui, 2009; Saura and Miguel-Ayanze, 2002; Donoghue and Mironnet, 2002). In this study the mosaic image was classified into four classes .Once the training sites and classes were assigned, the full panorama image was classified using three upervised classification algorithms which are Maximum Likelihood, Minimum-to-Distend, and Parallelepiped. Accuracy assessment was made to the image after classified .among the various methods of accuracy assessment discussed in remote sensing literatures, three measures of accuracy were selected and tested in this study, namely overall accuracy, kappa coefficient, and error matrix (Thiemann and Kaufmann, 2002).

DATA ANALYSIS AND RESULTS DISCUSSION

A total of 100 training samples were randomly generated in this study. The three supervised classifiers performed to the mosaic image after registered in UTM coordinate system. The image was classified into four legends which are trees/vegetation, water, soil field and urban. Overall accuracy and kappa coefficient results of the three classification methods are shown in Table 2 and error matrix results are shown in Table 3.

The overall accuracy is expressed as a percentage of the test pixels successfully assigned to correct legends. Based on the findings Maximum Likelihood classifier produced the highest degree of accuracy with overall accuracy 90.02% and kappa coefficient 0.81, Minimum-to-Distend gave overall accuracy 79.46% with kappa coefficient 0.562 and Parallelepiped classifier result was the lowest in overall accuracy of 31.29% and kappa coefficient 0.14.A classified image using Maximum Likelihood classifier is shown in (*Fig. 7*).

TABLE 2
The overall classification accuracy and Kappa coefficient

Classification method	Overall classification accuracy (%)	Kappa coefficient
Maximum likelihood	90.02	0.81
Minimum distance to mean	79.46	0.562
Parallelepiped	31.29	0.14

TABLE 3
The confusion matrix results

Classified data	Reference data				
	V	W	S	U	Total
V	52	3	4	0	59
W	4	2	6	1	13
S	0	1	19	6	26
U	0	0	0	2	2
Total	56	6	29	9	100

Class: V: tress Vegetation; W: Water; S: Soil filed; U: Urban

The results show a good agreement between the image and the ground. During supervised classification processing we had some misplacing pixels or mixed pixels between the four classes

this is happened because we using limited channels (RGB) specially when we was classified the trees and other vegetation.

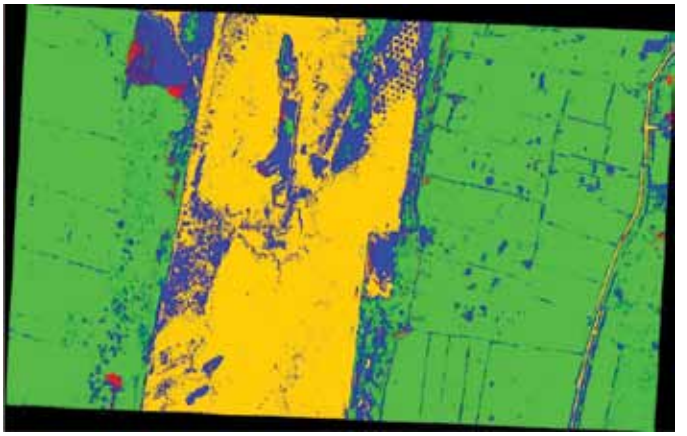

Fig. 7: The classified image obtained using Maximum likelihood classifier (Green = Trees/ vegetation, Blue = Water, yellow = Soil field, red = Urban and black = unprocessed area)

CONCLUSION

From the classified map, Maximum Likelihood method gives a good result for LULC mapping. This analysis has demonstrated that the capability of the digital camera with high spatial resolution to capture images from a low elevation attached to a CropCam can give more accurate results and consider low cost compare with others remote sensing data collected from satellite or manned airborne. This study showed that the normal digital can provides an alternative way to capture useful data for LULC mapping. The study showed also that the CropCam UAV as an ideal and new remote sensing system for collecting data, this includes that the fact that it can be transported and deployed easily. The study confirmed that using CropCam system can give high resolution and real time images for accurate further processing and at a relatively low cost.

REFERENCES

Bruzzone, L., Cossu, R., & Vernazza, G. (2002). Combining parametric algorithms for partially supervised classification of multitemporal remote-sensing images. *Information Fusion*, *3*, 289-297.

CropCam. (2008). Retrieved from www.cropcam.com.

Donoghue, D. N. M., & Mironnet, N. (2002). Development of an integrated geographical information system prototype for coastal habitat monitoring. *Computers and Geosciences*, *28*, 129-141.

Grenzdoreff, G., & Zuev, S. (2007). Bestimmung des photogrammetrischin Genauigkeitspotentials des online-systems ANTAR zur Verkehrsuberwachung. *Publikationen der DGPF*, *16*, 571-578.

Lewis, G. (2007). *Evaluation the use of a low-cost unmanned aerial vehicle platform in acquiring digital imagery for emergency response*. Springer Berlin Heidelberg.

Lim, H. S., & MatJafri, M. Z., Abdullah, K., Wong, C. J., & N. Mohd. Saleh. (2009). Regional land cover/ use classification in Malaysia based on conventional digital camera imageries. *Proceeding of the 2009 IEEE Conference.* Big Sky, Montana ,USA.

Pentax optio A40. (2009). www.pentax.com

PTGui. (2009). http://www.ptgui.com.

Saura S., & Miguel-Ayanze J. S. (2002). Forest cover mapping in central Spain with IRS-WIFS images and multi-extent textual-contextual measures. *International Journal of Remote Sensing*, *23*(3), 603-608.

Tan, K. C., Lim, H. S., MatJafri, M. Z., & Abdullah, K. (2009). Landsat data to evaluate urban expansion and determine land use/ land cover changes in Penang Island, Malaysia. *Journal of Environmental Earth Sciences*, 1866-6299.

Thiemann, S., & Kaufmann, H. (2002). Determination of chlorophyll content and tropic state of lakes using field spectrometer and IRS-IC satellite data in the Mecklenburg lake district, Germany. *Remote Sensing of Environment*, *73*, 227-235.

Weng, Q. (2001). A remote sensing-GIS evaluation of urban expansion and its impact on surface temperature in the Zhujiang Delta, southern China. *International Journal of Urban and Regional Studies*, *22*, 425-442.

ISSN: 0128-7680
Pertanika J. Sci. & Technol. **19 (S)**: 77 - 82 (2011)

Digital Elevation Model (DEM) Generation from Stereo Images

C. E. Joanna Tan*, M. Z. Mat Jafri, H. S. Lim and K. Abdullah
School of Physics, Universiti Sains Malaysia,
Minden 11800 Penang, Malaysia
**E-mail: vincci_jo@hotmail.com*

ABSTRACT

Digital elevation model (DEM) generation from stereo images is an effective and economical method in topography mapping. This paper used the stereo pair methodology to generate the digital elevation model (DEM) from PRISM (Panchromatic Remote-Sensing Instrument Satellite) sensor which is onboard of ALOS (Advanced Land Observing Satellite). The pair of forward-backward is used as stereoscopic imagery in this study. Ten ground control points (GCPs) are collected with residual error 0.49 pixels to generate an absolute DEM. This generated DEM with 2.5 m spatial resolution is then matched with the 90 m spatial resolution of SRTM (Space Shuttle Radar Topography Mission) DEM to compare the result. Although SRTM-DEM has a much coarser resolution, the positional accuracy of the matching is found. The difference of the height from the mean sea level (MSL) between the SRTM-DEM and the PRISM-DEM is analyzed and the correlation between the two DEMs is R^2=0.8083. The accuracy of the DEM generated is given by the RMSE value of 0.8991 meter.

Keywords: PRISM, DEM, stereoscopic imagery

INTRODUCTION

A Digital Elevation Model (DEM) is digital data in which each point represents X-, Y-, and Z-coordinates or latitude, longitude, and height describing the bare soil (Lee *et al*., 2003). Extraction of accurate DEMs is important for flood planning, map generation, three-dimensional GIS, erosion control, environmental monitoring, and others. The accuracy of DEMs based on space images is mainly depending upon the image resolution, the height-to-base-relation, and the image contrast. Currently, several different technologies are being used to generate large area DEMs at various resolutions and accuracies, each with their own various resolution and limitation (Chekalin and Fomtchemko, 2000).

DEM generation requires many processing steps such as camera modeling, stereo matching, editing, interpolating, and so on. All these steps contribute to the quality of DEM. Among all the steps, stereo matching is crucial to the accuracy and completeness of a DEM. Stereo matching is a process of finding conjugate points in a stereo image pair. A number of publications regarding stereo matching techniques for various applications have been published using processing software of DEM and ortho-rectified image using triplet image matching technique (Hashimoto, 2000; Takaku *et al*., 2005; Dhond and Anggarwal, 1989).

With the strong advantage in providing high resolution of 2.5 m with three independent optical systems in viewing forward, nadir, and backward that provides along-track overlapping images, PRISM sensor on-board ALOS (Advanced Land Observation Satellite) is capable to provide along-track stereoscopic imagery. PRISM is a panchromatic radiometer with a wavelength of 0.52μm to

Received: 1 August 2010
Accepted: 22 June 2011
*Corresponding Author

0.77µm and 2.5m spatial resolution. Its high resolution of 2.5 m has a good potential for 1:25,000 scale maps (Takaku *et al*., 2005; Bignono and Umakawa, 2008; Trisakti and Pradana, 2007).

The nadir view telescope provides a swath of 70 km width while the forward and backward view telescope provide a swath of 35km. The forward and backward view telescopes are inclined by ±24º from nadir to realize a base to height ratio of one at an orbital altitude of 692 km.

This paper describes DEM generation method from ALOS-PRISM stereo pair imagery and evaluates the accuracy of generated ALOS-DEM by comparing it to SRTM-DEM of 90 m spatial resolution. The SRTM obtained elevation data on a near global scale (80% of the land mass) to generate the most complete high resolution digital topographic database of Earth. It consists of a specially modified radar system that flew onboard the Space Shuttle Endeavour during an 11 days mission in February 2000. Data in a resolution of 90 m at the Equator is freely provided for most of the planet (Rodriguez *et al*., 2006).

METHODOLOGY

The study area is located in Penang Island, Malaysia, within latitudes 5º 12'N to 5º 30'N and longitudes 100º 09'E to 100º 26' E. The map region is shown in *Fig. 1*. However, in this study our focus was on Georgetown area.

Fig. 1: The location of the study area

The imagery of ALOS-PRISM dated 7th December 2006 was used to generate the elevation. The forward-backward pair used in this paper is shown in *Fig. 2(a)* and *(b)*.

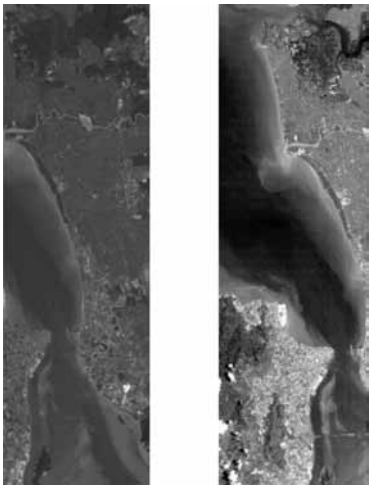

(a) (b)

Fig. 2: (a) Forward-viewing imagery; (b) Backward-viewing imagery

In DEM generation process, PCI OrthoEngine software was used. It supports the reading of different satellite data, GCP collection, geometric modeling, orthorectification, image matching, DEM generation, and so on. Different correction methods are provided in the software. However, the rational polynomial function method was selected during the image processing.

During epipolar generation process forward view imagery was used as left stereo pair while the backward viewing imagery was used as right stereo pair. To define the relationship between the two stereo imageries the GCP points play important role. 10 GCP points were collected in the pair of tile imagery, with residual error of 0.49 pixels. The generated DEM is absolute in the sense that the horizontal and vertical reference systems are tied to geodetic coordinates. The generated GCPs must be checked and corrected to reduce the parallax error. The epipolar geometry was calculated and generated automatically by the software. It is important to re-project the stereo pair so that the left and right images have a common orientation, matching feature between the images appear along the x-axis. It helps to reduce the possibility of incorrect matches. The last step is generating the DEM.

After generating the PRISM-DEM, the result was then matched with SRTM-DEM to find the positional accuracy. Next, a comparison between PRISM-DEM and the SRTM-DEM was made by taking 30 ground points randomly to obtain the elevation from both DEMs. The accuracy was found through plotting the correlation graph between the data of SRTM-DEM and of PRISM-DEM.

RESULTS AND DISCUSSION

PRISM-DEM was generated from the forward-backward viewing pair by using 10 GCPs with the residual error of 0.49 pixels. The generated PRISM-DEM is shown in *Fig. 3*.

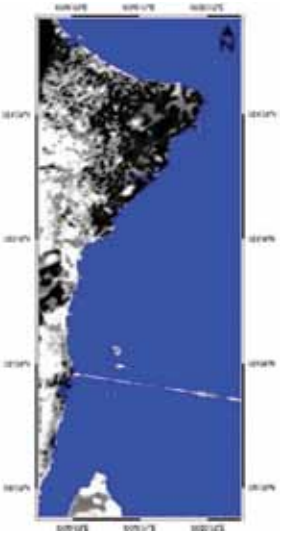

Fig. 3: Generated PRISM-DEM

The colour indicates the elevation value where:
White colour – ≥ 20 m
Grey colour – 6 m – 19 m
Black colour – ≤ 5 m
Blue colour – sea

From *Fig. 3*, it shows that the black and grey colour areas are urban area with the elevation less than 20 m.

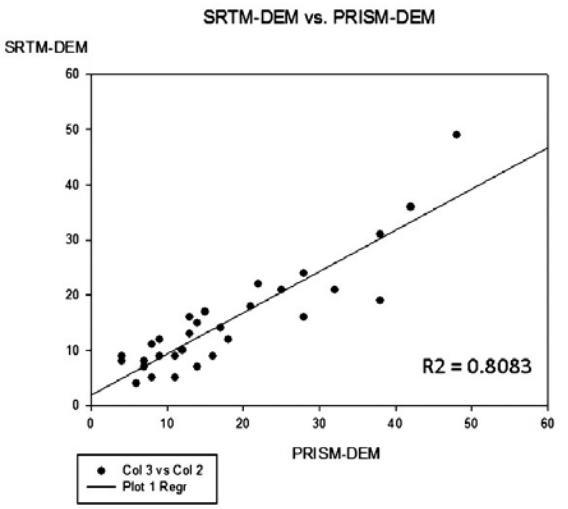

Fig. 4: SRTM-DEM data vs. PRISM-DEM data

Validation analysis was carried out to determine the accuracy of PRISM-DEM by comparing the elevation data with the SRTM-DEM. It was found that, the height distribution between PRISM-DEM and SRTM-DEM has few differences in m.

The correlation between the two DEMs data was analyzed as well. 30 control points were collected to plot the graph with linear regression. The graph gives a correlation of $R^2 = 0.8083$ as shown in *Fig. 4* and the RMSE (root mean square error) of 0.8991 m.

In this study, the sea area often gives misleading elevation values; therefore the sea area was set to a constant value to improve the model. However, the study will be continued and the problem of misleading elevation values will be studied in future.

CONCLUSION

This paper describes DEM generation from forward-backward viewing stereoscopic pair of ALOS-PRISM using commercial software PCI OrthoEngine. The stereo pair data can be used to generate DEM with high spatial resolution of 2.5 meter. Visual observation result shows that it has a smooth elevation pattern. However, the sea area provides misleading elevation and it is still under research process.

ACKNOWLEDGEMENTS

This research is conducted under the agreement of JAXA Research Announcement titled "2nd ALOS Research Announcement for the Advanced Land Observation Satellite between the Japan Aerospace Exploration Agency and the Research – The use of ALOS data in studying environmental changes in Malaysia."

Special thanks dedicated to Universiti Sains Malaysia for supporting and funding this research. Thanks to JAXA for providing the satellite images.

REFERENCES

Chekalin, V. F., & Fomtchemko, M. M. (2000). Comparative characteristics of DEM obtained from satellite images SPOT-5 and TK-350. Sovinformsputnik, 47 Leningrad Sky Pri, 125167 Moscow, Russia.

Bignono, F., & Umakawa, H. (2008). Assessment of ALOS PRISM digital elevation model extraction over Japan. *The International Achieves of the Photogrammetry, Remote Sensing and Spatial Information Sciences*, *XXXVII*(B1). Beijing.

Dhond, U. R., & Anggarwal, J. K. (1989). Structure from stereo – A review. *IEEE Transaction on System, Man and Cybernetics*, *19*(6), 1489-1510.

Hashimoto, T. (2000). DEM generation from stereo AVNIR images. *Adv. Space Res*., *25*(5), 931-936.

Lee, H-Y., Kim, T., Park, W., & Lee, H. K. (2003). Extraction of digital elevation models from satellite stereo images through stereo matching based on epipolarity and scene geometry. *Image and Vison Computing*, *21*, 789-796.

Rodriguez, E., Morris, C. S., Belz, J. E., Chapin, E. C., Martin, J. M., Daffer, W., & Hensley, S. (2006). An Assessment of SRTM Topographic Product JPL Report.

Takaku, J., Futamura, N. Iijima, T., Tadono, T., shimada, M., Shibasaki, R. (2005). High resolution DSM generation from ALOS PRISM data – Pre-launch simulation and assessment plans. *Proceeding IGARSS 2005*. Seoul, IEEE.

Trisakti, B., & Pradana, F. A. (2007). DEM generation from PRISM ALOS and ASTER. *Proceeding Geo-Marin Research Forum.*

ISSN: 0128-7680
Pertanika J. Sci. & Technol. **19 (S)**: 83 - 88 (2011)

Land Cover Classification of ALOS PALSAR Data Using Maximum Likelihood and Dual Mode Polarization

C. K. Sim*, K. Abdullah, M. Z. Mat Jafri and H. S. Lim
School of Physics, Universiti Sains Malaysia,
Minden 11800 Penang, Malaysia
**E-mail: cksim_83@yahoo.com*

ABSTRACT

Microwave Remote sensing data have been widely used in land cover and land use classification. The objective of this research paper is to investigate the feasibility of the multi-polarized ALOS-PALSAR data for land cover mapping. This paper presents the methodology and preliminary result including data acquisitions, data processing and data analysis. Standard supervised classification techniques such as the maximum likelihood, minimum distance-to-mean, and parallelepiped were applied to the ALOS-PALSAR images in the land cover mapping analysis. The PALSAR data training areas were chosen based on the information obtained from optical satellite imagery. The best supervise classifier was selected based on the highest overall accuracy and kappa coefficient. This study indicated that the land cover of Butterworth, Malaysia can be mapped accurately using ALOS PALSAR data.

Keywords: ALOS-PALSAR, land cover, land use

INTRODUCTION

The availability of remote sensing data applicable for global, regional, and local environment monitoring has greatly increased over recent years (Ehlers *et al*., 2003). Over the past few decades, manual and computer-assisted image interpretation techniques were applied to optical Landsat MSS, Landsat TM, and SPOT imagery to classify land cover (Johnson and Rohde, 1981; Hutchinson, 1982; Franklin and Logan, 1986; Gross *et al*., 1988; Tucker *et al*., 1985). In recent years, researchers have been investigating the use of longer wavelength radar imagery to obtain additional land cover information. Radar remote sensing is one of the main tools used for natural resource mapping and monitoring. Its ability to produce images independently of sun illumination and weather conditions makes it particularly suitable for monitoring tropical forest, where optical systems fail to provide timely and continuous information (Kasischeke *et al*., 1997). It has been shown that radar returns can be used to effectively identify forested areas and to create models of their structural composition. Many studies have indicated the correlation between radar returns and the different land cover types. Correlations were found between backscattering and forest structure, leading to increasing interest in the use of radar systems for estimating above ground biomass (Imhoff, 1995). Supervised classification of Maximum Likelihood, Minimum Distance-to-mean, and Parallelepiped classifier method was applied to the digital image. The monitoring task can be accomplished by supervised classification techniques, which have proven to be effective categorization tools (Bruzzone *et al*., 2002). The objective of supervised classification in remote sensing is to identify and partition the

Received: 1 August 2010
Accepted: 22 June 2011
*Corresponding Author

pixels comprising of the noisy image of the area according to its class (Yu and Ekstrom, 2003). Supervised classification of multispectral remote sensing imagery is commonly used for land cover determination (Duda and Canty, 2002). Post-classification of accuracy assessment also was carried out in this study.

The objective has been to evaluate high-resolution ALOS-PALSAR data in a variety of applications involving land use and land cover mapping. The application of optical data, such as that obtained by LANDSAT and SPOT has a limitation on weather conditions, especially cloud coverage in equatorial region. Many studied have been done using SAR data for land cover mapping, particularly in tropical countries. The traditional method of collecting data for planning is surveying samples at field.

STUDY AREA

The study area is Butterworth, Malaysia, located within latitudes 5° 08' N to 5° 33' N and longitudes 100° 21' E to 100° 32' E. The map of the region is shown in *Fig. 1*. The satellite image was acquired on 1 November 2007.

Fig. 1: Study area

DATA ANALYSIS AND RESULTS

All image-processing tasks were carried out using PCI Geomatica version 10.1 digital image processing. Geocoded ALOS-PALSAR L-band polarimetric data with 12.5 m spatial resolution

and 21.5 degree incident angle recorded on 1 November 2007 was used in the analysis of land cover classification in Butterworth, Malaysia. *Fig. 2* shows the ALOS PALSAR raw satellite image.

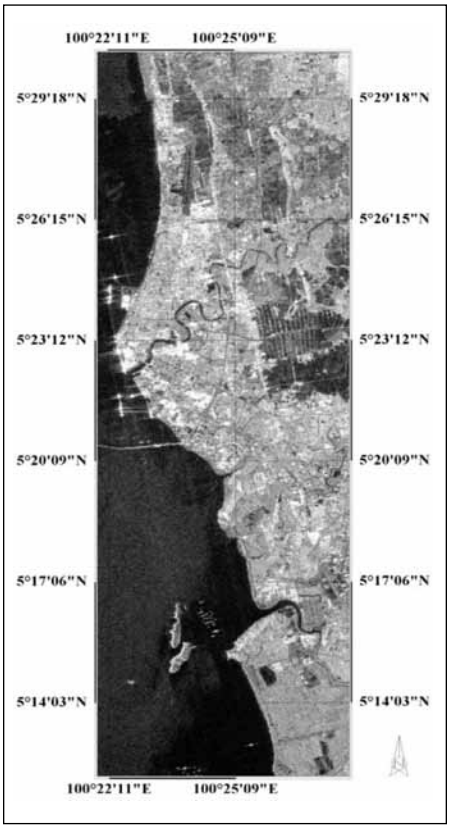

Fig. 2: ALOS-PALSAR raw satellite image

The ASF MapReady program from Alaska satellite Facility Geographical Institute at the University of Alaska Fairbanks was used for radiometric correction, geometric correction and terrain correction of the ALOS-PALSAR data. Digital elevation model (DEM) of Shuttle Radar Topographic Mission (SRTM, http://srtm.usgs.gov) 90 m resolution elevation data was used for geometric correction of ALOS PALSAR data with different incident angles. This process also removed artifacts commonly seen in SAR data such as layover and shadow.

Radiometric and geometric corrections were applied to the ALOS PALSAR data acquired on 1 November 2007. For analyzing the synergistic effects of SAR data with different polarization and incident angles it is essential to work with geometric highly referenced data. After converting DN to Sigma-naught to obtain radar backscattering coefficients, geometric terrain correction using DEM data to prevent relief displacement was calculated. DN values were converted to sigma-naught to obtain radar backscattering coefficients. In this study, a medium filter with a 3 × 3 window size to reduce speckle noise of ALOS-PALSAR image.

A Landsat TM satellite image of 128/56 (path/row) on 8 February 2007 was use for the selection of training areas and validation purposes. Standard supervised classification techniques such as the maximum likelihood, minimum distance-to-mean, and parallelepiped were used for land cover

classification. Every single acquisition mode was classified using the same training areas derived from the optical satellite data. The satellite image was classified into 3 classes namely vegetation, water, and urban. Accuracy assessments determined the correctness of the classified map.

A total of 200 samples were chosen randomly for the accuracy assessment. Two methods of accuracy assessments were tested in this study, the overall classification accuracy and kappa coefficients. In this study, dual mode microwave ALOS PALSAR was used for land cover mapping and the accuracies of the final land use/land cover map has been improved significantly. The overall classification accuracy and Kappa coefficient by using single mode polarization microwave (HH) ALOS PALSAR are shown in Table 1. The overall classification accuracy and Kappa coefficient by using dual mode polarization microwave ALOS PAISAR are shown in Table 2.

TABLE 1
The overall classification accuracy and Kappa coefficient by using single mode polarization microwave (HH) ALOS PALSAR data

Classification method	Overall classification accuracy (%)	Kappa coefficient
Maximum likelihood	77.9	0.65
Minimum distance-to-mean	64.5	0.47
Parallelepiped	0.5	0.003

TABLE 2
The overall classification accuracy and Kappa coefficient by using dual mode polarization microwave ALOS PAISAR data

Classification method	Overall classification accuracy (%)	Kappa coefficient
Maximum likelihood	80.0	0.70
Minimum distance-to-mean	70.0	0.55
Parallelepiped	1.0	0.007

In this study, the Maximum Likelihood classifier produced the highest accuracy with overall classification accuracy of 80.0% and Kappa coefficient of 0.70. These results showed the advantage of using high spatial resolution ALOS PALSAR data to characterize land cover using Maximum Likelihood classifier. Due to frequent cloud cover of satellite imagery and the time consuming activities, we recommend the use of ALOS PALSAR data to provide remotely sensed data for land cover classification at local scale. A classified image using Maximum Likelihood classifier with dual mode polarization microwave ALOS PAISAR is shown in *Fig. 3*.

In this study, an increase of the overall classification accuracy and kappa coefficient were obtained with dual mode polarization microwave data compared to the single mode polarization microwave data (Tables 1 and 2). The overall classification accuracy and kappa coefficient using dual mode polarization microwave data (80.0% and 0.70 respectively) were always better than the single mode polarization microwave data (77.9% and 0.65 respectively) for Maximum Likelihood classifier.

The assessment results showed a reasonably good agreement between the land cover data set and the reference data. The overall classification accuracies obtained with single mode polarization microwave data achieved by the supervised classification of Maximum Likelihood, Minimum Distance-to-mean and Parallelepiped classifier were 77.9%, 64.5%, and 0.5% respectively.

While the overall classification accuracies obtained with dual mode polarization microwave data achieved by the supervised classification of Maximum Likelihood, Minimum Distance-to-mean, and Parallelepiped classifier were 80.0%, 70.0%, and 1.0% respectively. The overall accuracy and kappa coefficient values for the three classification techniques are shown in Tables 1 and 2 for single mode polarization microwave data and dual mode polarization microwave data respectively.

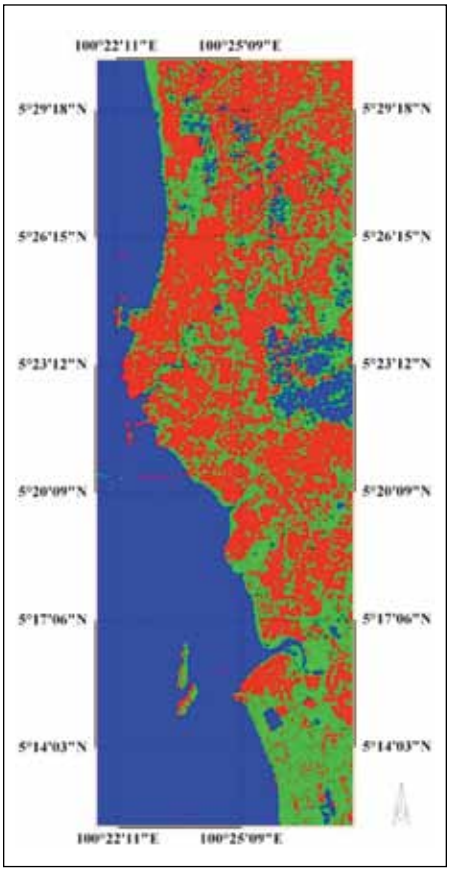

Fig. 3: The land cover map using ALOS-PALSAR image [color Code: Green= Vegetation, Blue = Water, and Red = Urban]

CONCLUSION

The decision based on dual mode polarization microwave ALOS PALSAR data is quite simple but effective to classify different land features from satellite data. The use of multimode data increases the accuracy in land cover identification. In this study, it was found that the Maximum Likelihood classifier with dual mode polarization microwave ALOS PALSAR data produced the highest degree of accuracy. This study also showed that the microwave remote sensing data provides an alternative solution to the land cover mapping problem in a cloudy equatorial region such as Malaysia. The classified map can be used to provide useful data for planning and management in this area.

ACKNOWLEDGEMENTS

This research is conducted under the agreement of JAXA Research Announcement entitled '2 nd ALOS Research Announcement for the Advanced Land Observation Satellite between the Japan Aerospace Exploration Agency and the Research - The use of ALOS data in studying environmental changes in Malaysia' (JAXA – 404). The authors would like to express special thanks to Alaska satellite Facility Geographical Institute at the University of Alaska Fairbanks for providing the ASF MapReady programs free software used in this study. Thanks are extended to USM for support and encouragement.

REFERENCES

Bruzzone, L., Cossu, R., & Vernazza, G. (2002). Combining parametric and non-parametric algorithms for a partially unsupervised classification of multitemporal remote-sensing images. *Information Fusion*, *3*, 289-297.

Duda, T., & Canty, M. (2002). Unsupervised classification of satellite imagery: Choosing a good algorithm. *International Journal of Remote Sensing*, *23*(11), 2193-2212.

Ehlers, M., Gahler, M., & Janowsky, R. (2003). Automated analysis of ultra high resolution remote sensing data for biotope type mapping: New possibilities and challenges. *ISPRS Journal of Photogrammetry & Remote Sensing*, *57*, 315-326.

Franklin, J., Logan, T. L., Woodcock, C. E., & Strahler. A. H. (1986). Coniferous forest classification and inventory using LANDSAT and digital terrain data. *IEEE Transactions on Geoscience and Remote Sensing*, *26*, 139-149.

Gross, M. F., Klemas, V., & Levasseur, J. E. (1988). Remote sensing of biomass of salt marsh vegetation in France. *International Journal of Remote Sensing*, *9*, 397-408.

Hutchinson, C. F. (1982). Techniques for combining LANDSAT and ancillary data for digital classification improvement. *Photogrammetric Engineering and Remote Sensing*, *48*, 123-130.

Imhoff, M. L. (1995). A theoretical-analysis of the effect of forest structure on synthetic-aperture radar backscatter and the remote-sensing of biomass. *IEEE Transactions on Geoscience and Remote Sensing*, *33*(2), 341-352.

Johnson, G. R., & Rohde, W. G. (1981). LANDSAT digital analysis techniques required for wild land resource classification. *Proc. Arid Land Resource Inventories: Developing Cost- Effective Method* (pp. 204-213). LaPaz, Mexico.

Kasischke, E. S., Melack, J. M., & Dobson, M. C. (1997). The use of imaging radars for ecological applications-A review. *Remote Sensing of Environment*, *59*(2), 141-156.

Tucker, C. J., Townshend, R. G., & Goff, T. E. (1985). African land-cover classification using satellite data. *Science*, *227*, 369-375.

Yu, J., & Ekstrom, M. (2003). Multispectral image classification using wavelets: A simulation study. *Pattern Recognition*, *36*, 889-898.

ISSN: 0128-7680
Pertanika J. Sci. & Technol. **19 (S)**: 89 - 96 (2011)

Monthly Distribution Map of Carbon Monoxide (CO) from AIRS over Peninsular Malaysia, Sabah and Sarawak for the year 2003

Jasim M. Rajab*, M. Z. Mat Jafri, H. S. Lim and K. Abdullah
School of Physics, Universiti Sains Malaysia,
Minden 11800 Penang, Malaysia
**E-mail: jasim_rijab@yahoo.com*

ABSTRACT

Carbon monoxide (CO) is a ubiquitous, an indoor and outdoor air pollutant. It is not a significant greenhouse gas as it absorbs *little* infrared radiation from the Earth. It is produced by the incomplete combustion of fossil fuels, and biomass burning. The CO data are obtained from Atmospheric Infrared Sounder (AIRS) onboard NASA's Aqua satellite. The AIRS provides information for several greenhouse gases, CO_2, CH_4, CO, and O_3 as a one goal of the AIRS instrument (included on the EOS Aqua satellite launched, May 4, 2002) as well as to improve weather prediction of the water and energy cycle. The results of the analysis of the retrieved CO total column amount (CO_total_column_A) as well as effective of the CO volume mixing ratio (CO_VMR_eff_A), Level-3 monthly (AIR*3STM) 1º*1º spatial resolution, ascending are used to study the CO distribution over the East and West Malaysia for the year 2003. The CO maps over the study area were generated by using Kriging Interpolation technique and analyzed by using Photoshop CS. Variations in the biomass burning and the CO emissions where noted, while the highest CO occurred at late dry season in the region which has experienced extensive biomass burning and greater draw down of CO occurred in the pristine continental environment (East Malaysia). In all cases, the CO concentration at West Malaysia is higher than East Malaysia. The southeastern Sarawak (lat. 3.5˚ - long. 115.5˚) is less polluted regions and less the CO in most of times in the year. Examining satellite measurements revealed that the enhanced CO emission correlates with occasions of less rainfall during the dry season.

Keywords: AIRS, carbon monoxide, Malaysia, AMSU, Sabah and Sarawak

INTRODUCTION

Many gases occur naturally in the atmosphere, while other from industrial wastes emissions. Global air pollution became increasingly dangerous to the health of the earth over the past two decades and minimal environmental limitations in many nations. In Malaysia, industrialization, urbanization, and rapid traffic growth has contributed significantly to economic growth. With this believed to be responsible for increasing emissions of gaseous pollutants. Pockets of heavy pollution are being created by emissions from major industrial zones, a dramatic increase in the number of residences, office buildings, manufacturing facilities, and increases in the number of motor vehicles.

Southeast Asia is experiencing a similar rapid economic growth to that in Northeast Asia. Also a large source of several air pollutants may make to regional and global pollution because of increasing anthropogenic emissions associated with biogenic emissions from large tropical forests. The greater oxidizing capacity in the tropical regions is due to a higher UV intensity, humidity, rapid development, and industrialization (Kato and Akimoto, 1992; Lavorel *et al*., 2007; Marshall *et al*., 2006; Streets *et al*., 2001).

Received: 1 August 2010
Accepted: 22 June 2011
*Corresponding Author

A concentration of as little as 400ppm (0.04%) carbon monoxide in the air can be fatal. The levels of normal carboxyhemoglobin in an average person are less than 5%, whereas cigarette smokers (two packs/day) may have levels up to 9% (Delaney *et al*., 2001). The carbon monoxide (CO) is a tasteless gas that slightly lighter than air. It is the most abundant pollutant in urban atmospheres and very stable, having an average lifetime of 2-4 months in the atmosphere, produced by human activities approximately 50% of emissions come from anthropogenic sources, the remainder from biomass burning and oxidation of naturally occurring volatile hydrocarbons accounting for nearly 50% of tropospheric CO (Thompson, 1992). The CO has an influence on oxidization in the atmosphere by interaction with hydroxyl radicals (OH), halocarbons, tropospheric ozone, and methane but not considered a direct greenhouse gas because it does not absorb terrestrial thermal IR since it account for 75% of hydroxyl radicals (OH) sinks (Thompson *et al*., 1994).

Fires are considered as one of the largest anthropogenic influences on terrestrial ecosystems after agricultural and urban activities (Lavorel *et al*., 2007). In the Southeast Asia, many factors such as social, economic, and environmental impacts caused by forest and land fires. Tropical haze from peat fires has serious negative impacts on the human health and regional economy, and peat land fires affect global carbon dynamics (De Groot *et al*., 2007).

Trace gas abundances in the troposphere during the past two decades were obtained from sparsely distributed measurement sites, and observations were mostly confined to the surface (Clerbaux *et al*., 2003). The measurement of atmosphere pollution from satellite (MAPS) instrument onboard the space Shuttle with subsequent MAPS flights in 1984 and 1994 was the first satellite observations of the carbon monoxide (Connors *et al*., 1994).

Launched onboard NASA's Aqua satellite on 4 May 2002, Aqua's cross-track scanning Advanced Microwave Sounding Unit (AMSU) with AIRS cross-track scanning grating spectrometer coupled, provide vertical profiles of the atmosphere with a nadir 45 km field-of-regard (FOR) across a 1650 km swath. AIRS broad spectral coverage (3.7 to 16 μm with 2378 channels) includes spectral features of CH_4, CO, O_3, and CO_2. The objectives of the AIRS is to determine the factors that control the global energy and water cycles, investigation of atmosphere-surface interactions, improving numerical weather prediction, assessing climate variations and feedbacks and detection of the effects of increased carbon dioxide, methane, ozone, and other greenhouse gases. The term "sounder" in the instrument's name refers to the fact that water vapor and temperature are measured as functions of height. AIRS measure CO total column by (36) channels with uncertainty estimate 15-20% at 500mb, vertical coverage 1000 - 1 mb, global non-polar, mid-tropospheric total, (7 - 9) layers, troposphere carbon monoxide (CO) abundance are retrieved in the 4.58-4.50 μm (2180-2220 cm^{-1}) region from the AIRS measured radiances of the IR spectrum (Chahine *et al*., 2006).

This study is based on the CO retrievals from a research version of the current AIRS operational physical algorithm, used Standard Level-3 Monthly gridded product (AIRX3STM) 1º×1º spatial resolution, Version 5 data, using AIRS IR and AMSU, without-HSB, to investigate Monthly, Yearly, wet season and dry season distribution map of the carbon monoxide over peninsular Malaysia, Sabah and Sarawak for the year 2003. By using Retrieved the CO total column amount (CO_total_column_A) as well as effective of the CO volume mixing ratio (CO_VMR_eff_A). The CO concentration maps of the study area were processed and analyzed using Photoshop CS and SigmaPlot 11.0 software to assess the carbon monoxide distribution in the atmosphere over the study area.

STUDY AREA AND DATA

An area covering 1.725×10^6 km^2, with a center at South Chinese sea (109.5º E and 3.5º N) was selected for this study .The extent of the domain was chosen so that it is sufficiently large to contain

the CO plumes. The central dimensions of the study domain are 2300 km E-W and 750 km N-S. The period from (2003) was selected to study the CO distribution. The data used for this study include the CO data from AIRS; they were extracted for the study area and were processed to match in space and time. The carbon monoxide data were derived from the Atmospheric Infrared Sounder (AIRS) Version 5 Level 3 data available at http://disc.sci.gsfc.nasa.gov/data/datapool/AIRS_DP/, as well as auxiliary data that include the corresponding location and time along the satellite track in HDF (Hierarchical Data Format) format on monthly basis. Using the location information, CO data were gridded Monthly at Geospatial Resolution: 1 degrees x 1 degree (lat x long).

Fig.1: Study area

ACQUISITION AND SPECIFICATION

The AIRS spectrometer is devised to operate in synchronism with the microwave instruments AMSU-A1, AMSU-A2, and HSB and its science objectives is to determined of the factors that control the global energy and water cycles, inquisition of atmosphere-surface interactions, improving numerical weather prediction, evaluating climate variations and feedbacks and diagnosis of the effects of increased the carbon dioxide, methane, ozone, and other greenhouse gases. Table 1 describes AIRS Technology – specifications. AIRS infrared spectrometer acquires 2378 spectral samples at resolutions, $\lambda/\Delta\lambda$ ranging from 1086 to 1570, in three bands: 3.74 μm to 4.61 μm, 6.20 μm to 8.22 μm, and 8.8 μm to 15.4 μm. Tropospheric carbon monoxide abundance is retrieved in the 4.58-4.50 μm (2180-2220 cm^{-1}) region from the AIRS measured radiances of the IR spectrum

and using the AIRS 1600-km cross-track swath and cloud-clearing retrieval capabilities. It is capable to retrieve daily global CO maps cover approximately 70% of the Earth (Chahine *et al*., 2006). Monthly (AIRX3STM) 1°x1° spatial resolution, Level-3 ascending (day time), results from the analysis of the retrieved CO total column amount (CO_total_column_A) as well as effective CO volume mixing ratio (CO_VMR_eff_A) are used in this work. The V5 Level-3 gridded product is derived from the Level 2 standard swath products. (36) Channels at 500mb, Vertical Coverage 1000 - 1 mb, (7 - 9) layers, are used in the Version 5.0 for retrieved troposphere.

TABLE 1
AIRS technology – specification

Instantaneous Field of View (IFOV)	1.1°
Spectral resolution	13.5x13.5 km in the nadir
Coverage	pole-to-pole & covers the globe two times a day
Orbit	438 miles (705.3km) polar, sun synchronous, 98.2+/- .1 degrees inclination, ascending node 1:30pm +/- 15 minutes, period 98.8 minutes
Ground coverage	+/- 49.5 degrees around nadir
Ground footprint	90 per scan, 22.4 ms footprint
Temporal coverage	Global, twice daily swath (daytime and nighttime)
Radiometric calibration	+/- 3% absolute error
Spatial coverage	Scan Angle: +/- 49.5 around nadir IFOV: 0.185
Power / Mass	256 W / 166 kg
Swath width	

RESULTS AND DISCUSSION

Southeast Asia is in the tropics, seasons are not as precise as in more temperate zones, and typically only dry and wet seasons can be clearly distinguished. The dry and wet seasons in the insular Southeast Asia and in continental Southeast Asia are at opposite times of the year because of the various circulations in the southern and northern hemispheres. The strong monsoon and the associated movement of the inter-tropical convergence zone (ITCZ) were dominated by the climatology of continental Southeast Asia and air mass transport in this region. When the inter-tropical convergence zone (ITCZ) relocates southern across Southeast Asia into the southern hemisphere, the winter monsoon brings marine air masses from the northern Asia to the region. This region experiences a dry season for about six months (November - April) before the ITCZ moves back to the northern hemisphere and long-range transport of continental air masses from the Indian Ocean in the summer monsoon prevails during the subsequent wet season (May - October). Unlike boreal forest fires, the tropical biomass burning is a major source of the atmospheric pollutants in the Southeast Asia. It is strongly influenced by anthropogenic post-agricultural waste burning, and occurs consistently each year (Christopher *et al*., 1998).

The AIRS/AQUA (AIRX3STM), level 3 CO retrieval product monthly (calendar), 1°×1° spatial resolution, version 5 data, using AIRS IR and AMSU, without-HSB, were used to investigate monthly, yearly, wet season and dry season distribution map of carbon monoxide over peninsular Malaysia, Sabah and Sarawak for the year 2003. By using Photoshop CS & SigmaPlot 11.0 software, map was generated for the retrieved total column CO (molecules/cm²) (CO_total_Column_A) as well as (CO_VMR_eff_A) Effective CO Volume Mixing Ratio over study area.

The six maps in *Figs. 2a-2f* illustrate the extent of AIRS monthly coverage CO total column, the nominal peak of airs vertical sensitivity and the magnitude of the seasonal variations CO at wet season (May – October) 2003. Note that the decrease in the values of the carbon monoxide total column during wet season with rather abrupt decreases, relatively high values, on June at Peninsular Malaysia and on September at west Sarawak & Johor, because of some small fires that have occurred in Pulau Perdamaran and Kalimantan Barat, Indonesia. The CO total column is lowest in the north Perak, east Sarawak and pristine marine environment of Sabah (1.482×10^{18} molecules/cm²) on July (lat. 3.5° – long. 115.5°), increase at the west Sarawak, and highest in the peninsular Malaysia (2.2945×10^{18} molecules/cm²) on June (lat. 4.5° – long. 100.5°).

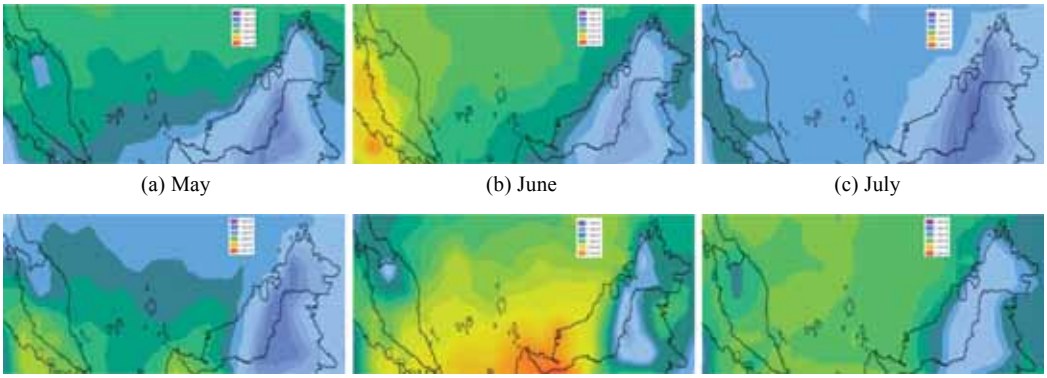

(a) May (b) June (c) July

(d) August (e) September (f) October

Fig. 2: Monthly coverage retrieved total column CO, from [May to October 2003] wet season

During the wet season, the Southeast Asia is govern by marine air masses from the middle and low latitudes of the Southern Hemispheric Indian Ocean, which bring small to moderate amounts of air pollution to continental Southeast Asia also there is no clear observational evidence that the transport of air pollution exerts a strong effect on the Southeast Asia. Particularly due to the transport attributes of the region, as well as previous study and investigations showed minimum values of the CO occurs at wet season (Tsutsumi and Matsueda, 2002).

Figs. 3a-3f illustrate the extent of AIRS monthly coverage Carbon Monoxide at dry season (November – April) 2003. It clearly showed, elevated CO values appear over west Malaysia especially over Penang, Johor, along the coast of Sarawak and Selangor. These regions represent biomass burning sources, long-rang transport, and industrial/domestic fuel sources, respectively and contributes to the burning of agricultural residues occur at this season. Enhanced CO values in Sabah and Southeast Sarawak on April. During the late months of dry season, biomass burning is a large source of atmospheric in the Southeast Asia, and also long-rang transport of air masses from the Middle East, western Asia, and from as far away may be found but because of the strong impact of regional burning makes it very difficult to detect any evidence of the long-rang transport of air pollution from other regions to Southeast Asia.

The CO total column is lowest in the Southeast Sarawak and pristine continental environment of Sabah (1.6252×10^{18} molecules/cm²) on April (lat. 3.5° – long. 115.5°), increase at the west and along the coast of Sarawak, and highest in the peninsular Malaysia (2.3218×10^{18} molecules/cm²) on December (lat. 4.5° – long. 100.5°).

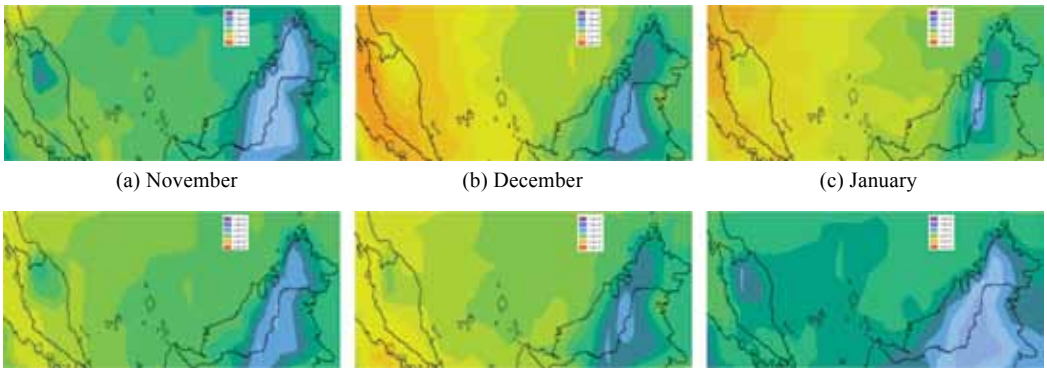

(a) November (b) December (c) January

(d) February (e) March (f) April

Fig. 3: Monthly coverage retrieved total column CO, from [November to April 2003] dry season

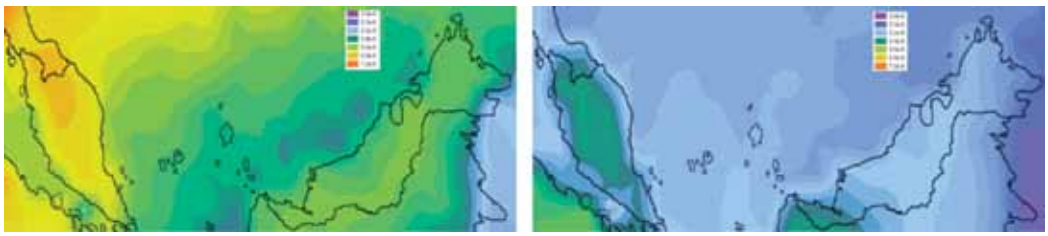

Dry season Wet season

Fig. 4: CO VMR [Volume Mixing Ratio] coverage for dry and wet season 2003

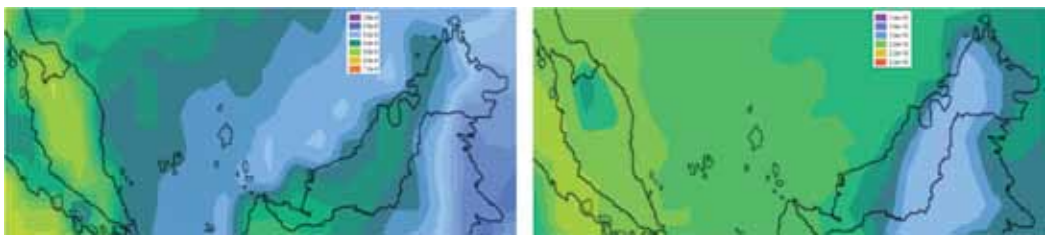

CO VMR (Volume Mixing Ratio) 2003 CO total column 2003

Fig. 5: CO Volume Mixing Ratio [VMR] & CO total column, yearly for 2003

Fig. 4 illustrate the extent of AIRS seasonally coverage of carbon monoxide VMR (Volume Mixing Ratio) [wet and dry seasons] 2003. Note the difference value of carbon monoxide between the two parts of Malaysia, on dry season, high value in the west and moderate values in the east, while on wet season, moderate values in the west and lowest values on the east. This seasonal dichotomy results primarily from seasonal photochemical cycle of OH, the primary oxidizer for CO.

In the wet season, OH abundance is near a maximum degree; the CO is near minimum degree. In contrast, the dry season coincides with the minimum of OH concentrations and thus a maximum for CO. The extensive sources are evident in Peninsular Malaysia and exhibits a large carbon monoxide abundances as well as its near the peak of the biomass burning seasons in Sumatra, so that CO in west Malaysia is higher than the east.

Fig. 5 illustrates the annual distribution of CO Volume Mixing Ratio & CO total column for 2003.The local CO maximum just west Malaysia occurs precisely in a region that experienced extensive biomass burning, Industrial area and congested urban zones in 2003. In contrast, it showed that less CO over Sabah and southeastern Sarawak, where the green lands and vast forests, and moderate over western Sarawak. AIRS sensitivity of CO over Sabah and southeastern Sarawak may be due to its vast forests and lack sources of pollution. Both of these time series showed the same seasonal cycle with rather abrupt decreases on June and September. The Selangor, Penang, and Perak have the highest values of pollution. Selangor presents the largest variations indicating a substantial number of the polluted days at times other than the seasonal peak.

CONCLUSION

As demonstrated in this study, the AIRS' monthly views of atmosphere CO across the study area enables detailed analyses of both the spatial and temporal variations in emissions and the visualization of subsequent transport. Investigation was carried out based on the information contained in the one year of AIRS data. The AIRS/Aqua Level 3 monthly CO retrieval Standard (Version 5.0) data, using AIRS IR and AMSU, without-HSB were used to evaluate the monthly, yearly, wet season, and dry season CO distributions, and quality of the satellite measurements.

Plainly evident of the highest values of the CO occurred when biomass burning during dry season (especially at late dry season), and also over the industrial and congested urban zones. The local maximum CO for west Malaysia occurs in a region that experienced extensive biomass burning in 2003 (lat. 4.5° – long. 100.5°). A greater draw down of the CO occurs in the pristine continental environment at East Malaysia on wet season (lat. 3.5° – long. 115.5°), where the green lands and vast forests and lack sources of pollution. In short, in all cases, the CO concentration at West Malaysia is higher than East Malaysia, and the southeastern Sarawak (lat. 3.5° – long. 115.5°) was cleaner regions and the less CO in most times of the year.

Continuing analyses combining chemical transport with the AIRS CO observations and inverse models will yield new insights on dynamical mixing during long-range transport and emission sources.

Satellite measurements are able to measure the increase of CO concentration in the troposphere over different regions of the Southeast Asia, from the AIRS data. From this study, it is expected that the CO maps will lead to a more understanding of the CO budget. Further study will be conducted to assess the effect of other pollutant and greenhouses gases based on the observation and measurement of the satellite (AIRS).

ACKNOWLEDGEMENTS

This project was carried out using the USM short term grants and Science Fund. We would like to thank the technical staff who participated in this project. Special thanks are extended to Brian Curtiss who provides the methods of measuring the sky transmittance using spectroradiometer. Thanks are also extended to USM for support and encouragement.

REFERENCES

Chahine, M. T., Thomas, S. P., Hartmut, H. A., Robert, A., Christopher, B., John, B., Luke, C., Murty, D., Eric, J. F., Mitch, G., Catherine, G., Stephanie, G., Scott, H., Fredrick, W. I., Ramesh, K., Eugenia, K., Bjorn, H. L., Sung-Yung, L., John, L. M., Mcmillan, W. W., Larry, M., Christopher, S. A., Chou, J., Welch, R. M., Kliche, D. V., & Connors, V. S. (1998). Satellite investigations of fire, smoke and carbon monoxide during April 1994 MAPS mission: Case studies over tropical Asia. *J. Geophys Res*., *103*, 19327-19336.

Clerbaux, C., Hadji-Lazaro, J., Turquety, S., M´egie, G., & Coheur, P.-F. (2003). Trace gas measurements from infrared satellite for chemistry and climate applications. *Atmos. Chem. Phys*., *3*, 1495-1508.

Connors, V. S., Gormsen, B. B., Nolf, S., & Reichle Jr. H. G. (1999). Spaceborne observations of the global distribution of carbon monoxide in the middle tropsphere during April and October 1994. *J. Geophys. Res.*, *104*, 21,455-21,470.

De Groot, W. J., Field, R. D., Brady, M. A., Roswintiarti, O., & Mohamad, M. (2007). Development of the Indonesian and Malaysian fire danger rating systems. *Mitig Adapt Strat Glob Change*, *12*, 165-180.

Delaney, K. A., Ling, L. J., & Erickson T. (2001). In M. D. Ford (Ed.), *Clinical toxicology.* WB Saunders Company.

Edward, O. T., Henry, R., Philip, R., William, S. L., David, S., Strow, L. L., Joel, S., David, T., Walter, W., & Lihang, Z. (2006). The atmospheric infrared sounder (Airs): Improving weather forecasting and providing new data on greenhouse gases. *American Meteorological Society*, *87*, 911- 926. DOI: 10.1175/BAMS-87-7-911.

Kato, N., & Akimoto, H. (1992). Anthropogenic emissions of SO2 and NOx in Asia: Emissions inventories (plus errata). *Atmos. Environ*., *26A*, 2997-3017.

Lavorel, S., Flannigan, M. D., Lambin, E. F., & Scholes, M. C. (2007). Vulnerability of land systems to fire: Interactions among humans, climate, the atmosphere, and ecosystems. *Mitig Adapt Strat Glob Change*, *12*, 33-53.

Marshall, J. L., Jung, J., Derber, J., Chahine, M., Treadon, R., Lord, S. J., Goldberg, M., Wolf, W., Liu, H. C., Joiner, J., Woollen, J., Todling, W., Delst, P. V., & Ahara, Y. (2006). Improving gobal aalysis and frecasting wth airs. *American Meteorological Society*, 891-894. DOI: 10.1175/BAMS-87-7-891.

Streets, D. G., Tsai, N. Y., Akimoto, H., & Oka, K. (2001). Trends in emissions of acidifying species in Asia, 1987-1997. *Water, Air, and Soil Pollution*, *130*, 187-192.

Thompson, A. M. (1992). The oxidizing capacity of the earth's atmosphere: Probable past and future changes. *Science*, *256*, 1157-1165.

Thompson, A. M., Pickering, K. E., Dickerson, R. R., Ellis, W. G., Jacob, D. J., Scala, J. R., Tao,W., McNamara, D. P., & Simpson, J. (1994). Convective transport over the central United States and its role in regional CO and ozone budgets. *J. Geophys. Res*., *99*, 18703-18711.

Tsutsumi, Y., & Matsueda, H. (2002). Relationship of ozone and CO at the summit of Mt. Fuji (35.35°N, 138.73°E, 3776 m above sea level) in summer 1997., 2002. *Atmospheric Environment*, *34*, 553-56.

ISSN: 0128-7680
Pertanika J. Sci. & Technol. **19 (S)**: 97 - 105 (2011)

Comparison of Fusion of Different Algorithms in Mapping of Melaleuca Forest in Marang District, Malaysia

M. M. Saberioon[1*], M. Mardan[1], L. Nordin[2] and A. Mohd Sood[3]
[1]Department of Agriculture Technology,
Faculty of Agriculture, Universiti Putra Malaysia,
[2]BlockC3, UPM-MTDC Technology Center, Universiti Putra Malaysia,
[3]Faculty of Forestry, Universiti Putra Malaysia,
43400 UPM, Serdang, Selangor, Malaysia
[*]E-mail: saberioon@gmail.com

ABSTRACT

Melaleuca cajuputi and Acacia auriculiformis trees are major sources of nectar and pollen for Apis dorsata and the colonies are a major source of honey to the rural poor, honey hunters. Honey is a supplementary income to many of these people (including school children) in the Marang district, Terengganu. In this study, Marang area with 270 square kilometers was chosen as pilot study area in Terengganu state for mapping M. cajuputi and A. auriculiformis as two dominant species in low land secondary forest in Terengganu state.

To inventory and produce land use map of Melaleuca forest in Marang area, in this study SPOT-5 satellite image in multispectral mode with 10 meter resolution which is acquired in 2007 as optical satellite was utilized. Most images from optical satellites have some null data from ground because of clouds and shadow of clouds. To solve this problem, Hue, Saturation and value (HSV) and Principal Component Analysis (PCA) were used as fusion techniques to replace null data with microwave data which taken from Radarsat-1 image in C-band with 25 meter resolution image. Accordingly, fusion technique which was used in this research not only was a technique to improve information but also caused the accuracy increasing than land use map by just only SPOT-5 image. Also between two different fusion techniques, PCA shows the better result than HSV as two different fusion techniques.

Keywords: Fusion, Optical, SAR, RADARSAT-1, SPOT-5, Marang, Malaysia

INTRODUCTION

Forests are important natural resource that play a major role in supporting the livelihood of human like in providing material goods, such as fuel wood, commercial timber, non-wood products, water for irrigation and drinking; preventing landslides or debris flows, providing protection from strong winds and purifying the atmosphere. It is a trove of biodiversity and genetic resource, as well as provider of other environmental services and a key player in poverty alleviation (F.A.O., 2005; Myers, 1992; Sellers, 1985).

Malaysia is located within the equator belt which currently has 32.8 million hectares of land area, of which 17.13 million hectares – 52 percent of total land – are classified as forest and tree cover in the end of 2007. 8.07 million hectares (47.11 percent) are found in Sarawak, 4.74 million hectares (27.6 Percent) are found in Peninsular Malaysia and 4.32 million hectares (25.2 Percent) in Sabah (Anon., 2007).

Received: 1 August 2010
Accepted: 22 June 2011
[*]Corresponding Author

In low land rainforest along the coastal corridor of Kelantan and North Terengganu in Peninsular Malaysia, *Melaleuca cajuputi* (*Gelam*) and *Acacia auriculiformis* (*Acacia*) are the two dominant trees. These trees are major sources of nectar and pollen for giant honey bee (*Apis dorsata*). The honey from these trees has strong flavor and weak density. It granulates quickly, with grain varying from fine creamy to coarse brown and dark if more than moderate heat is used during extraction, straining or packing. On the other hand, the trunk and branches of the Gelam trees are almost upright and the bark are papery and loose that it is unsuitable to serve as nesting support for *A. dorsata*. Therefore, other smooth barked trees with sloping branches in the vicinity of the *Melaleuca* forest are chosen as nesting supports for the *A. dorsata* colonies. It is important to understand what would be the choices of nesting support for *Apis dorsata* in the Melaleuca forest when there is plenty of nectars and pollen sources for the bees.

In order to find out the potential of Melaleuca forest to predict behavior of *A. dorsata* for nesting and collecting nectar and pollen, it is necessary to map vegetation coverage and land measurement of Melaleuca forest in the study area.

The manual (traditional) mapping method to measure and inventories the vegetation coverage of the Melaleuca forest will take a long time and cost. Better means are needed for land use inventory. In many of the developed countries and some of developing countries, Remote Sensing (RS) and Geographic Information System (GIS) are widely used to provide up-to-date information (Luney and Dill, 1970). Recent advances in RS and GIS technology have become cost effective and affordable, by virtue of the following reasons: (a) satellite images are sufficiently accurate and reliable, (b) changes over time can be identified, (c) computers have the power to rapidly process large quantities of data, and (d) object-oriented GIS provide enormous flexibility in storing and analyzing any type of data, providing decision support modeling for effective management (Buchan, 1997).

RS technology is particularly useful tool to produce a broadly consistent database at spatial, spectral, and temporal resolution which is useful for forest. As well, RS data can be made effective and economical for periodic preparation of accurate inventories and also for managing and monitoring forests. Different techniques are available for differentiating and mapping forest units. Studying large area, data can be processed in an automated way; for thematic mapping, images are visually interpreted, enabling the forestry experts to use their knowledge and experience.

In this investigation two different types of RS images were used as source for digital image processing. The first one was optical sensor which has been used to determine and map the distribution of *M. cajuputi* (Gelam) and *A. auriculiformis* (Acacia) trees, the two main sources of nectar and pollen in study area. Because of cloud and shadow of cloud, microwave images was used to fusion with optical sensor which enables penetration of atmospheric conditions to replace null pixels (Goetz *et al.* nod).

The objective of this research was determine processing techniques that improve land classification of Melaleuca forest, Marang district, Malaysia by using optical and radar data when compared to classifications using only the optical sensor data. By combining specially processed Radarsat-1 data with SPOT-5 data, the radar data can provide complementary information that can aid in land-cover mapping.

Data fusion is a process dealing with data and information from multiple sources to achieve refined/improved information for decision making (Hall, 1992). A general definition of image fusion is given as "image fusion is the combination of two or more different image to form a new image by using a certain algorithm (Genderen and Pohl, 1994).

In general, the fusion techniques can be grouped into two classes: (1) Color related techniques and (2) Statistical/numerical methods. The first comprises the color composition of three image channels in the RGB color space as well as more sophisticated color transformations, e.g. HSV and IHS. Statistical approach is developed on the basis of channel statistics including correlation and

filters. Techniques like PCA which belongs to this group. The numerical methods follow arithmetic operations such as image differencing and ratios but also adding of a channel to other image bands. A sophisticated numerical approach uses wavelets in a multi-resolution environment(Pohl & Genderen, 1998).

The main function of the HSV is to separate the spectral information in the hue (H) and saturation (S) components, and the value that represents the image brightness in which high values indicate brighter color (V) component, starting from a RGB image (Pohl, 1998). Firstly, the process begins with the transformation of a RGB color composite into HSV. After that, radiometric normalization is applied between the PAN and I bands. Band I is substituted by PAN, returning to the RGB space, thereby obtaining a hybrid image with the spectral characteristics of the color composite and the spatial qualities of the panchromatic band. In the literature Cheisa and Tyler (1990) was used HSV technique as fusion technique.

The PCA is useful for image encoding, image data compression, image enhancement, digital change detection, multitemporal dimensioality, and image fusion. It is a statistical technique that transforms a multivariate data set of intercorrelated variables into a data set of new uncorrelated linear combination of the original variables (Pohl and Genderen, 1998). The exit images are called Principal Components (PCs) in which the diverse targets that are present in the scene are the most distinct because they are not spectrally correlated. The PCs are calculated simultaneously for a set of bands formed from multispectral and panchromatic images. Troya (1999) and Marcelino (2003) used a variation of this technique using PCA pairs from the PAN and TM bands. Next an inverse transformation to the RGB space was used on the first PCs, thus obtaining a hybrid image.

This study aims to evaluate the accuracy of HSV and PCA fusion techniques in mapping two main bee plants as sources of nectar and pollen for *Apis dorsata* in Marang district, Terengganu state of Malaysia.

STUDY AREA

This study was conducted in Marang district, located in the state of Terengganu at the northern east of Peninsular Malaysia (*Fig. 1*); between upper left of 5 01' N, 103 11' E and lower right of 4 50' N, 103 24'50" E. The district's topography consists of the South China Sea coast, peat swamps, hills, and plains.

The sub-districts of Rusila, Pulau Kerengga and Merchang lie on the coast with sandy plains gradually giving way to hills in the interior. The Jerong sub-district is mainly hilly, while the sub-districts of Bukit Payong and Alor Limbat consist of rolling plains and peat swamps. The dominant trees species in this area are Mangrove, Melaleuca, Acacia, Rubber, and Coconut trees.

Fig. 1: A map of study area

MATERIAL AND METHOD

The following steps were carried out to achieve the objectives of this research: (i) study area definition; (ii) pre-processing (images acquisition/band selection/radiometric normalization, speckle filter); (iii) implementation of the image fusion techniques; (iv) evaluation of the methods (spatial quality assessment, spectral quality assessment, visual assessment).

Two satellite images were used for this current inventory (Table 1), taken on acquisition dates that were near to each other so as to minimize the influence of time on landscape elements (Pohl & Genderen, 1998). However, according to these authors, in landscapes with low-spectro-temporal variability, the result of the image fusion is not significantly affected by this temporal aspec

TABLE 1
Satellite images used in mapping Melaleuca forest

Sensor/satellite	Pixel size	Bands	Resolution	Date
SPOT-5	10m × 10m	B1(B1: 0,50–0,59 μm/(Green) B2: 0,61–0,68 μm/(Red) B3: 0,79–0,89 μm/(Near-infrared)	10 m	03-05-2007
RADARSAT-1	12.5m × 12.5m	C-band/ HH Polarization/Standard 7	25 m	23-11-2007

Preprocessing

Before the image fusion process SAR images were pre-processed by the commonly used speckle reducing filter techniques. For the filtering of SAR images lee filter at windows 7was chosen (Lopes *et al.*, 1990). This selection was made based on the analysis of the mean vectors before and after filtering operation as well as the coefficient of variance (Paudyal and Aschbacter, 1993).

In this study image fusion was conducted at the pixel level. In order to avoid the combination of unrelated data spatial registration accuracies should be at the sub pixel. Therefore in fusion applications geometric correction is very important for registration of the images. After reducing the speckle effects of SAR images by using lee filter in 13×13 windows, SAR images were registered to SPOT image by using image to image rectification method with a root mean square error of less than 1 pixel. Cadastral maps in 1/5000 scale and topographic maps in 1/25000 scale were used for the rectification of SPOT images.

Image Processing

In this study two image fusion techniques were tested to select the one that was most able to mapping *Melaleuca Cajuputi* and *Acacia Auriculiformis* as two main dominant sources of nectar and pollen for *Apis dorsata.* These techniques used to combine to Radarsat-1 as SAR image with 321 SPOT-5 images.

The many classification algorithms define some measures of similarity between a pixel and each class and assign the pixel to the most similar class. We used the maximum likelihood classification (MLC). This is a fairly good method and most commonly used. It allows for incorporating class variance, which is provided by the maximum likelihood rule. The probability of the pixel belonging to a given class is determined from the class mean and covariance from the class mean and covariance. The pixel is assigned to the class for which it has the highest probability of membership. Maximum likelihood algorithm was used on the fused images of SPOT-5 image and Radarsat-1 from two different HSV and PCA techniques. The fused images were classified in 4 classes. (i) *Melaleuca Cajuputi* (ii) *Acacia Auriculiformis* (iii) water bodies (iv) non-vegetation.

Accuracy assessment was run to determine the degree of 'correctness or correspondence of the classification to reality and is performed by comparing classes in the land-use map with reference (ground truth) data by establishing an error (confusion) matrix. The confusion matrix quantifies the similarity between ground truth and classified pixels. The diagonal indicates the number of pixels where map and ground truth concur.

RESULTS AND DISCUSSION

The performance of PCA and HSV techniques in these two different data combinations was analyzed statistically, visually, and graphically. Comparisons were also made among the output classified maps from the fused images.

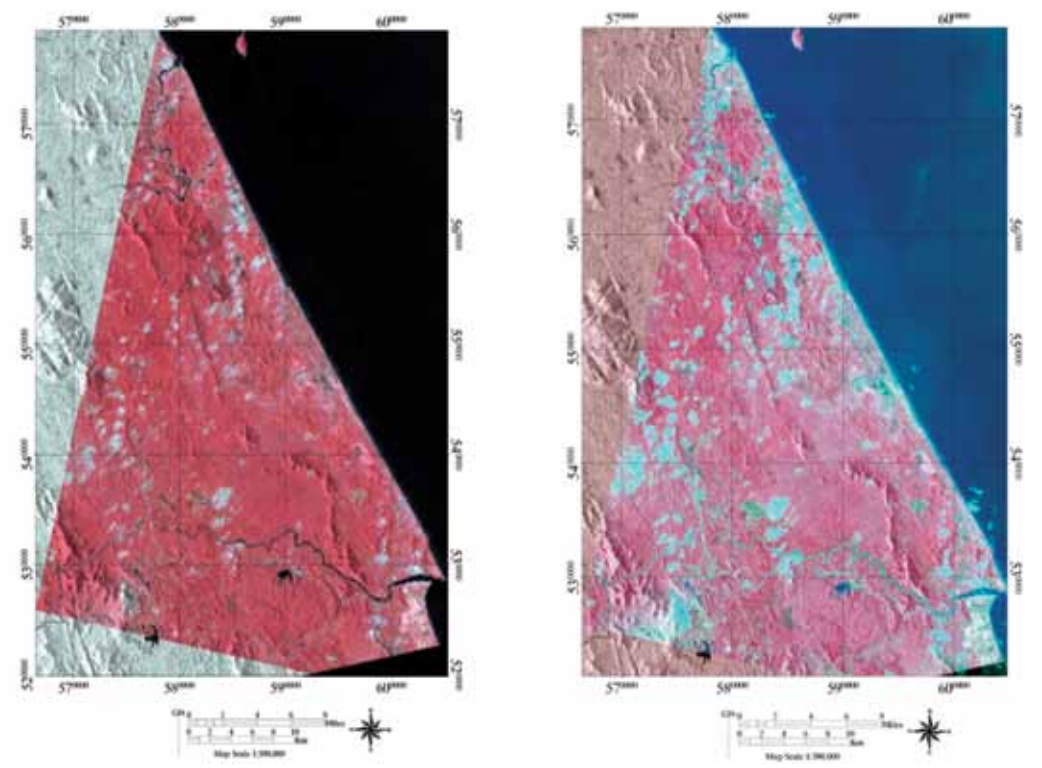

(a) (b)

Fig. 2: Fusion Radarsat1- with SPOT-5 (321) (a) HSV (b) PCA

These four classes were selected because they were readily interpreted and also were the main land cover type found in this study area. *Fig. 3* shows the output of the supervised classification while Table 3 illustrates the statistics results of the supervised classification for both classified fused images.

TABLE 2
Map legend

Melaleuca cajuputi	Light green
Acacia auriculiformis	Dark green
Water bodies	Blue
Non-vegetation	Red

In Table 2 the light green chosen for *Melaleuca cajuputi*, dark green for *Acacia auriculiformis*, red for non-vegetation and blue for water bodies.

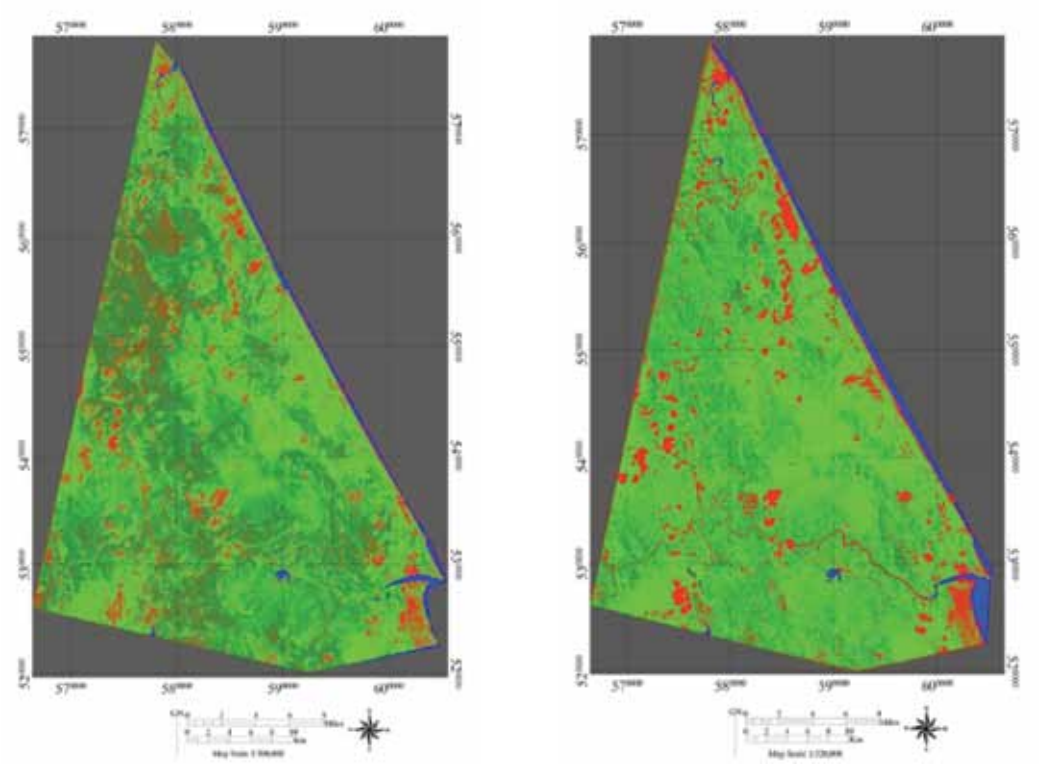

(a) (b)

Fig. 3: Maximum likelihood classification on (a) HSV fusion (b) PCA fusion

TABLE 3
Statistical result of maximum likelihood classification of fusion images

Classes	Area (ha)		Percent	
	PCA	HSV	PCA	HSV
Melaleuca cajuputi	68465	50471	56.05	42.25
Acacia auriculiformis	32887	47988	26.98	40.17
Non-vegetation	17081	19103	13.98	15.9
Water bodies	3597	1907	2.99	1.59

The classified maps from HSV techniques of two data combination showed overall accuracy 70.02% and kappa 0.4236 and for PCA technique the overall accuracy shows the 82.08% and kappa for classified HSV fused image was 0.42 and for classified image from PCA fused technique was 0.69 (Table 4). Refer to Landis & Koch (1977) Kappa's coefficient of near to +1 shows the best performance.

This means that the PCA fusion technique has better results in fusion Radarsat-1 and SPOT-5 to mapping land cover in Marang area.

TABLE 4
Accuracy assessment for two different fusion techniques

Fusion technique	Overall accuracy	Kappa coefficent
HSV	70.02%	0.42
PCA	82.08%	0.69

CONCLUSION

Radarsat-1 imagery fused with satellite optical imagery can provide accurate information about forest mapping especially in tropical rainy forest. Usually optical images from tropical rainy forest are covered by clouds. Fusion techniques can improve the quality and quantity of information from tropical rainy forest because of penetrates of radar wavelengths into clouds. In other word, these feature can help to fill in the null data in optical images because of clouds and shadows by microwave data.

Based on the assessment results, it may be concluded that PCA fusion of Radarsat-1 with SPOT-5 321 is the best available technique for preserving spatial and spectral information from the original images, so as to more clearly identify distribution of trees in tropical rainy forests.

ACKNOWLEDGEMENT

I gratefully acknowledge the funding sources that made my Master work possible. I was funded by the Universiti Putra Malaysia fellowship (GRF). My work was also supported by the Malaysian Remote sensing Agency and the The Sultan Mizan Royal Foundation (YDSM).

REFERENCES

Anon. (2007). Annual report of forestry department of peninsular malaysia. Retrieved on May 27, 2009.

Buchan, P. (1997). Satellite imagery for regulatory control. Modern agriculture. *Journal for Site-Specific Crop Management*, *1*(2), 20-23.

Cheisa, C. C., & Tyler, W. A. (1990). Data fusion of off-nadir spot panchromatic images with other digital data sources. Paper presented at the *ACSM-ASPRS Annual Convention, Image Processing and Remote Sensing.*

F.A.O. (2005). Global forest resources assessment 2009.

Genderen, J. A. V., & Pohl, C. (1994). Image fusion: Issure, techniques and applications. Inteligent image fusion. Paper presented at the *EARSel Workshop*. Strasbourg, France.

Goetz, S. J., Prince, S. D., Thawley, M. M., Smith, A. J., Wright, R., & Weiner, M. (nod). Applications of multi-temporal land cover information in the mid-atlantic region: A resac initiative. *IEEE IGARSS*, *1*, 357-359.

Hall, D. L. (1992). *Mathematical techniques in multisensor data fusion*. Norwood: Artech House Inc.

Landis, J. R., & Koch., G. G. (1977). The measurement of observer agreement for categorical data. *Biometrics., 33*, 159-174.

Lopes, A., Touzi, R., & Nezry, E. (1990). Adaptive filters and scene heterogeneity. *IEEE Trans. Geosci. Remote Sensing, 28*(6), 992- 1000.

Luney, P. R. H. W., & Dill, J. (1970). Uses, potentialities, and needs in agriculture and forestry. In remote sensing with special reference to agriculture and forestry. *Natural Academic of Science*, 1-34.

Marcelino, E. V., Fonseca, L. M. G., Ventura, F., & Rosa, A. N. C. S. (2003). Evaluation of his, pca and wavelet transform fusion techniques for the identification of landslide scars using satellite data. Paper presented at the *Proceedings of IX Simpósio Brasileiro de Sensoriamento Remoto Belo Horizonte*, Brasil.

Mardan, M. (1989). Some aspects of honey collection from colonies of *Apis dorsata* in Peninsular Malaysia. Paper presented at the *International Conference Apiculture Tropical Climates.*

Myers, N. (1992). *The primary source: Tropical forests and our future*. New York: W.W. Norton.

Othman, M. S. H. (1997). Promoting beekeeping as apotential trump card in a drive to conserve selected pockets of melaleuca (gelam) forest in peninsular malaysia. Paper presented at the *International conference on Tropical bees and The environement,* UPM, Malaysia.

Paudyal, D. R., & Aschbacter, J. (1993). Evaluation and performance test of selected sar speckles filter. Paper presented at the *International Symposium "Operationalization Org. Remote Sensing" ITC Enschede,* The Netherlands.

Pohl, C. (1998). Tools and methods used in data fusion. Paper presented at the *Future Trends in Remote Sensing*, Balkema, Rotterdam.

Pohl, C., & Genderen, J. A. V. (1998). Multisensor image fusion in remote sensing: Concepts, methods and applications. *Int. J. Remote Sensing, 19*(5), 823-854.

Sellers, P. J. (1985). Canopy reflectance, photosynthesis, and transpiration. *International Journal of Remote Sensing, 6*, 1335-1372.

Troya, H. (1999). Fusión de imágenes satelitales irs-1c y tm para identificación de elementos urbanos. Paper presented at the *INPE, São José dos Campos,* monograph.

ISSN: 0128-7680
Pertanika J. Sci. & Technol. **19 (S)**: 107 - 114 (2011)

The Use of Morlet Wavelet Coefficients for Identifying Fatigue Damage Features

S. Abdullah*, T. E. Putra, M. Z. Nuawi and Z. M. Nopiah
Department of Mechanical and Materials Engineering,
Universiti Kebangsaan Malaysia,
43600 UKM, Bangi, Selangor, Malaysia
**E-mail: shahrum@eng.ukm.my*

ABSTRACT

This paper presents a new approach to identify fatigue damaging potential locations using the Morlet wavelet coefficients. For solving the subject matter, the 122.4 second SAESUS strain signal was selected for the simulation purpose. As the result, the Morlet wavelet coefficients predicted that the maximum fatigue damage occurs at 40.4 - 42.6 seconds and 67.4 - 70 seconds. For the validation purpose, the Morrow's fatigue damaging value was calculated and was obtained that the maximum fatigue damage occurs at 0 seconds and 99.7 seconds. The fatigue damaging value at the points was 0.0047 cycles to failure. Since both the plots had similar pattern, the Morlet wavelet coefficients could be used as the early warning of the fatigue damaging potential locations, although the locations were not entirely correct.

Keywords: Fatigue strain signal, Morlet wavelet coefficient, fatigue damage

INTRODUCTION

August Wöhler was the first engineer to study fatigue failure and proposed an empirical analysis technique. Between 1852 and 1870, he studied the progressive failure of railway axles. Two railways were suspended from the ends of the axles and the axles rotated till failure. He then plotted the nominal stress versus the numbers of rotation to failure on what has become known as the stress-life (*S-N*) diagram. The S-N - analysis is valid between the transition and the endurance limit (approximately 10^6 cycles for steel). Above the endurance limit, the slope of the curve reduces dramatically and as such this is often referred to as the 'infinite life' region. Several effects are notable about the approach. At below the transition point (approximately 1000 cycles), the S-N curve is not valid because the nominal stresses are now elastic-plastic. For this case, the strain-life (*-N*) - based approach is appropriate method and is commonly used to predict fatigue life for ductile materials at relatively short fatigue life. The crack initiation method relates the plastic deformation that occurs at a localized region where fatigue cracks begin to the durability of the structure under influence of mean stress.

Most fatigue life predictions are based on the Palmgren-Miner's linear cumulative damaging rule normally applied with the established strain-life fatigue damaging models. However, several limitations were found in the implementation of the rule. Using this approach, the fatigue damage is accurately calculated for constant amplitude loadings, but it may lead to the erroneous prediction for variable amplitude loading (Fatemi and Yang, 1998). Such rule assumes no load sequence effect and does not consider the load-interaction accountability that occurs in fatigue service loadings

Received: 1 August 2010
Accepted: 22 June 2011
*Corresponding Author

(Abdullah, 2005). Considering the importance of the influence of load sequence effects and the limitation of the rule, therefore, a suitable improved approach of fatigue live prediction for analyzing components subjected to variable amplitude loadings needs to be identified.

This paper presents a novel approach to indentify the fatigue damaging potential locations. This method utilized the Morlet wavelet coefficients which indicate how energy in the signal is distributed in the time-frequency plane (Darpe, 2007). The energy spectrum (the energy density over frequency) is plotted in order to observe the signal behaviour and its content gives significant information about the random signal pattern. This study uses the Morlet wavelet coefficients to indentify the fatigue damage features based on the wavelet coefficient plot. The schematic flow of the process is illustrated in *Fig. 1*. The strain signal selected for the simulation purpose was obtained from the database of Society of Automotive Engineers (SAE) profiles, named the SAESUS. The signal (in the unit of microstrain) was collected from a suspension component of a car and it was assumed to be sampled at 204.8 Hz for 25,061 data points. It gave the total record length of the signal of 122.4 seconds.

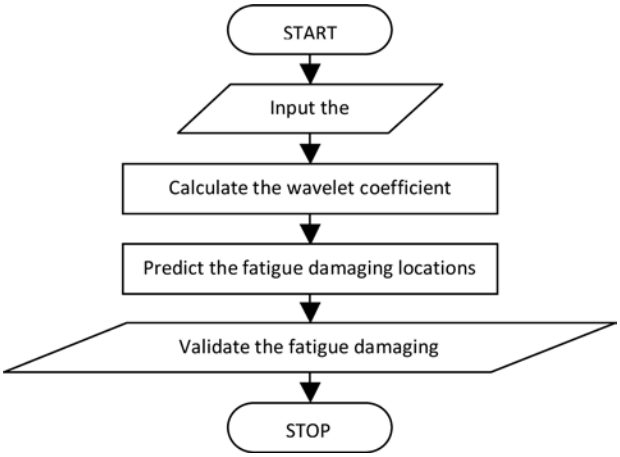

Fig. 1: The flowchart of the effectiveness of the wavelet coefficients in predicting the fatigue damaging potential locations

ANALYSIS OF THE MORLET WAVELET COEFFICIENT

The Wavelet Transform (WT) approach is probably the most recent solution to overcome the nonstationary signals. This time-frequency technique is applied by cutting time domain signal into various frequency components through the compromise between time and frequency - based views of the signal. It presents information in both time and frequency domain in a more useful form (Valens, 1999; Addison, 2002; Percival and Walden, 2000).

The analysis is started with a basic function (called the mother wavelet) scaled and translated to represent the signal being analyzed (Berry, 1999). The transform shifts a window along the signal and calculates the spectrum for every position. The process is repeated many times with a slightly shorter (or longer) window for every new cycle. In the end, the result will be a collection of time-frequency representations of the signal with different resolutions. The WT provides information on when and at what frequency the signal occurs (Valens, 1999). Obviously, the WT represents a windowing technique with variable-sized regions. This technique allows the use of long time intervals (more precise low frequency information) and shorter regions (high frequency

information). The major advantage is the ability to analyze a localized area of larger signal (local analysis) (Misiti *et al*., 2008).

The Continuous Wavelet Transform (CWT) can operate at every possible scale, generates an awful lot of data, and is used to know all values of a continuous decomposition to reconstruct the signal exactly. In addition, it is easier to interpret, makes all information more visible, and is sufficient for exact reconstruction. The Morlet wavelet is one of functions which are the most generally used in the CWT analyses (Gao *et al*., 2001). The name of the wavelet family is written "morl". The wavelet decomposition calculates a resemblance index between signal being analyzed and the wavelet, called coefficient. It is a result of a regression of an original signal produced at different scales and different sections on the wavelet. It represents correlation between the wavelet and a section of the signal. If the index is large, the resemblance is strong, otherwise it is slight (Misiti *et al*., 2008).

The WT of any time-varying signal $f(t)$ is defined as the sum of all of the signal time multiplied by a scaled and shifted version of the wavelet function $\psi(t)$ (Kim *et al*., 2007). The CWT is expressed by the following integral:

$$CWT_{(a,b)} = \int_{-\infty}^{+\infty} f(t)\psi_{a,b}(t)dt \tag{1}$$

The parameter a represents the scale factor which is a reciprocal of frequency, the parameter b indicates the time shifting or translation factor, and t is time.

$\psi_{a,b}(t)$ denotes the mother wavelet (Purushotham *et al*., 2005):

$$\psi_{a,b}(t) = \frac{1}{\sqrt{a}}\psi\left(\frac{t-b}{a}\right) a,b \in R; a \neq 0 \tag{2}$$

$$CWT_{(a,b)} = \int_{-\infty}^{+\infty} f(t)\frac{1}{\sqrt{a}}\psi\left(\frac{t-b}{a}\right)dt \tag{3}$$

The original signal was transformed into the Morlet wavelet using the CWT. This algorithm presented the distribution of the wavelet coefficients in time-frequency domain. *Fig. 2* shows the SAESUS strain signal and the wavelet coefficient distribution.

In the scalogram, the x-axis denoted the time parameter, the y-axis represented the scale that has an inversely related to the frequency value, and the colour intensity at each x-y point was proportional to the absolute value of the wavelet coefficients as a function of the dilation and translation parameters. It provided the energy distribution display with respect to the particular time and frequency information. Accordingly, a lower scale indicated higher frequency and had small amplitude that means that these cycles had lower energy. They gave minimal or no fatigue damaging potential. A large scale was indicative of lower frequency and higher amplitude that indicates that these cycles had higher energy causing the fatigue damage.

Using the newly Morlet wavelet - based developed computational algorithm, the wavelet coefficient magnitude segments were transposed into time domain SAESUS signal, as presented in *Fig. 3*. The representation showed a two dimensional view of the energy distribution, as observed in time-frequency plane. On this plot, the higher coefficients occur at 40.4 - 42.6 seconds and 67.4 - 70 seconds. Since the higher Morlet wavelet coefficients indicate higher fatigue damage, it indicates that the fatigue damaging events also will occur at the same points.

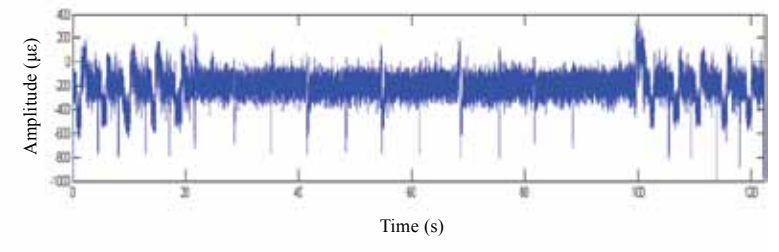

(a)

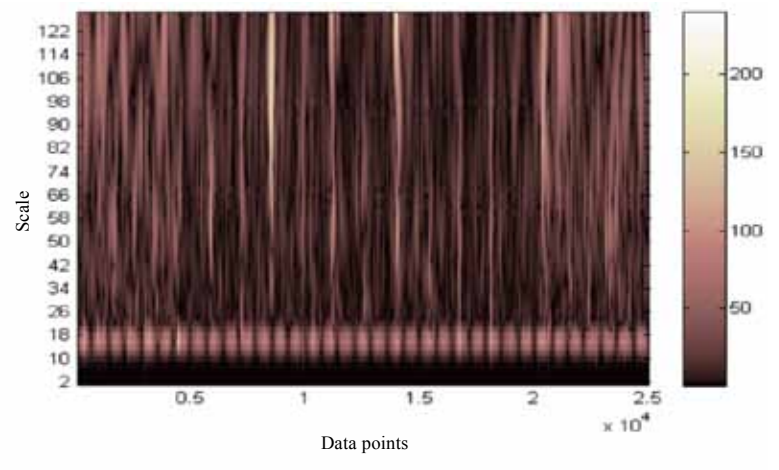

(b)

Fig. 2: (a) Time history of the SAESUS strain signal, and (b) the distribution of the Morlet wavelet coefficients

FATIGUE LIFE PREDICTION

For the validation purpose, the fatigue damaging value was estimated using a specific commercial software package. Comparing the Morlet wavelet coefficients and the fatigue damage, it was obtained the effectiveness of the wavelet coefficients in identifying the fatigue damaging potential locations. The signal is compressed data since the mean value is minus. In a case of the loading being predominantly compressive, particularly for wholly compressive cycles, the Morrow's model provides more realistic live estimates. The mean stress correction effect seems to work reasonably well for steels. The model is mathematically defined as the following expression (nCode):

$$\varepsilon_a = \frac{\sigma'_f}{E}\left(1 - \frac{\sigma_m}{\sigma'_f}\right)(2N_f)^b + \varepsilon'_f\ (2N_f)^c \tag{4}$$

where ε_a is the true strain amplitude, σ'_f is the fatigue strength coefficient, E is the material modulus of elasticity, σ_m is the mean stress, N_f is the numbers of cycle to failure for a particular stress range and mean, b is the fatigue strength exponent, ε'_f is the fatigue ductility coefficient, and c is the fatigue ductility exponent.

The fatigue damage caused by each cycle of repeated loading is calculated by reference to material live curves, such as *S-N* or ε-*N* curves. The fatigue damage *D* for one cycle and the total fatigue damage ΣD caused by cycles are expressed respectively as (Abdullah, 2005):

$$D = \frac{1}{N_f} \tag{5}$$

$$\sum D = \sum \frac{N_i}{N_f} \tag{6}$$

where D N_i is the numbers of cycle within a particular stress range and mean.

For the fatigue damaging calculation, the selected material for the simulation purpose was the SAE1045 carbon steel shaft. This material was chosen because it was commonly used in automotive industries for fabricate a vehicle lower suspension arm structure (Khalil and Topper, 2003). The material properties and their definitions are given in Table 1 (nCode, 2005).

From the fatigue damaging analysis using the Morrow's strain-life model, it was obtained that the maximum fatigue damaging events occur at 0 seconds and 99.7 seconds. The fatigue damaging value at the points was 0.0047 cycles to failure. The fatigue damaging distribution is presented in *Fig. 4* and *Fig. 5* plots the fatigue damaging and cycle counting histograms.

TABLE 1
The mechanical properties of the SAE1045 carbon steel shaft

Properties	Values
Ultimate tensile strength, S_u (MPa)	621
Modulus of elasticity, E (GPa)	204
Fatigue strength coefficient, σ'_f(MPa)	948
Fatigue strength exponent, b	-0.092
Fatigue ductility exponent, c	-0.445
Fatigue ductility coefficient, ε'_f	0.26

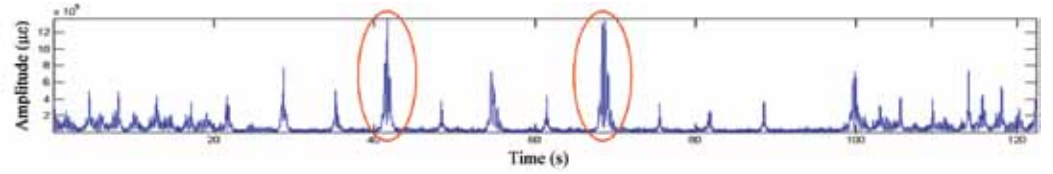

Fig. 3: The Morlet wavelet coefficients in time representation

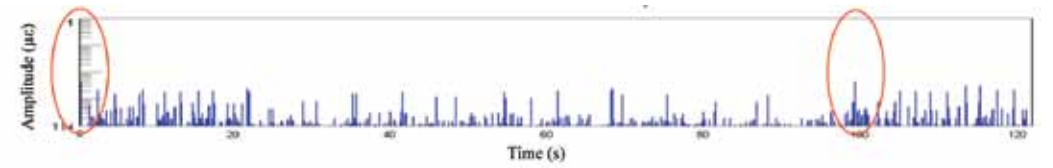

Fig. 4: Time series of the Morrow's fatigue damaging events

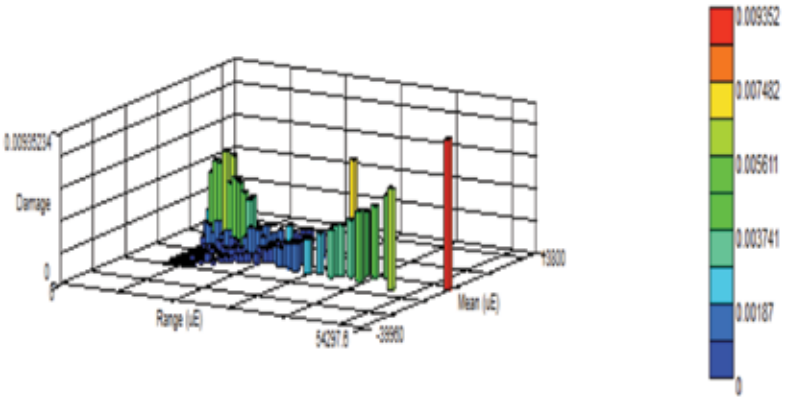

(a)

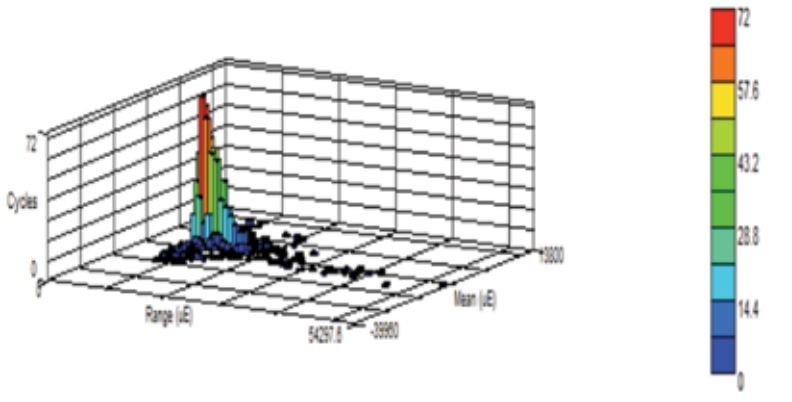

(b)

Fig. 5: The histograms: (a) the fatigue damage, and (b) the cycle counting

IDENTIFICATION OF FATIGUE DAMAGING FEATURES

According to the analysis findings, the Morlet wavelet coefficients have been found to be able in identifying the fatigue damaging potential locations. Although the fatigue damaging events predicted by the Morlet wavelet coefficients were not entirely correct, but they can be used as the early warning of the fatigue damaging locations. *Fig. 6* shows the plot of the Morlet wavelet coefficients when compared to the fatigue damaging event plot, and both plots had similar pattern. Therefore, the resemblance index representing correlation between the Morlet wavelet and the signal was strong.

CONCLUSION

This paper discussed on the effectiveness of the Morlet wavelet coefficients in predicting the fatigue damaging potential locations. The used signal was obtained from the database of SAE profiles, named the SAESUS. In overall, this study found that the Morlet wavelet coefficients can be used to locate the fatigue damaging events. Although the results were not entirely correct, but it could be used as the early warning of the fatigue damaging potential locations, since the Morlet wavelet coefficient plot type was similar to the fatigue damaging plot pattern.

In the future, the authors suggest some works related to development of a relationship model between the Morlet wavelet coefficients and the fatigue damage. In this aspect, it was suggested that the wavelet coefficients are not only used to predict the locations, but the wavelet also can be used to predict the fatigue damaging values.

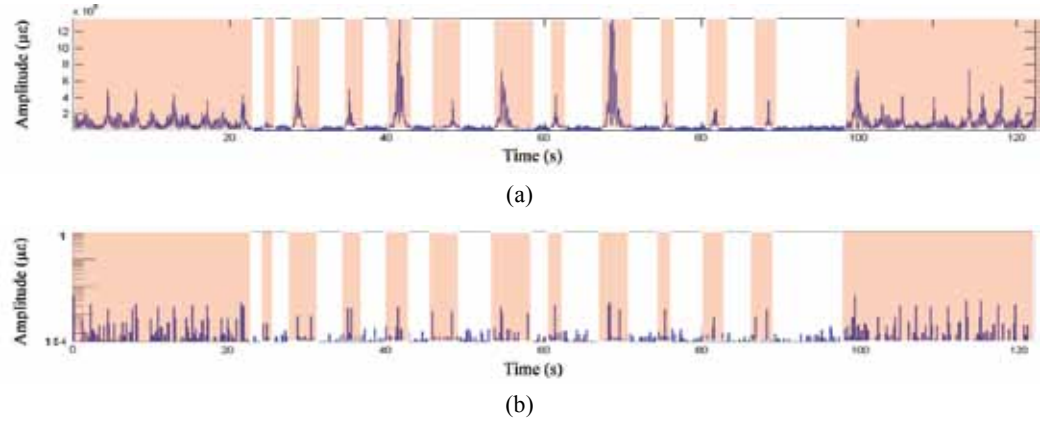

Fig. 6: Plot comparison: (a) The Morlet wavelet coefficients, and (b) the fatigue damaging events

ACKNOWLEDGEMENT

The authors would like to express their gratitude to Universiti Kebangsaan Malaysia through the fund of UKM-GUP-BTT-07-25-158, for supporting the research.

REFERENCES

Abdullah, S. (2005). Wavelet Bump Extraction (WBE) for editing variable amplitude fatigue loadings. Ph.D. Thesis. The University of Sheffield, July 2005.

Addison, P. S. (2002). *The illustrated wavelet transform handbook*. UK: Institute of Physics Publishing.

Berry, S. (1999). Practical wavelet signal processing for automated testing. IEEE, 0-7803-5432-X/99, 653-659.

Darpe, A. K. (2007). A novel way to detect transverse surface crack in a rotating shaft. *Journal of Sound and Vibration*, *305*, 151-171.

Fatemi, A., & Yang, L. (1998). Cumulative fatigue damage and life prediction theories: A survey of the state of the art for homogeneous materials. *International Journal of Fatigue*, *20*(1), 9-34.

Gao, J. H., Wu, R. S., & Wang, B. J. (2001). A new type of analyzing wavelet and its applications for extraction of instantaneous spectrum bandwidth. *SEG International Exposition and Annual Meeting*. San Antonio, Texas.

Khalil, M., & Topper, T. H. (2003). Prediction of crack-opening stress levels for 1045 as-received steel under service loading spectra. *International Journal of Fatigue*, *25*, 149-157.

Kim, B. S., Lee, S. H., Lee, M. G., Ni, J., Song, J. W., & Lee, C. W. (2007). A comparative study on damage detection in speed-up and coast-down process of grinding spindle-typed rotor-bearing system. *Journal of Materials Processing Technology*, 187-188, 30-36.

Misiti, M., Misiti, Y., Oppenheim, G., & Poggi, J. M. (2008). *Matlab user's guide: wavelet toolbox™ 4*. MA, USA: The Math Works Inc.

nCode. *The nCode book of fatigue theory.* nCode International Ltd., Sheffield, UK.

nCode. *ICE-flow: glyphWorks 4.0 tutorials.* nCode International Ltd., Sheffield, UK, 2005.

Percival, D. B., & Walden, A. T. (2000). *Wavelet methods for time series analysis*. UK: Cambridge University Press.

Purushotham, V., Narayanan, S., & Prasad, S. A. N. (2005). Multi-fault diagnosis of rolling bearing elements using wavelet analysis and hidden Markov model based fault recognition. *NDT & E International*, *38*, 654-664.

Valens, C. (1999). A really friendly guide to wavelets. Retrieved from http://pagesperso-orange.fr/polyvalens/clemens/wavelets/wavelets.html.

ISSN: 0128-7680
Pertanika J. Sci. & Technol. **19 (S)**: 115 - 124 (2011)

The ASTER DEM Generation for Geomorphometric Analysis of the Central Alborz Mountains, Iran

Seyed Ramzan Mousavi[1, 2*], Saied Pirasteh[2], Biswajeet Pradhan[2], Shattri Mansor[2] and Ahmad Rodzi Mahmud[2]

[1]Department of Watershed Management, Faculty of Natural Resources, Sari Agriculture Sciences and Natural Resources, Badeleh, Sari, Iran
[2]Institute of Advanced Technology (ITMA), Universiti Putra Malaysia, 43400 UPM, Serdang, Selangor, Malaysia
[*]E-mail: srmmousavi@gmail.com

ABSTRACT

This research focuses on the ASTER DEM generation for visual and mathematical analysis of topography, landscapes and landforms, as well as modeling of surface processes of Central Alborz, Iran. ASTER DEM 15 m generated using tie points over the Central Alborz and Damavand volcano with 5671 m height from ASTER (Advanced Space borne Thermal Emission and Reflection Radiometer) satellite data using PCI Geomatica 9.1. Geomorphic parameters are useful to identify and describe geomorphologic forms and processes, which were extracted from ASTER DEM in GIS environment such as elevation, aspect, slope angle, vertical curvature, and tangential curvature. Although the elevation values are slightly low in altitudes above 5500 m asl., the ASTER DEM is useful in interpretation of the macro- and meso-relief, and provides the opportunity for mapping especially at medium scales (1:100,000 and 1:50,000). ASTER DEM has potential to be a best tool to study 3D model for to geomorphologic mapping and processes of glacial and per glacial forms above 4300 m asl.

Keywords: Remote sensing, GIS, ASTER DEM, geomorphometry, Central Alborz

INTRODUCTION

Digital elevation models (DEMs) are best tools for visual and mathematical analysis of topography, landscapes and land forms, as well as modeling of surface processes (Dikau *et al*., 1995; Giles, 1998; Millaresis and Argialas, 2000; Tucker *et al*., 2001)). Bishop *et al*. (2001) used a DEM of Nanga Parbat to map glaciers in the rough mountain terrain of the western Himalayas. A DEM offers the most common method for extracting vital topographic information and even enables the modeling of flow across topography, a controlling factor in distributed models of landform processes (Dietrich *et al*., 1993; Desmet and Govers, 1995). DEMs play also an important tool for the analysis of glaciers and glaciated terrains (Etzelmüller *et al*., 1997; Baral and Gupta, 1997; Krzytek, 1995). To accomplish this, the DEM must represent the terrain as accurately as possible, since the accuracy of the DEM determines the reliability of the geomorphometric analysis. Currently, the automatic generation of a DEM from remotely sensed data with sub-pixel accuracy is possible (Krzytek, 1995). DEMs can be generated from stereo satellite data derived from electro-optic scanners such as ASTER (Advanced Spaceborne Thermal Emission and Reflection Radiometer). The ASTER sensor offers simultaneous along-track stereo-pairs, which eliminate variations caused by multi-date stereo data acquisition.

Received: 1 August 2010
Accepted: 22 June 2011
[*]Corresponding Author

This paper presents a DEM derived from ASTER satellite data of the Central Alborz in North Iran. Fieldwork at the Damavand Volcano was conducted only on the western side during March and April 2008 and focused on geomorphological mapping with special respect to geomorphologic processes as well as glacial and per glacial forms above 4300 m asl. Aerial photographs with a resolution of 2/5 m from 1997 were used for orientation and to monitor the geomorphologic mapping. The climatic conditions in the Damavand of Alborz region are treated in the Damavand book from (Al-Rousan *et al*., 1997). In one of its detailed study deals with the topo-climatic structure around the volcanic cone, identifying four slope zones and two valley zones. The topographic information was derived from a section of the ASTER DEM data. As fieldwork was not possible on the southeastern side, a detailed, realistic geomorphologic mapping of the entire study area is only possible with the help of DEM data.

STUDY AREA

The study area is a part of the Alborz range of Alp- Himalaya belt in the north of Iran. The Central Alborz corresponds to the East-West trending mountain range bounding the Caspian domain to the South. It is located between 35° 30' N to 37° 05' N latitudes and 51° 19' E to 54° 03' E longitudes (*Fig. 1*). It connects to the Talesh and the Lesser Caucasus structures to the West and the Eastern Alborz structures to the East. Central Alborz contains different geological units from Precambrian to Quaternary ages. These units, assembled in complex systems of thrusts and folds, deformed during several orogeneses related to the closure of Tethyan basins (Proto Tethys, Paleo Tethys, and Neo Tethys). Since Neogene, Iran is undergoing the N-S collision process between Arabian and Eurasian plates and the lateral force of the northwards converging Indian plate along its eastern border. Old structures are uplifted and reactivated, especially along the ancient margins. In Central Alborz, the recent activity is controlled by the E-W trending structures such as the North Tehran fault, the Musha fault in the South and the north Alborz fault, and the Khazar fault in the north.

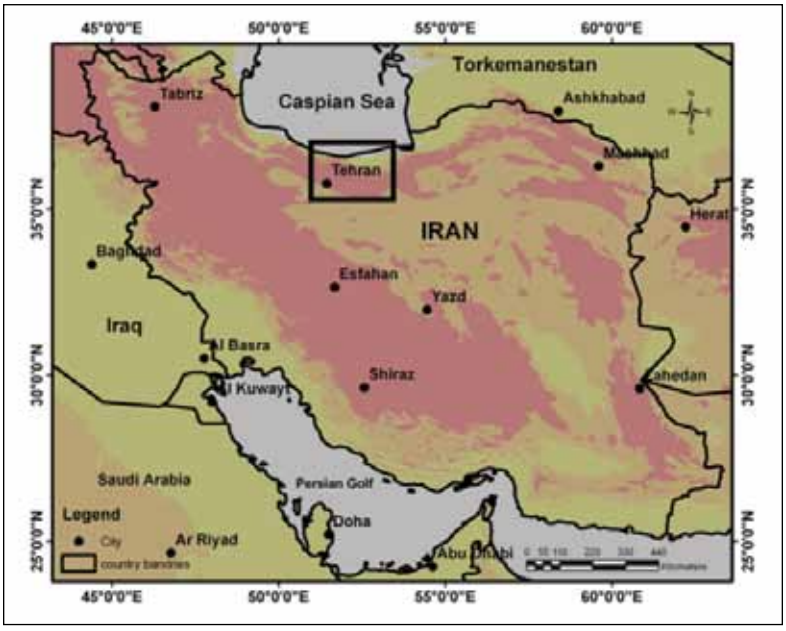

Fig.1: Location map of the study area in the Central Elburz of North Iran over ASTER Imagery

ASTER INSTRUMENT AND DATA SET

ASTER is a high-spatial-resolution, multispectral imaging system flying aboard TERRA, a satellite launched in December 1999 as part of NASA's Earth Observing System (EOS). An ASTER scene covering 61.5-km × 63-km contains data from 14 spectral bands. ASTER is comprised of three separate instrument subsystems representing different ground resolutions: three bands in the visible and near infrared spectral range (VNIR, 0.5-1.0 μm) with 15 m spatial resolution, six bands in the shortwave infrared spectral range (SWIR, 1.0-2.5 μm) with 30 m resolution, and five bands in the thermal infrared spectral range (TIR, 8- 12 μm) with 90 m resolution. In the VNIR one nadir looking (3N, 0.76-0.86 μm) and one backward-looking (3B, 27.7° off-nadir) telescope provide black-and-white stereo images, which generate an along-track stereo image pair with a base-to-height ratio of about 0.6. The potential accuracy for the DEM from ASTER could be on the order of ±7 to ±50 m (RMSE). ASTER is capable of recording 771 digital stereo pairs per day, and cross-track pointing out to 136 km allows viewing of any spot on Earth at least once every sixteen days. One ASTER-level 1A raw data scene, acquired on July 28, 2005, was downloaded from the USGS EROS Data Center (EDC) EOSDIS Core System (ECS).

DEM GENERATION AND 3D-VISUALIZATION

ASTER scenes are distributed in a data format called HDF-EOS, which can be imported by the software Ortho-Engine as part of the PCI Geomatica 9.1. Using this software, DEMs can be generated automatically. For DEM extraction only the VNIR nadir and backward images (3N and 3B) are used. Al-Rousan *et al*. (1997) described a detailed procedure of the DEM generation using the Geomatica software. The geometric model being used is a rigorous one; it reflects the physical reality of the complete viewing geometry and corrects distortions that occur in the imaging process due to platform, sensor, earth, and cartographic projection conditions. After rigorous models (co-linearity and co-planarity equations) are computed for the 3N and 3B images, a pair of quasi-epipolar images is generated from the images in order to retain elevation parallax in only one direction. An automated image-matching procedure is used to generate the DEM through a comparison of the respective gray values of these images. As ground control points (GCPs) were not available, 23 tie points (TPs) were collected between the stereo-pair. For 11 TPs the elevation value was known. The total RMS of the TPs was < 1.17 pixel. The DEM was generated at 30 m resolution with the highest possible level of detail, and the holes were filled by automated interpolation (*Fig. 2*). The overall quality of the DEM was outstanding, with only few artifacts mostly representing lakes. The DEM was re-sampled to 15 m to exploit full ortho-image resolution. The three-band VNIR nadir-looking image (1, 2, 3N) was orthorectified using the extracted DEM. Several perspective scenes and 'fly-by' simulations were developed showing the Damavand peak from different views and in different scales. Although GCPs were not available, the absolute elevation of the ASTER DEM is of good accuracy and allows analysis of the macro- and mesorelief. In the altitudes above 5500 m asl., elevation values are low, due to the internal smoothing procedures of the Geomatica software. ASTER DEMs in general are known to be often too low (personal communication, PCI). Nevertheless, the developed 3D-views demonstrate the high quality of the DEM and the potential for more detailed image interpretation.

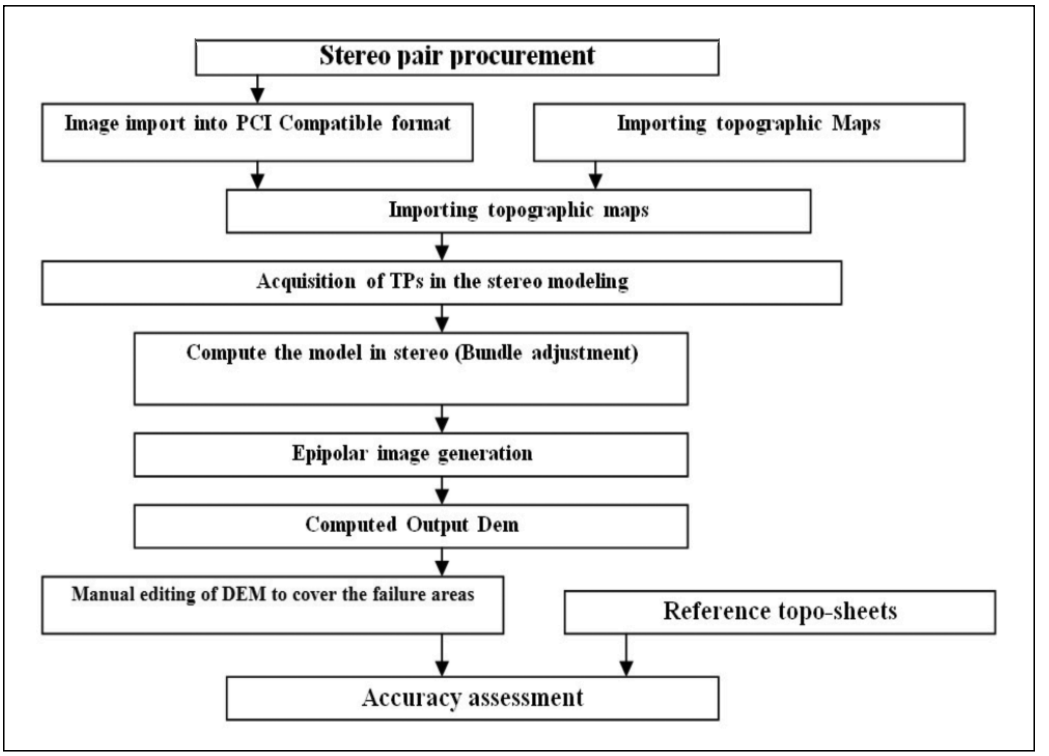

Fig. 2: Diagram of generating DEM from ASTER data

GEOMORPHOMETRIC ANALYSIS

Five geomorphic parameters, which are useful to identify and describe geomorphologic forms and processes (Pirasteh *et al*., 2010a, b), were extracted using the ArcGIS software V9.2 and ArcView GIS: elevation, aspect, slope angle, vertical curvature, and tangential curvature. Flow lines and the catchment areas of the rock glaciers were extracted using the 'hydrologic modeling' tool of the ArcView software. The elevation is graphically presented in a hypsometric map with eight classes, which at Damavand volcano at the same time represent altitudinal belts (*Fig. 3*), e.g. the green class is vegetation cover, the yellow class is a transition zone, and the gray class represents firn fields. In general the ASTER DEM is to low if compared with reality: the summit is only at 5565 m asl. (reality: 5671 m asl.), and the mean altitude is only 4842 m asl. (reality: ~ 4930 m asl.). This fact is mainly caused by the lack of GCPs and smoothing procedures of the Geomatica software. Topography can be generalized into eight aspect classes, and this may also help to identify geomorphologic features (*Fig. 4*). For example, differences in aspect may be an indicator of valley asymmetry. Another map demonstrates the slope angle in ten classes (*Fig. 4*). The class with the lowest slope has a relatively steep upper boundary (5°) in accordance with the general relief, which comprises nearly no flat areas. Other slope classes may be useful to identify specific geomorphic forms: for example, rectilinear slopes have a slope of 25-35° per definition and should be found in the corresponding two classes of the slope map. Slope curvature is of special interest for morphological and hydrological problems. Both curvatures are shown in maps of five classes: The vertical curvature is the second derivation of elevation regarding slope (*Fig. 4*); and the tangential curvature is the second derivation of elevation relating to aspect (*Fig. 4*).

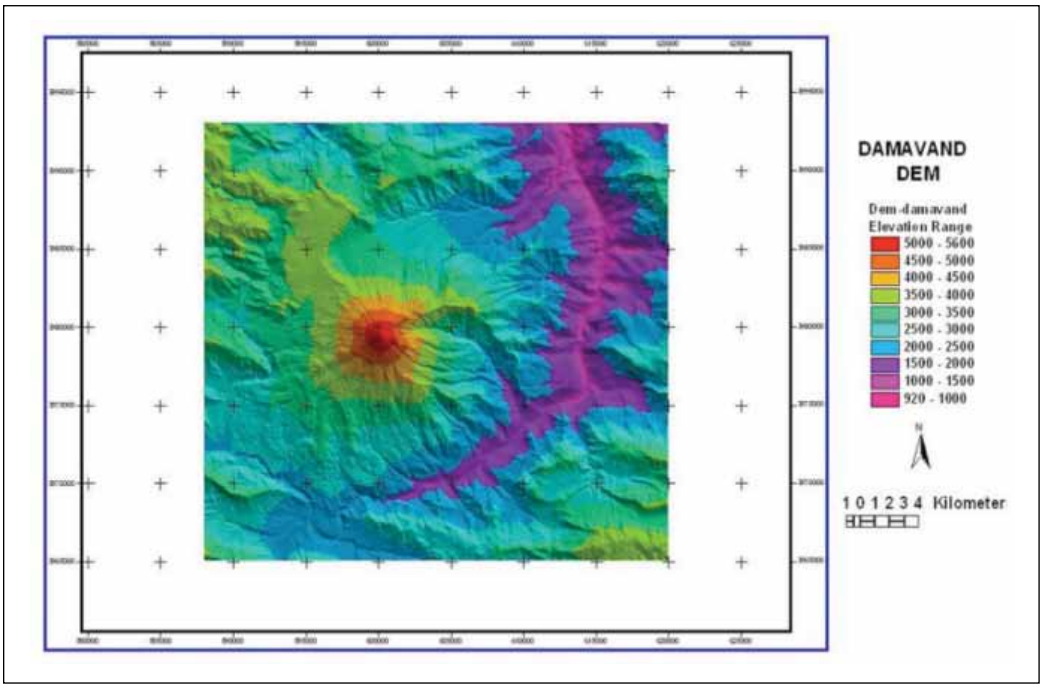

Fig. 3: Morphometric parameters of Central Alborz, deriving from the ASTER DEM: The digital elevation model (DEM) derived from ASTER satellite data of Central Alborz, representing elevation in eight classes

Obviously, ridges have (very) convex and divergent profiles, and valleys have mostly (very) concave and convergent profiles. Meso-scale objects such as rock glaciers can be identified in several locations; the rock glacier front is characterized by a convex profile curvature and convex tangential curvature. In general, profile and tangential curvature are realistic even though the ASTER DEM contains a few artifacts caused by perspective. A special interest of the study was a focus on the per glacial forms at Damavand volcano peak. A per glacial map could be produced using the DEM (*Fig. 4*), and the area of each per glacial form was calculated. Recti-linear slopes cover most of the study area. Non-vegetated solifluction mainly appears on the rectilinear slopes; slightly vegetated solifluction reaches up to the lower limit of the rectilinear slopes; and vegetated solifuction is very exceptionally. Also, rock glaciers occur very rarely in general, but in some valleys they may cover up to 5 % of the area. Striated and patterned ground, breaking blocks, and firn cover smaller areas. A more detailed analysis was undertaken for the rock glaciers in the Gaznak Valley. Knowledge about the geomorphometry is also important for a hydrologic modeling. The more accurate the DEM is the better the modeling results. Flow lines and surface run-off were calculated to delimit the catchment areas of the rock glaciers. The ASTER DEM seems to be precisely regarding the flow lines by comparing it with the virtual image (*Fig. 5-7*). The surface run-off shows very good results especially for the most active rock glaciers.

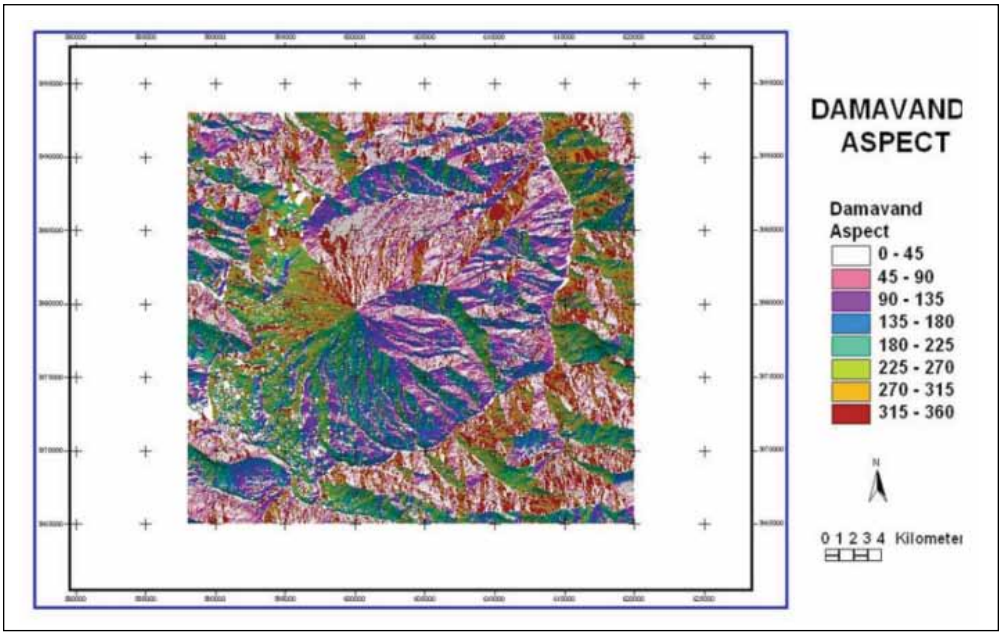

Fig. 4: The digital elevation model (DEM) derived from ASTER satellite data of Central Alborz, representing aspect of Damavand Volcano

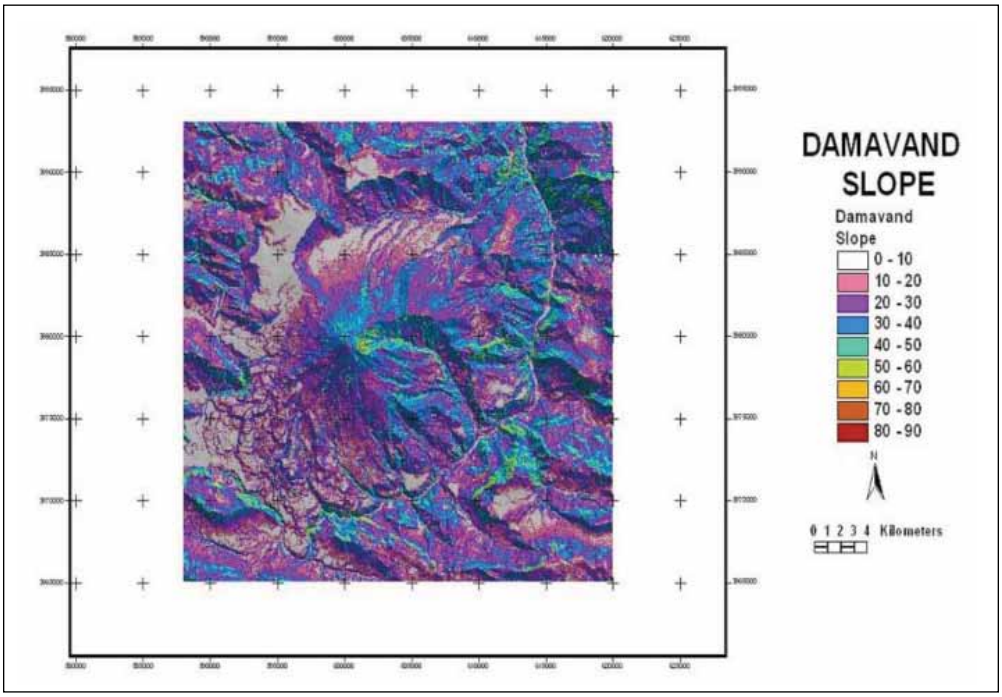

Fig. 5: Morphometric parameters of Central Alborz, deriving from the ASTER DEM, representing slope angle

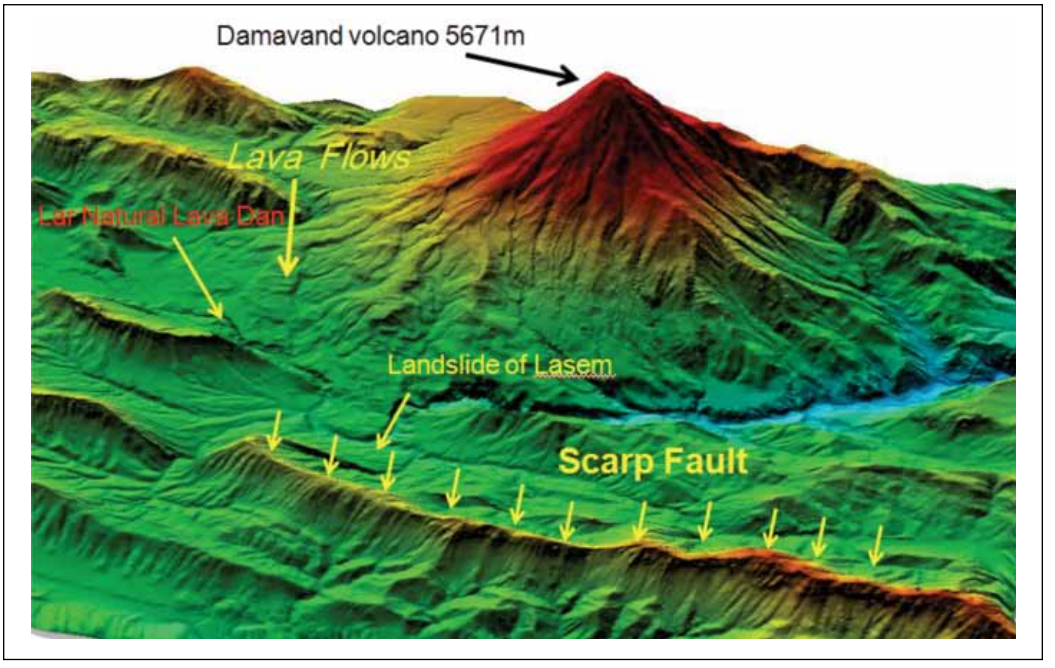

Fig. 6: Morphometric parameters of Central Alborz, deriving from the ASTER DEM, representing hill-shaded relief

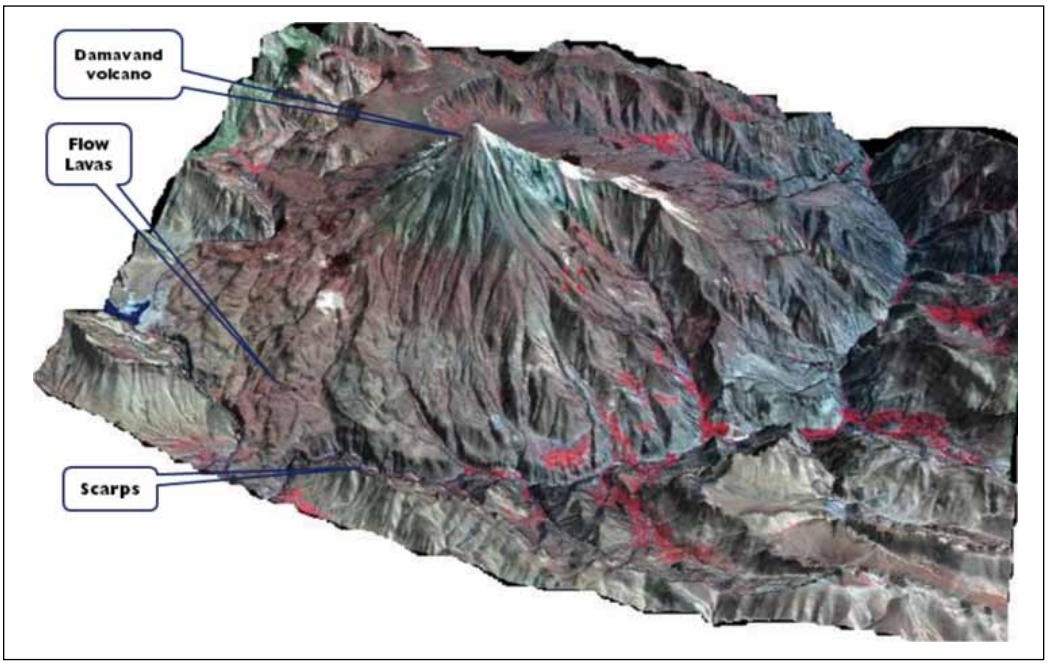

Fig. 7: Morphometric parameters of Central Alborz, deriving from the ASTER imagery, representing 3D surface view

ASTER DEM ACCURACY ASSESSMENT

The result of the stereocorrelation over the Central Alborz is summarized in Table 1, along with the vertical accuracy determined by comparing the computed Z-coordinate values at check points with those collected from the topographic maps and GPS surveys.

TABLE 1
Detail of accuracy assessment of ASTER DEM over the Central Alborz

Image to image registration (Pixel)	Image to ground registration		RMSEz (m)	Number of check points (source)	Completeness of stereocorrelation (%)
	Number of GCPs (source)	RMSExy (pixel)			
± 0.78	11 map points (1: 25,000)	5 m (±0.5)	± 18	36 map points (1: 25,000)	96

An elevation transect developed to further compare the ASTER DEM with a topographic map DEM (*Fig. 8*). At the lower elevations, transects from the ASTER DEM agree with those from the topographic map DEM (*Fig. 8*).

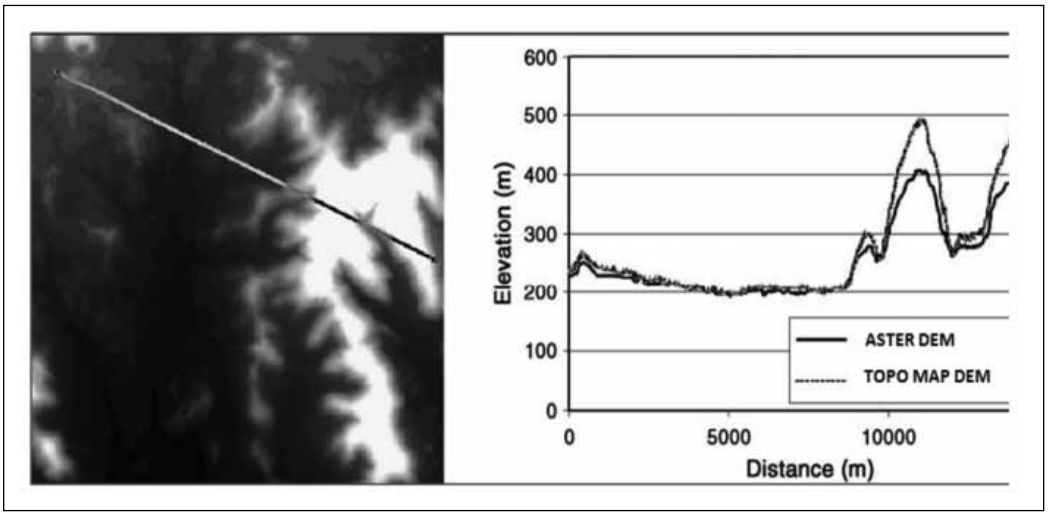

Fig. 8: Profile comparison between ASTER DEM elevations and Topographic map DEM over the Central Alborz

DISCUSSION

While developing an ASTER DEM by using a special commercial software package, the DEM algorithm cannot be changed easily. Often, the software offers only a few parameters for free selection by the operator. For identifying TPs, the operator needs experience in landforms and land covers, because the quality of the TPs is essential for the DEM quality. But when familiar with the software, an operator can develop an ASTER DEM relatively quickly. ASTER DEMs are excellent for virtual-reality visualizations, because they represent quasi ortho-images. The Algorithm Theoretical Basis Document for ASTER Digital Elevation Models (Lang & Welch,

1999) suggests that RMSE values for ASTER DEMs should be on the order of 10 to 50 meters. DEMs produced in other mountainous areas have a preferential failure mode, which is, facets with an aspect of 340 – 140 degrees or slopes over 35 degrees. This is likely due to two factors. First, relative to the ground being examined, the after looking ASTER sensor is set at an azimuth of roughly 10 degrees, making slopes with an aspect of 10 degrees the least likely to be well imaged. Second, these slopes receive the least direct solar illumination, which, by reducing image contrast, increases the probability of image-to-image correlation failure.

CONCLUSION

For Damavand peak, a volcano in the Central Alburz of North Iran, a DEM was developed using ASTER remote sensing data. The results presented here demonstrate that the DEM is useful for morphometric analysis. The scale of a DEM sets the limits for the level of detail for geomorphologic analysis. Today, DEMs from ASTER remote sensing data are reliable sources for an interpretation of the macro- and mesorelief. ASTER DEMs offer relatively great detail, are often easy to develop, and available for many parts of the Earth. In general, the ASTER DEM is accurate, e.g. cliff faces and steep slopes are easy to identify. Analyzing the micro-relief requires a level of detail, which today's DEM resolutions deriving from satellite data do not offer. Here, aerial photographs still are the better choice. ASTER data provides the opportunity for mapping at medium scales (1:100,000 and 1:50,000), and for extracting elevation information from nadir and aft images. The simultaneous along-track stereo data eliminates radiometric variations caused by multi-date stereo data acquisition while improving image-matching performance. In cases where precise GCPs cannot be obtained, it is possible to generate DEMs through tie points (TPs) alone.

ACKNOWLEDGEMENT

The authors wish to thank the Iranian geographic organization for providing satellite data for this research.

REFERENCES

Al-Rousan, N., Cheng, P., Petrie, G., Toutin, T., & Valadan Zoej, M. J. (1997). Automated DEM extraction and orthoimage generation from SPOT level 1B imagery. *Photogrammetric Engineering and Remote Sensing*, *63*, 965-974.

Baral, D. J., & Gupta, R. P. (1997). Integration of satellite sensor data with DEM for the study of snow cover distribution and depletion pattern. *International Journal of Remote Sensing*, *18*, 3889-3894.

Bishop, M. P., Bonk, R., Kamp, U., & Shroder, J. F. (2001). Topographic analysis and modeling for alpine glacier mapping. *Polar Geography*, *25*, 182-201.

Desmet, P. J. J., & Govers, G. (1995). GIS-based simulation of erosion and deposition patterns in an agricultural landscape: A comparison of model results with soil map information. *Catena*, *25*, 389-401.

Dietrich, W. E., Wilson, C. J., Montgomery, D. R., & McKean, J. (1993). Analysis of erosion thresholds, channel networks, and landscape morphology using a digital terrain model. *Journal of Geology*, *101*, 259-278.

Dikau, R., Brabb, E. E., Mark, R. K., & Pike, R. J. (1995). Morphometric landform analysis of New Mexico. *Zeitschrift für Geomorphologie*, *N.F., Suppl.-Bd.*, *101*, 109-126.

Etzelmüller, B., & Sollid, J. L. (1997). Glacier geomorphometry - an approach for analysing long-term glacier surface changes using grid-based digital elevation models. *Annals of Glaciology*, *24*, 135-141.

Giles, P. T. (1998). Geomorphological signatures: classification of aggregated slope unit objects from digital elevation and remote sensing data. *Earth Surface Processes and Landforms*, *23*, 581-594.

Krzystek, P. (1995). New investigations into the practical performance of automatic DEM generation. Proceedings*, ACSM/ASPRS Annual Convention*, Charlotte, North Carolina, American Society for Photogrammetry and Remote Sensing, *2*, 488-500.

Millaresis, G. C., & Argialas, D. P. (2000). Extraction and delineation of alluvial fans from digital elevation models and Landsat Thematic Mapper images. *Photogrammetric Engineering and Remote Sensing*, *66*, 1093-1101.

Pirasteh, S., Rizvi, S. M. A., Ayazi, M. H., & Amir Mahmoodzadeh. (2010a). Using microwave remote sensing for flood study in Bhuj Taluk, Kuchch District Gujarat, India. *International Geoinformatics Research and Development Journal*, *1*(1), 13-24. Retrieved from www.igrdg.com.

Pirasteh, S., Safari, H. O., Pradhan, B., & Attarzadeh, I. (2010b). Litho-morphotectonics analysis using Landsat ETM data and GIS techniques: Zagros Fold Belt (ZFB), SW Iran. *International Geoinformatics Research and Development Journal*, *1*(2), 28-36.

Sidjak, R. W., & Wheate, R. D. (1999). Glacier mapping of the Illecillewaet icefield, British Columbia, Canada, using Landsat TM and digital elevation data. *International Journal of Remote Sensing*, *20*, 273-284.

Tucker, G. E., Catani, F., Rinaldo, A., & Bras, R. L. (2001b). Statistical analysis of drainage density from digital terrain data. *Geomorphology*, *36*, 187-202.

ISSN: 0128-7680
Pertanika J. Sci. & Technol. **19 (S)**: 125 - 129 (2011)

Surface UV Irradiance Obtained by Ozone Monitoring Instrument (OMI) Over Peninsular Malaysia

N. H. Hisamuddin Shah*, H. S. Lim and M. Z. Mat Jafri
School of Physics, Universiti Sains Malaysia, 11800 Penang, Malaysia
**E-mail: hidayah_hisamuddin@yahoo.com*

ABSTRACT

Ultraviolet radiation is at shorter wavelengths than the visible spectrum (400 to 700 nm) and is divided into three components: UV-A (315 to 400 nm), UV-B (280 to 315 nm), and UV-C (less than 280 nm). Global increases in UV-B fluxes from decreasing stratospheric ozone amounts caused by anthropogenic chlorine releasing gases (mostly chlorofluorocarbons) have been a matter of public concern for the past 20 years. This surface UV irradiance data retrieved from Ozone Monitoring Instrument (OMI) from AURA spacecraft with the filename OMUVB. OMUVB contains surface UV irradiance data along with supplementary information generated using the OMI global mode measurements. In this mode each file contains the sunlit portion of a single orbit from pole-to-pole, with an approximately 2600 km wide swath composed of 60 ground pixels. The OMI measurements are used to estimate the ultraviolet (UV) radiation reaching the Earth's surface. The product contains spectral irradiances at 305.1, 310.1, 324.1, and 380.1 nm corresponding to both the overpass time and the local solar noon. Using the correspondence latitude and longitude of Peninsular Malaysia, we can develop the pattern of distribution of UV irradiance interpolations using Sigma Plot and Adobe Photoshop.

Keywords: Surface UV irradiance, Ozone Monitoring Instrument (OMI), AURA spacecraft, Peninsular Malaysia

INTRODUCTION

The sun radiates energy in a wide range of wavelengths, most of which are invisible to human eyes. The shorter the wavelength, the more energetic the radiation, and the greater the potential for harm. Ultraviolet (UV) radiation that reaches the Earth's surface is in wavelengths between 290 and 400 nm (nanometers, or billionths of a meter). This is shorter than wavelengths of visible light, which are 400 to 700 nm. The solar UV radiation has positive and negative effects to human life, animals and plants. For human, solar UV enables the synthesis of vitamin D in skin whereas skin cancer or eye diseases when expose to excessive doses of UV radiation (WMO 2007). Surface UV radiation has several factors that affect it, but the main factor is existence of atmospheric ozone. Stratospheric ozone absorbs completely UV-C, that extremely dangerous for us and UV-B, but UV-A was not absorbed significantly. Absence of ozone depletion can increase the UV-B radiation on earth, and it can be harmful to us. The other factors that effect surface UV irradiance are cloud cover, solar zenith angle, aerosols, elevation, reflectivity of the earth's surface, and water depth.

OMI is a Dutch/Finnish instrument onboard the NASA Earth Observing System (EOS) Aura spacecraft (Levelt *et al*., 2006a). OMI is a nadir-viewing UV/Visible spectrometer with a spectral resolution about 0.63 nm for the visible channel (349-504 nm) and about 0.42 nm for the UV channel (307-383 nm). It measures the solar light scattered by the atmosphere in the 270-5—nm

Received: 1 August 2010
Accepted: 22 June 2011
*Corresponding Author

wavelength range with a spatial resolution at nadir of 13 km x 24 km. The sun-synchronous orbit of Aura and the wide viewing angle of OMI enable daily global coverage of the sunlit portion of the Earth. Omi is the successor of TOMS instruments and contributes to monitoring of the atmospheric ozone, trace gases, aerosols and surface UV radiation (Levelt *et al*.,2006b)

STUDY AREA AND METHODOLOGY

The study area for this paper is peninsular Malaysia area starting from (1˚N, 99˚E) until (9˚N, 106˚E) is taken (*Fig. 1*). The date taken for the study are on 9, 16, 25, and 30th August 2005 and 9, 15, 25, and 29th August 2008, based on the date that Aura satellite is passed. The data of surface UV irradiance is downloaded from website Mirador Earth Science Data Search Tool, and the area of Surface UV irradiance data over study area was viewed using HDF Explorer software.

Daily Level 3 global gridded data products (Ozone, Aerosol, Effective Cloud Fraction, Surface UV-B Spectral Irradiance and Erythemal Daily Dose at 0.25x0.25 deg and 1x1 deg global grids and the wavelength 305.1 nm was used to investigate the distribution of satellite observed from (OMI) and surface UV irradiance distribution over peninsular Malaysia. By using Adobe Photoshop 7.0 and Sigma Plot 11.0 software, map was generated for surface UV irradiance over peninsular Malaysia.

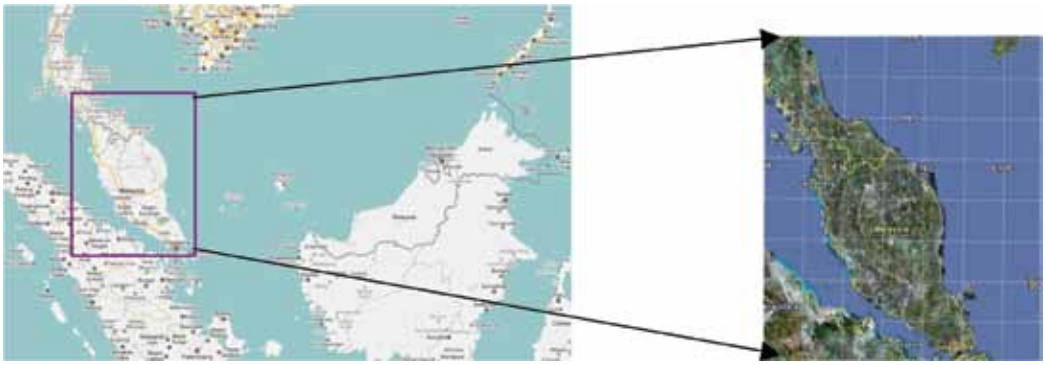

Fig. 1: Location map of the study area

DATA AND ANALYSIS

Fig. 2 shown the distribution of surface UV irradiance at 305 nm over peninsular Malaysia observed by Aura satellite. The highest irradiance on 9th August is 118.278 W/m²/nm. On 16th August, the highest surface irradiance recorded is 118.894 W/m²/nm. This value is not really high and considered as normal distribution for lower latitude region because peninsular Malaysia is near the equator and the skies over Malaysia was covered with cloud, so the surface UV irradiance distribution is almost unchanged for this study area. On 25 August, several places were record a high distribution of UV irradiance such as at Sumatera and Kuala Lumpur's area. There are a number of causes can effect the UV irradiance like presence of cloud and aerosols' effect. On mid-August 2005, Indonesia forest fires was badly affected and caused air pollution and this presence of aerosols can affect the surface UV irradiance. All particles on air tend to reduce the UV irradiance (defined as the radiation incident on a horizontal surface). However, scattering by non-absorbing aerosols can actually increase the UV exposure on non-horizontal surfaces due to the additional radiation incident from low angles (Blumthaler *et al*. 1997; Dickerson *et al*., 1997; Loxsom & Kunkel, 1997). The highest point on 30th August was at Penang and Perak.

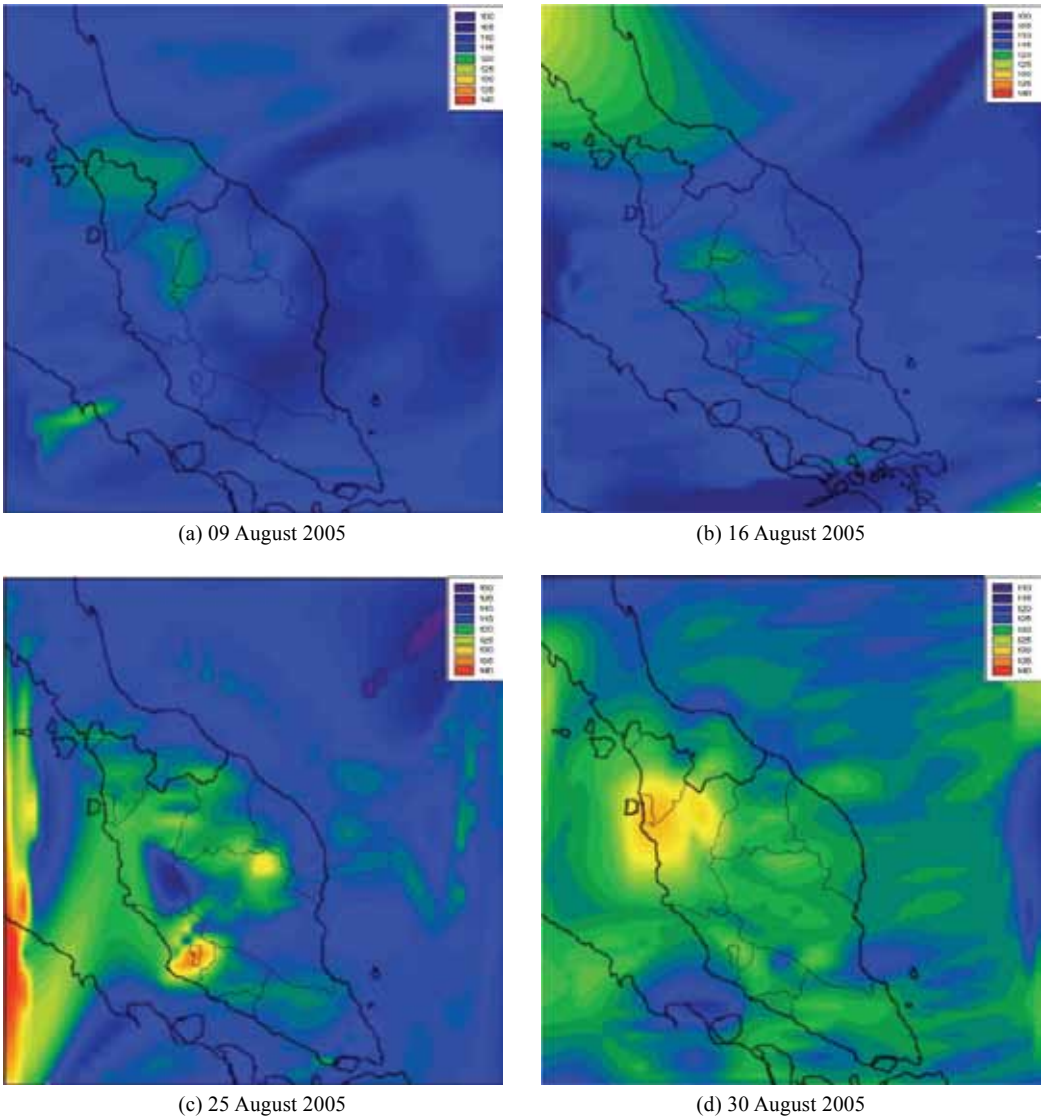

(a) 09 August 2005 (b) 16 August 2005

(c) 25 August 2005 (d) 30 August 2005

Fig. 2: OMI surface UV irradiance at 305 nm over peninsular Malaysia on August 2005 for various days

Fig. 3 shows the distribution of surface UV irradiance over peninsular Malaysia on August 2008. All study days show that the distribution of surface UV irradiance was quite normal for all area, except at middle peninsular Malaysia, where the surface UV irradiance is higher than other area. This is because middle peninsular Malaysia was consists of hills and mountains and high altitudes reflect back higher irradiance than lower altitudes.

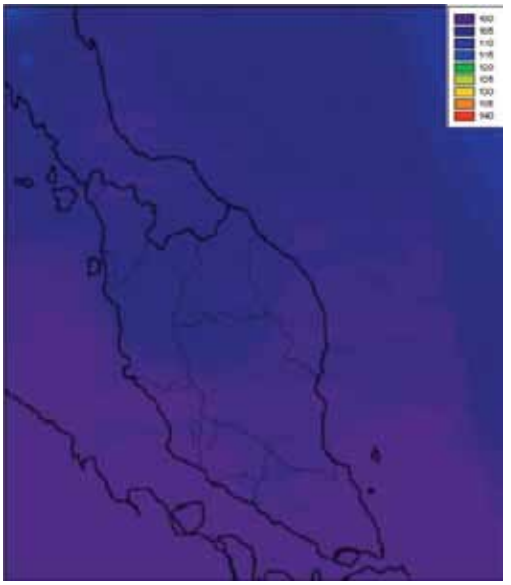

(a) 09 August 2008

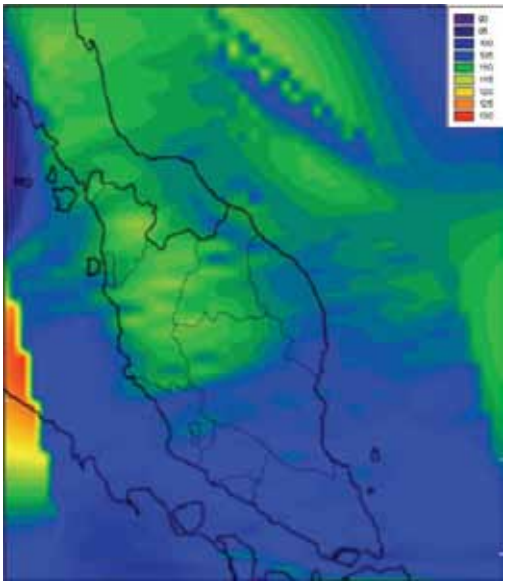

(b) 16 August 2008

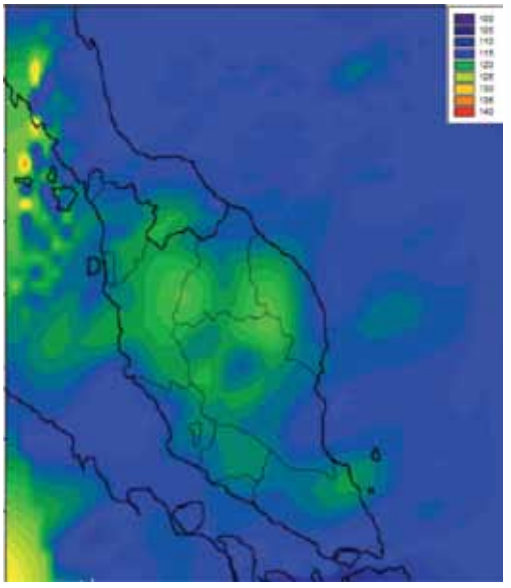

(a) 25 August 2008

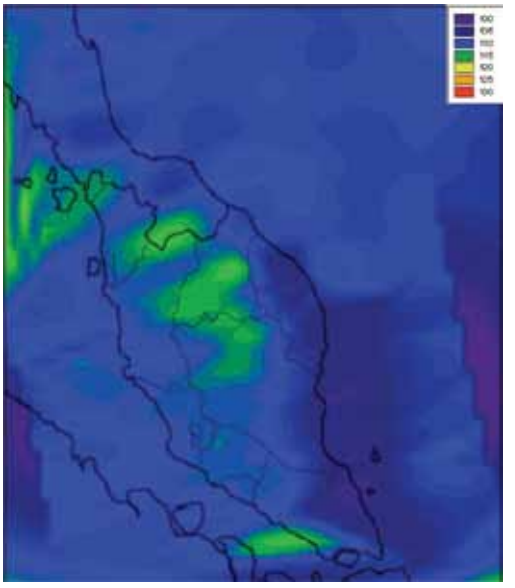

(b) 29 August 2008

Fig. 3: OMI surface UV irradiance at 305 nm over peninsular Malaysia on August 2008

CONCLUSION

As expressed here, OMI has been designed to provide daily global coverage of clouds, aerosols, and surface UV irradiance with a spatial resolution of 13 × 24 km² (OMI ATBD Vol. I) and the result is shown in this study. UV distribution on August 2005 is higher than August 2008 due to forest fire at Indonesia on mid-August.

For further study, this data have to compared with the ground-based measurement over the study area in order to validate the data. Most validation comes from high latitude countries such as French, Italy, Finland and etc. because ozone depletion is greater at higher latitudes (toward the North and South poles). Even though ozone depletion is negligible at lower latitudes, the concern of the harmful of UV effects is still considerable. So this OMI data can helps the study on UV distribution over peninsular Malaysia.

ACKNOWLEDGEMENTS

This project was conceded using the USM short term grants. We would like to thanks the technical staff who participated in this project. Thanks also extended to USM lecturers and staff for encouragement and support.

REFERENCES

Zhangqing Li, Pucai Wang, & Cihlar, J. (2000). A simple and efficient method for retrieving surface UV radiation dose rate from satellit. *Journal of Geophysical Research*, *105*, nº D4, 4777-5080 (48 ref.), pp. 5027-5036.

Buchard, V., Brogniez, C., Auriol, F., Bonnel, B., Lenoble, J., Tanskanen, A., Bojkov, B., & Veefkind, P. (2008). Comparison of OMI ozone and UV irradiance data with ground-based measurement at two French sites. *Atmos. Chem. Phys*., *8*, 4517-4528.

Diffey, B., & McKinlay, A. F. (1987). A reference action spectrum for ultraviolet induced erythema in human skin – human exposure to UV radiation: Risks and regulations, 83-87. Elsevier, NY, USA.

Estupinan, J. G., Raman, S., Crescenti, G. H., Streicher, J. J., & Barnard, W. F. (1996). Effects of clouds and haze on UV-B radiation. *J. Geophys. Res*. *101*, 16807-16816.

REFEREES FOR THE PERTANIKA
JOURNAL OF SCIENCE AND TECHNOLOGY
VOL 19 (S) OCT 2011

(JST Special Issues)

The Executive Editor and the Editorial Board of the Journal of Science and Technology wishes to thank the following for acting as referees for manuscripts published in this Special Issue.

A. Rashid M. Shariff
Anuar Ahmad
Atamurat Kuchkarov
Biswajeet Pradhan
Gafurjan Ibragimor
Helmi Zulhaidi Mohd Shafri
Isamiddin S. Rakhimov
Lawal Billa
Mohd Hasmadi Ismail
Rausham Ashurov
Saied Pirasteh

While every effort has been made to include a complete list of referees for the period stated above, however if any name(s) have been omitted unintentionally or spelt incorrectly, please notify the Executive Editor, *Pertanika* Journals at ndeeps@admin.upm.edu.my.

Any inclusion or exclusion of name(s) on this page does not commit the Pertanika Editorial Office, nor the UPM Press or the University to provide any liability for whatsoever reason.

Pertanika

Our goal is to bring high quality research to the widest possible audience

Journal of Science and Technology

INSTRUCTIONS TO AUTHORS

(Manuscript Preparation & Submission Guidelines)

Revised July 2011

We aim for excellence, sustained by a responsible and professional approach to journal publishing.
We value and support our authors in the research community.

Please read the guidelines and follow these instructions carefully; doing so will ensure that the publication of your manuscript is as rapid and efficient as possible. The Editorial Board reserves the right to return manuscripts that are not prepared in accordance with these guidelines.

About the Journal

Pertanika is an international peer-reviewed journal devoted to the publication of original papers, and it serves as a forum for practical approaches to improving quality in issues pertaining to tropical agriculture and its related fields. *Pertanika* began publication in 1978 as Journal of Tropical Agricultural Science. In 1992, a decision was made to streamline *Pertanika* into three journals to meet the need for specialised journals in areas of study aligned with the interdisciplinary strengths of the university. The revamped Journal of Science and Technology (JST) is now focusing on research in science and engineering, and its related fields. Other *Pertanika* series include Journal of Tropical Agricultural Science (JTAS); and Journal of Social Sciences and Humanities (JSSH).

JST is published in **English** and it is open to authors around the world regardless of the nationality. It is currently published two times a year i.e. in **January** and **July**.

Goal of *Pertanika*

Our goal is to bring the highest quality research to the widest possible audience.

Quality

We aim for excellence, sustained by a responsible and professional approach to journal publishing. Submissions are guaranteed to receive a decision within 12 weeks. The elapsed time from submission to publication for the articles averages 5-6 months.

Indexing of *Pertanika*

Pertanika is now over 30 years old; this accumulated knowledge has resulted in *Pertanika* JST being indexed in SCOPUS and EBSCO.

Future vision

We are continuously improving access to our journal archives, content, and research services. We have the drive to realise exciting new horizons that will benefit not only the academic community, but society itself.

We also have views on the future of our journals. The emergence of the online medium as the predominant vehicle for the 'consumption' and distribution of much academic research will be the ultimate instrument in the dissemination of the research news to our scientists and readers.

Aims and Scope

Pertanika Journal of Science and Technology aims to provide a forum for high quality research related to science and engineering research. Areas relevant to the scope of the journal include: *bioinformatics, bioscience, biotechnology and bio-molecular sciences, chemistry, computer science, ecology, engineering, engineering design, environmental control and management, mathematics and statistics, medicine and health sciences, nanotechnology, physics, safety and emergency management*, and related fields of study.

Editorial Statement

Pertanika is the official journal of Universiti Putra Malaysia. The abbreviation for *Pertanika* Journal of Science & Technology is *Pertanika J. Sci. Technol.*

Guidelines for Authors

Publication policies

Pertanika policy prohibits an author from submitting the same manuscript for concurrent consideration by two or more publications. It prohibits as well publication of any manuscript that has already been published either in whole or substantial part elsewhere. It also does not permit publication of manuscript that has been published in full in Proceedings. Please refer to Pertanika's **Code of Ethics** for full details.

Editorial process

Authors are notified on receipt of a manuscript and upon the editorial decision regarding publication.

Manuscript review: Manuscripts deemed suitable for publication are sent to the Editorial Board members and/or other reviewers. We encourage authors to suggest the names of possible reviewers. Notification of the editorial decision is usually provided within to eight to ten weeks from the receipt of manuscript. Publication of solicited manuscripts is not guaranteed. In most cases, manuscripts are accepted conditionally, pending an author's revision of the material.

Author approval: Authors are responsible for all statements in articles, including changes made by editors. The liaison author must be available for consultation with an editor of *The Journal* to answer questions during the editorial process and to approve the edited copy. Authors receive edited typescript (not galley proofs) for final approval. Changes **cannot** be made to the copy after the edited version has been approved.

Please direct all inquiries, manuscripts, and related correspondence to:

The Executive Editor
Pertanika Journals
Office of the Deputy Vice Chancellor
IDEA Tower II, UPM-MTDC Technology Centre
Universiti Putra Malaysia
43400 UPM, Serdang, Selangor
Malaysia
Phone: + (603) 8947 1622
ndeeps@admin.upm.edu.my

or visit our website at http://www.pertanika2.upm.edu.my/jpertanika/index.htm for further information.

Manuscript preparation

Pertanika accepts submission of mainly four types of manuscripts. Each manuscript is classified as **regular** or **original** articles, **short communications**, **reviews**, and proposals for **special issues**. Articles must be in **English** and they must be competently written and argued in clear and concise grammatical English. Acceptable English usage and syntax are expected. Do not use slang, jargon, or obscure abbreviations or phrasing. Metric measurement is preferred; equivalent English measurement may be included in parentheses. Always provide the complete form of an acronym/abbreviation the first time it is presented in the text. Contributors are strongly recommended to have the manuscript checked by a colleague with ample experience in writing English manuscripts or an English language editor.

Linguistically hopeless manuscripts will be rejected straightaway (e.g., when the language is so poor that one cannot be sure of what the authors really mean). This process, taken by authors before submission, will greatly facilitate reviewing, and thus publication if the content is acceptable.

The instructions for authors must be followed. Manuscripts not adhering to the instructions will be returned for revision without review. Authors should prepare manuscripts according to the guidelines of *Pertanika*.

1. Regular article

Definition: Full-length original empirical investigations, consisting of introduction, materials and methods, results and discussion, conclusions. Original work must provide references and an explanation on research findings that contain new and significant findings.

Size: Should not exceed 5000 words or 8-10 printed pages (excluding the abstract, references, tables and/or figures). One printed page is roughly equivalent to 3 type-written pages.

2. Short communications

Definition: Significant new information to readers of the Journal in a short but complete form. It is suitable for the publication of technical advance, bioinformatics or insightful findings of plant and animal development and function.

Size: Should not exceed 2000 words or 4 printed pages, is intended for rapid publication. They are not intended for publishing preliminary results or to be a reduced version of Regular Papers or Rapid Papers.

3. Review article

Definition: Critical evaluation of materials about current research that had already been published by organizing, integrating, and evaluating previously published materials. Re-analyses as meta-analysis and systemic reviews are encouraged. Review articles should aim to provide systemic overviews, evaluations and interpretations of research in a given field.

Size: Should not exceed 4000 words or 7-8 printed pages.

4. Special issues

Definition: Usually papers from research presented at a conference, seminar, congress or a symposium.

Size: Should not exceed 5000 words or 8-10 printed pages.

5. Others

Definition: Brief reports, case studies, comments, Letters to the Editor, and replies on previously published articles may be considered.

Size: Should not exceed 2000 words or up to 4 printed pages.

With few exceptions, original manuscripts should not exceed the recommended length of 6 printed pages (about 18 typed pages, double-spaced and in 12-point font, tables and figures included). Printing is expensive, and, for the Journal, postage doubles when an issue exceeds 80 pages. You can understand then that there is little room for flexibility.

Long articles reduce the Journal's possibility to accept other high-quality contributions because of its 80-page restriction. We would like to publish as many good studies as possible, not only a few lengthy ones. (And, who reads overly long articles anyway?) Therefore, in our competition, short and concise manuscripts have a definite advantage.

Format

The paper should be formatted in one column format with the figures at the end. A maximum of eight keywords should be indicated below the abstract to describe the contents of the manuscript. Leave a blank line between each paragraph and between each entry in the list of bibliographic references. Tables should preferably be placed in the same electronic file as the text. Authors should consult a recent issue of the Journal for table layout.

There is no need to spend time formatting your article so that the printout is visually attractive (e.g. by making headings bold or creating a page layout with figures), as most formatting instructions will be removed upon processing.

Manuscripts should be typewritten, typed on one side of the A4 paper with at least 4cm margins and double spacing throughout. Every page of the manuscript, including the title page, references, tables, etc. should be numbered. However, no reference should be made to page numbers in the text; if necessary, one may refer to sections. Underline words that should be in italics, and do not underline any other words.

Authors are advised to use Times New Roman 12-point font. Be especially careful when you are inserting special characters, as those inserted in different fonts may be replaced by different characters when converted to PDF files. It is well known that 'μ' will be replaced by other characters when fonts such as 'Symbol' or 'Mincho' are used.

We recommend that authors prepare the text as a **Microsoft Word** file.

1. Manuscripts in general should be organised in the following order:

    - **Page 1: Running title.** (Not to exceed 60 characters, counting letters and spaces). This page should **only** contain your running title of your paper. In addition, the **Subject areas m**ost relevant to the study **must be indicated on this page.** Select one or two subject areas (refer to the *Scope Form)*.
      A **list** of n**umber of black and white / colour figures and tables should also be indicated on this page.** Figures submitted in color will be printed in colour. See "*5. Figures & Photographs"* for details.

    - **Page 2: Author(s) and Corresponding author information.** This page should contain the **full title** of your paper with name(s) of all the authors, institutions and corresponding author's name, institution and full address (Street address, telephone number (including extension), hand phone number, fax number and e-mail address) for editorial correspondence. The names of the authors **must** be abbreviated following the international naming convention. e.g. Salleh, A.B., Tan, S.G., or Sapuan, S.M.

Authors' addresses. Multiple authors with different addresses must indicate their respective addresses separately by superscript numbers:

George Swan[1] and Nayan Kanwal[2]
[1]Department of Biology, Faculty of Science, Duke University, Durham, North Carolina, USA.
[2]Research Management Centre, Universiti Putra Malaysia, Serdang, Malaysia.

- **Page 3**: This page should **repeat** the **full title** of your paper with only the **Abstract** (the abstract should be less than 250 words for a Regular Paper and up to 100 words for a Short Communication). **Keywords** must also be provided on this page (Not more than eight keywords in alphabetical order).

- **Page 4 and subsequent pages**: This page should begin with the **Introduction** of your article and the rest of your paper should follow from page 5 onwards.

Abbreviations. Define alphabetically, other than abbreviations that can be used without definition. Words or phrases that are abbreviated in the introduction and following text should be written out in full the first time that they appear in the text, with each abbreviated form in parenthesis. Include the common name or scientific name, or both, of animal and plant materials.

Footnotes. Current addresses of authors if different from heading.

2. **Text.** Regular Papers should be prepared with the headings **Introduction**, **Materials and Methods**, **Results and Discussion, Conclusions** in this order. Short Communications should be prepared according to "*8. Short Communications."* below.

3. **Tables.** All tables should be prepared in a form consistent with recent issues of *Pertanika* and should be numbered consecutively with Arabic numerals. Explanatory material should be given in the table legends and footnotes. Each table should be prepared on a separate page. (Note that when a manuscript is accepted for publication, tables must be submitted as data - .doc, .rtf, Excel or PowerPoint file- because tables submitted as image data cannot be edited for publication.)

4. **Equations and Formulae.** These must be set up clearly and should be typed triple spaced. Numbers identifying equations should be in square brackets and placed on the right margin of the text.

5. **Figures & Photographs.** Submit an original figure or photograph. Line drawings must be clear, with high black and white contrast. Each figure or photograph should be prepared on a separate sheet and numbered consecutively with Arabic numerals. Appropriate sized numbers, letters and symbols should be used, no smaller than 2 mm in size after reduction to single column width (85 mm), 1.5-column width (120 mm) or full 2-column width (175 mm). Failure to comply with these specifications will require new figures and delay in publication. For electronic figures, create your figures using applications that are capable of preparing high resolution TIFF files acceptable for publication. In general, we require **300 dpi or higher resolution for coloured and half-tone artwork** and **1200 dpi or higher for line drawings**. For review, you may attach low-resolution figures, which are still clear enough for reviewing, to keep the file of the manuscript under 5 MB. Illustrations may be produced at extra cost in colour at the discretion of the Publisher; the author could be charged Malaysian Ringgit 50 for each colour page.

6. **References.** Literature citations in the text should be made by name(s) of author(s) and year. For references with more than two authors, the name of the first author followed by 'et al.' should be used.

   Swan and Kanwal (2007) reported that …
   The results have been interpreted (Kanwal et al. 2009).

   - References should be listed in alphabetical order, by the authors' last names. For the same author, or for the same set of authors, references should be arranged chronologically. If there is more than one publication in the same year for the same author(s), the letters 'a', 'b', etc., should be added to the year.

   - When the authors are more than 11, list 5 authors and then et al.

   - Do not use indentations in typing References. Use one line of space to separate each reference. The name of the journal should be written in full. For example:

     - Jalaludin, S. (1997a). Metabolizable energy of some local feeding stuff. *Tumbuh, 1,* 21-24.

     - Jalaludin, S. (1997b). The use of different vegetable oil in chicken ration. *Malayan Agriculturist, 11,* 29-31.

     - Tan, S.G., Omar, M.Y., Mahani, K.W., Rahani, M., Selvaraj, O.S. (1994). Biochemical genetic studies on wild populations of three species of green leafhoppers *Nephotettix* from Peninsular Malaysia. *Biochemical Genetics*, *32,* 415 - 422.

   - In case of citing an author(s) who has published more than one paper in the same year, the papers should be distinguished by addition of a small letter as shown above, e.g. Jalaludin (1997a); Jalaludin (1997b).

- Unpublished data and personal communications should not be cited as literature citations, but given in the text in parentheses. 'In press' articles that have been accepted for publication may be cited in References. Include in the citation the journal in which the 'in press' article will appear and the publication date, if a date is available.

7. **Examples of other reference citations**:
   Monographs: Turner, H.N. and Yong, S.S.Y. (2006). *Quantitative Genetics in Sheep Breeding*. Ithaca: Cornell University Press.

   Chapter in Book: Kanwal, N.D.S. (1992). Role of plantation crops in Papua New Guinea economy. In Angela R. McLean (Eds.), *Introduction of livestock in the Enga province PNG* (p. 221-250). United Kingdom: Oxford Press.

   Proceedings: Kanwal, N.D.S. (2001). Assessing the visual impact of degraded land management with landscape design software. In N.D.S. Kanwal and P. Lecoustre (Eds.), *International forum for Urban Landscape Technologies* (p. 117-127). Lullier, Geneva, Switzerland: CIRAD Press.

8. **Short Communications** should include **Introduction, Materials and Methods, Results and Discussion, Conclusions** in this order. Headings should only be inserted for Materials and Methods. The abstract should be up to 100 words, as stated above. Short Communications must be 5 printed pages or less, including all references, figures and tables. References should be less than 30. A 5 page paper is usually approximately 3000 words plus four figures or tables (if each figure or table is less than 1/4 page).

   *Authors should state the total number of words (including the Abstract) in the cover letter. Manuscripts that do not fulfill these criteria will be rejected as Short Communications without review.

STYLE OF THE MANUSCRIPT

Manuscripts should follow the style of the latest version of the Publication Manual of the American Psychological Association (APA). The journal uses British spelling and authors should therefore follow the latest edition of the Oxford Advanced Learner's Dictionary.

SUBMISSION OF MANUSCRIPTS

All articles submitted to the journal **must comply** with these instructions. Failure to do so will result in return of the manuscript and possible delay in publication.

The **softcopy** of your manuscript, along with the Form BR 25 comprising Declaration, Referral A and Scope form may be submitted **electronically** together with a **cover letter**. The forms and the sample of the cover letter are available from the *Pertanika*'s home page at http://www.rmc.upm.edu.my/j*Pertanika*/index.htm or from the Executive Editor's office upon request.

Please do **not** submit manuscripts to the editor-in-chief or to UPM Press directly. All manuscripts must be **submitted through the executive editor's office** to be properly acknowledged and rapidly processed:

Dr. Nayan KANWAL
Executive Editor
Pertanika Journals
Office of the Deputy Vice Chancellor
IDEA Tower II, UPM-MTDC Technology Centre
Universiti Putra Malaysia
43400 UPM, Serdang, Selangor, Malaysia
email: ndeeps@admin.upm.edu.my; tel: + 603-8947 1622

Cover letter

All submissions must be accompanied by a cover letter detailing what you are submitting. Papers are accepted for publication in the journal on the understanding that the article is original and the content has not been published or submitted for publication elsewhere. This must be stated in the cover letter.

The cover letter must also contain an acknowledgement that all authors have contributed significantly, and that all authors are in agreement with the content of the manuscript.

The cover letter of the paper should contain (i) the title; (ii) the full names of the authors; (iii) the addresses of the institutions at which the work was carried out together with (iv) the full postal and email address, plus facsimile and telephone numbers of the author to whom correspondence about the manuscript should be sent. The present address of any author, if different from that where the work was carried out, should be supplied in a footnote.

As articles are double-blind reviewed, material that might identify authorship of the paper should be placed on a cover sheet.

Peer review

In the peer-review process, three referees independently evaluate the scientific quality of the submitted manuscripts. The Journal uses a double-blind peer-review system. Authors are encouraged to indicate in **referral form A** the names of three potential reviewers, but the editors will make the final choice. The editors are not, however, bound by these suggestions.

Manuscripts should be written so that they are intelligible to the professional reader who is not a specialist in the particular field. They should be written in a clear, concise, direct style. Where contributions are judged as acceptable for publication on the basis of content, the Editor or the Publisher reserves the right to modify the typescripts to eliminate ambiguity and repetition and improve communication between author and reader. If extensive alterations are required, the manuscript will be returned to the author for revision.

The editorial review process

What happens to a manuscript once it is submitted to *Pertanika*? Typically, there are seven steps to the editorial review process:

1. The executive editor and the editorial board examine the paper to determine whether it is appropriate for the journal and should be reviewed. If not appropriate, the manuscript is rejected outright and the author is informed.
2. The executive editor sends the article-identifying information having been removed, to three reviewers. Typically, one of these is from the Journal's editorial board. Others are specialists in the subject matter represented by the article. The executive editor asks them to complete the review in three weeks and encloses two forms: (a) referral form B and (b) reviewer's comment form along with reviewer's guidelines. Comments to authors are about the appropriateness and adequacy of the theoretical or conceptual framework, literature review, method, results and discussion, and conclusions. Reviewers often include suggestions for strengthening of the manuscript. Comments to the editor are in the nature of the significance of the work and its potential contribution to the literature.
3. The executive editor, in consultation with the editor-in-chief, examines the reviews and decides whether to reject the manuscript, invite the author(s) to revise and resubmit the manuscript, or seek additional reviews. Final acceptance or rejection rests with the Editorial Board, who reserves the right to refuse any material for publication. In rare instances, the manuscript is accepted with almost no revision. Almost without exception, reviewers' comments (to the author) are forwarded to the author. If a revision is indicated, the editor provides guidelines for attending to the reviewers' suggestions and perhaps additional advice about revising the manuscript.
4. The authors decide whether and how to address the reviewers' comments and criticisms and the editor's concerns. The authors submit a revised version of the paper to the executive editor along with specific information describing how they have answered' the concerns of the reviewers and the editor.
5. The executive editor sends the revised paper out for review. Typically, at least one of the original reviewers will be asked to examine the article.
6. When the reviewers have completed their work, the executive editor in consultation with the editorial board and the editor-in-chief examine their comments and decide whether the paper is ready to be published, needs another round of revisions, or should be rejected.
7. If the decision is to accept, the paper is sent to that Press and the article should appear in print in approximately two to three months. The Publisher ensures that the paper adheres to the correct style (in-text citations, the reference list, and tables are typical areas of concern, clarity, and grammar). The authors are asked to respond to any queries by the Publisher. Following these corrections, page proofs are mailed to the corresponding authors for their final approval. At this point, only essential changes are accepted. Finally, the article appears in the pages of the Journal and is posted on-line.

English language editing

Authors are responsible for the linguistic accuracy of their manuscripts. Authors not fully conversant with the English language should seek advice from subject specialists with a sound knowledge of English. The cost will be borne by the author, and a copy of the certificate issued by the service should be attached to the cover letter.

Note When your manuscript is received at *Pertanika*, it is considered to be in its final form. Therefore, you need to check your manuscript carefully before submitting it to the executive editor.

Author material archive policy

Authors who require the return of any submitted material that is rejected for publication in the journal should indicate on the cover letter. If no indication is given, that author's material should be returned, the Editorial Office will dispose of all hardcopy and electronic material.

Copyright

Authors publishing the Journal will be asked to sign a declaration form. In signing the form, it is assumed that authors have obtained permission to use any copyrighted or previously published material. All authors must read and agree to the conditions outlined in the form, and must sign the form or agree that the corresponding author can sign on their behalf. Articles cannot be published until a signed form has been received.

Lag time

The elapsed time from submission to publication for the articles averages 5-6 months. A decision of acceptance of a manuscript is reached in 2 to 3 months (average 9 weeks).

Back issues

Single issues from current and recent volumes are available at the current single issue price from UPM Press. Earlier issues may also be obtained from UPM Press at a special discounted price. Please contact UPM Press at penerbit@putra.upm.edu.my or you may write for further details at the following address:

UPM Press
Universiti Putra Malaysia
43400 UPM, Serdang
Selangor Darul Ehsan
Malaysia.